STRUCTURE GUIDED EQUATION DISCOVERY WITH INFLUENCE-BASED FEEDBACK FOR LARGE LANGUAGE MODELS

Anonymous authors
Paper under double-blind review

ABSTRACT

Large Language Models (LLMs) hold significant promise for scientific discovery, particularly in identifying interpretable, closed-form equations from complex data. However, existing LLM-driven approaches often rely on coarse, scalar feedback (e.g., overall Mean Squared Error), limiting the LLM's ability to discern the individual contributions of components within a proposed equation. This forces the LLM to rely heavily on its priors or engage in inefficient trial-and-error exploration. We introduce *Structure Guided Equation Discovery* (SGED), a novel framework where LLMs act as dual agents in an iterative symbolic modeling pipeline. An LLM agent first proposes candidate basis functions $\psi_j(x)$ for a linear symbolic model $f(x) = \sum_j w_j \psi_j(x)$. A second LLM agent then refines this set of terms, critically guided by detailed, per-term *influence scores* Δ_j and fitted weights w_j. These scores quantify each basis function's contribution to predictive accuracy, providing the crucial granular feedback needed for effective model refinement. SGED can operate as a direct iterative refinement loop or be integrated into Monte Carlo Tree Search (MCTS) for a more comprehensive exploration of the equation space. We demonstrate that providing LLMs with this structured, influence-based feedback improves the accuracy of discovered equations and the efficiency of the discovery process on diverse biological and synthetic datasets. SGED highlights the broader principle that equipping LLMs with detailed, interpretable feedback about sub-components of their generative output can unlock more sophisticated reasoning and self-improvement capabilities.

1 INTRODUCTION

The quest for interpretable and generalizable mathematical models from data is a cornerstone of scientific advancement. In fields like biology, pharmacology, and physics, concise equations that accurately predict phenomena and offer mechanistic insights are invaluable for guiding research and fostering new discoveries. This paper focuses on discovering *closed-form, nonlinear symbolic models* of the form $f(\mathbf{x}) = \sum_j w_j \psi_j(\mathbf{x})$, where $\psi_j(\mathbf{x})$ are basis functions (potentially complex transformations of input features $\mathbf{x}$) and w_j are their corresponding weights. The goal is to find models that are not only accurate but also interpretable.

Large Language Models (LLMs) have emerged as powerful tools for scientific tasks, including equation discovery (Ma et al., 2023b; Holt et al., 2024b). Their vast knowledge priors and reasoning capabilities allow them to navigate the complex search space of potential equations. However, current methods often guide LLMs with only a single scalar metric, such as the overall validation loss (e.g., Mean Squared Error). This coarse feedback, while indicating *if* a proposed equation is good, fails to provide information on *why* it is good or bad, or *which specific parts* of the equation contribute most to its performance or its deficiencies. Without this granular credit assignment, the LLM must resort to less efficient exploration strategies, relying heavily on its pre-trained biases or engaging in near-random perturbations. This limitation becomes particularly acute when dealing with high-dimensional data, where the number of potential input features and their interactions is vast.

To overcome this, we propose **Structure Guided Equation Discovery (SGED)**. SGED transforms LLMs into sophisticated agents within an iterative discovery pipeline by providing them with *granular,*

Table 1: **Problem Settings and Method Applicability (SGED Context).** Comparison of typical problem characteristics, system focus, and applications for different modeling paradigms. SGED targets interpretable symbolic equations for static or dynamic systems, where LLMs propose and refine basis functions for a linear model using detailed influence-based feedback and optional tree search.

Method Paradigm	Input Dim (d)	Typical Data Regime	Target Model Form	Handles Feat. Eng. ($\phi(\psi_j)$)?	System Type Focus	Primary Objective	Example Applications
Classical Symbolic Reg. (e.g., GP-SR) [1]	Low (< 20) / Struggles with High	Small-Large	Symbolic Eq ($\mathcal{E}$)	Manual / Limited	Static (mostly)	Interpretation	Basic physics laws, simple regressions
Black-Box ML (NN, GBDT) [2]	Any	Large Pref.	Black-Box Prediction	Implicit (Learned Rep.)	Static / Dynamical	Prediction Accuracy	Image recognition, complex risk scoring
Neural ODEs [3]	Any (if deep)	Large Pref.	ODE / Dynamics	Implicit	Dynamical	Prediction (Dynamics)	Modeling physical processes
LLM for ODEs (e.g., D3) [4]	Low Focus	Small-Large	ODE / Dynamics	✗(Assumes features)	Dynamical	Interpretation (ODE)	Discovering physics ODEs
SGED (Ours)	**Any (LLM selects from d)**	**Small-Large**	**Symbolic Eq ($\sum w_j\psi_j(\mathbf{x})$)**	**✓(LLM proposes ψ_j)**	**Static / Dynamical**	**Accuracy, Interpretation, Generalization**	**Biomarker discovery, genomic risk models**

Notes: ✓: Supported/Designed for, ✗: Not primary focus/supported, Implicit: Learned internally. ψ_j are basis functions. "Low Dim": struggles beyond $d \approx 20$.
SGED's current focus is regression; exploring other model forms (e.g., ODEs) with influence feedback could be explored in future work.
References: [1] (Stephens, 2015; Cranmer et al., 2020b), [2] (Chen & Guestrin, 2016; Gorishniy et al., 2021), [3] (Chen et al., 2018), [4] (Holt et al., 2024b)

per-term influence feedback. In our framework, one LLM agent proposes candidate basis functions $\psi_j(\mathbf{x})$. After these terms are used to fit a linear model, we calculate influence scores Δ_j for each term, quantifying its impact on the model's predictive performance (e.g., the change in MSE if the term were removed).

This detailed feedback, along with the fitted weights w_j, is then provided to a second LLM agent, which decides which terms to keep, discard, or implicitly refine for the next iteration. This process provides the LLM with the critical missing information: a clear understanding of each component's utility. This targeted feedback enables more efficient and effective exploration of the equation space, leading to more accurate and interpretable models. Furthermore, SGED can employ this iterative propose-and-prune cycle within a Monte Carlo Tree Search (MCTS) framework, allowing for a more structured and robust exploration of complex hypothesis spaces, potentially avoiding local optima.

We argue that providing LLMs with such detailed, interpretable feedback about the structural components of their proposals is a key enabler for more advanced reasoning and self-improvement in scientific discovery tasks. By understanding not just the overall quality but the specific value of individual contributions, LLMs can make more informed decisions, leading to faster convergence and ultimately, more accurate and insightful scientific models (see Figure 2). Additionally, we situate SGED within the landscape of modeling paradigms, see Table 1.

Contributions:
① **Conceptual Innovation**: We reframe LLM-driven equation discovery by emphasizing the need for granular, interpretable feedback. We propose per-term influence scores as a powerful mechanism to provide LLMs with the component-level understanding necessary for effective model refinement.
② **Methodological Framework (SGED)**: We introduce a novel framework employing two LLM agents: one for proposing candidate basis functions and another for pruning them, guided by per-term influence scores and weights. We detail how this iterative cycle can be enhanced with Monte Carlo Tree Search for systematic exploration.
③ **Empirical Validation**: We demonstrate through experiments on diverse biological and synthetic datasets that SGED, by leveraging influence-based feedback, discovers more accurate symbolic equations and converges more efficiently than approaches relying on coarser feedback.

2 Methodology: Structure Guided Equation Discovery (SGED)

Structure Guided Equation Discovery (SGED) is an iterative framework where a Large Language Model (LLM) acts as an intelligent agent to discover symbolic mathematical models. The target models are of the form $f(\mathbf{x}) = \sum_{j=1}^{M} w_j \psi_j(\mathbf{x})$, where $\psi_j(\mathbf{x})$ are basis functions proposed by the LLM, and w_j are their corresponding weights determined by fitting to data.

The central idea of SGED is to guide the LLM's search process through detailed, per-term influence feedback, enabling it to make informed decisions about refining the set of basis functions. This process can either follow a direct iterative refinement path or be augmented with a Monte Carlo Tree Search (MCTS) to explore a broader space of potential equations more systematically. The overall workflow is depicted in Figure 1, and we provide a concrete illustration of the discovery process in Appendix E.2.

2.1 Core Iterative Step: Propose-and-Prune Cycle

The engine of SGED is a propose-and-prune cycle, which constitutes a single iteration of model generation and refinement. This cycle takes the current set of basis functions (which can be empty initially or be the result of a previous iteration) and a history of past interactions and attempts. It

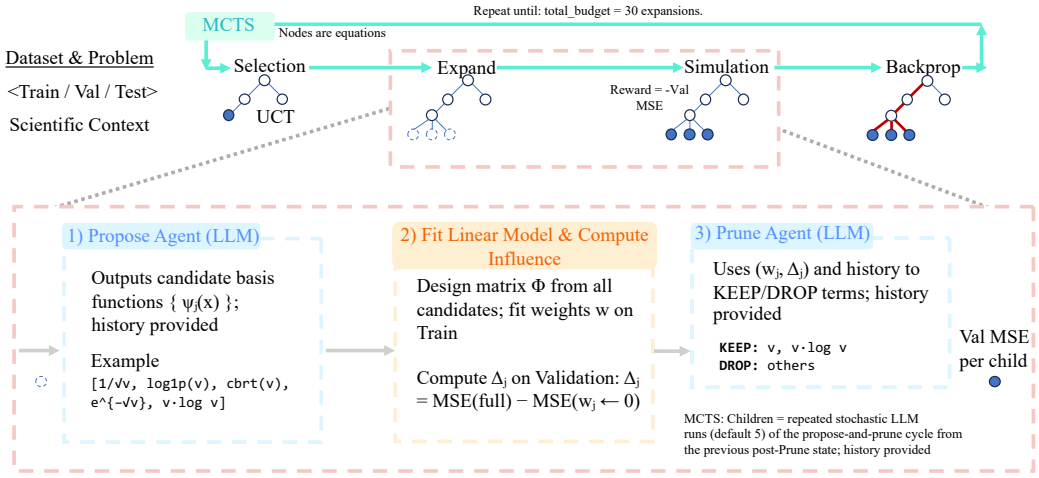

Figure 1: Conceptual block diagram of the Structure Guided Equation Discovery (SGED) method. The LLM agent iteratively proposes a set of basis functions $\{\psi_j\}$. A linear model $y = \sum w_j \psi_j(\mathbf{x})$ is fitted. The LLM receives detailed feedback, including weights w_j and influence scores Δ_j for each term, and uses this to refine its proposal for the next iteration. This iterative loop can be enhanced with MCTS for structured exploration. The process aims for accurate and interpretable models by leveraging the LLM's reasoning with granular, influence-based guidance.

consists of two main phases involving LLM interaction: term generation and term pruning, with an intermediate evaluation step that calculates the crucial influence scores (see Algorithm 2 in Appendix B.4 for pseudocode).

First, in the **Term Generation Phase**, the LLM is prompted to suggest new candidate basis functions. This prompt, provides substantial context: a detailed description of the dataset and the scientific problem, a preview of the input features and target variables, the currently active set of basis functions, the best equation found so far (if applicable), and, importantly, a history of previous rounds. This history includes a summary of which terms were kept or dropped in earlier cycles and their corresponding Mean Squared Errors (MSEs), enabling the LLM to learn from its past decisions (full prompt details are in Appendix B.6). The LLM is tasked with generating a list of new terms, expressed as NumPy-compatible mathematical expressions. The number of terms to propose can be guided by configuration, for instance, suggesting more terms in the initial round versus subsequent rounds.

Next, the **Candidate Evaluation and Feedback Preparation** stage begins. The newly proposed terms are aggregated with the existing basis functions to form an expanded candidate set. Each of these candidate terms is then evaluated on the training data to construct a design matrix $\mathbf{\Phi}$. A linear model (e.g. Ordinary Least Squares (OLS), Ridge, or Lasso) is fitted to this design matrix to predict the target variable $y \approx \mathbf{\Phi w}$. This step yields an initial set of weights $\mathbf{w}$ for all candidate terms and the corresponding training MSE. A critical computation then occurs: per-term influence scores are determined. For every candidate term ψ_j, its influence score Δ_j represents the change in validation MSE if that specific term were removed from the model (i.e., its weight w_j set to zero) while all other term weights remain fixed (see Appendix B.2 for calculation details). This vector of influence scores, $\mathbf{\Delta} = \{\Delta_j\}$, forms the core of the granular feedback provided to the LLM. The validation dataset is used for these calculations to assess generalization and mitigate overfitting. We use this computationally efficient 'no-refit' approach, which we empirically validated against more costly refit-aware alternatives and found to be as effective at guiding the discovery process in Appendix E.9.

Following this evaluation, the **Term Pruning Phase** commences. The LLM is again invoked, this time to prune the comprehensive set of candidate terms. It receives a detailed prompt, which includes: the dataset and problem description; the full list of candidate terms alongside their fitted weights w_j and their calculated influence scores Δ_j (obtained from the validation set); the overall validation MSE of the model incorporating all candidate terms; the history of prior keep/drop decisions; and the human-readable current equation. The LLM is explicitly guided to utilize the influence scores as a key heuristic for its decisions, with instructions like "$\Delta_j \approx 0 \implies$ drop" and "large $\Delta_j \implies$ keep", while also encouraging the use of its own judgment. The LLM's pruning decisions are returned as a dictionary specifying which terms to "keep" and which to "drop".

Finally, in the **Final Model Fitting and State Update** stage, the basis functions designated as "keep" by the LLM constitute the refined set of terms for the current iteration. A new linear model is trained exclusively with these surviving terms using the training data. Its performance metrics, namely MSE and optionally R^2 score, NRMSE, etc. are then evaluated on the validation set. An independent evaluation on the test set is also performed to record an unbiased measure of the model's generalization capability. All pertinent information from this entire propose-and-prune cycle — including the sets of terms before and after pruning, the LLM's keep/drop decisions, MSE values at different stages, other derived metrics, and the generated equations — is systematically collected. We also incorporate the updated history, which now includes a summary of the outcomes from the current iteration. This is the final output of one propose-and-prune cycle.

2.2 Search Strategies for Equation Discovery

SGED employs the propose-and-prune cycle as its core mechanism for generating and evaluating new candidate equations. Based on the configuration, SGED can adopt one of two main strategies to navigate the vast search space of possible equations.

The first strategy is a **Linear Iterative Refinement**. SGED operates by creating a linear sequence of model refinements. In this mode, the set of basis functions that survive the pruning phase directly becomes the input set of current terms for the immediately following propose-and-prune cycle. This iterative process is repeated for a predetermined number of iterations, or until a defined early stopping criterion is met. Such criteria might include observing no significant improvement in the validation MSE for a specified number of consecutive iterations, i.e., early-stopping. Each iteration in this chain is designed to incrementally enhance the quality of the equation by building upon the feedback and results from the preceding step. A comprehensive history of all generated is maintained throughout this process, enabling the system to monitor progress and, if needed, to revert to or reconsider previously high-performing solutions.

The second, more advanced strategy involves a **Tree-Based Search using Monte Carlo Tree Search (MCTS)**. The MCTS framework allows for a more structured and potentially more robust exploration of the complex hypothesis space of equations. In this configuration, the search for an optimal equation is formalized as an MCTS problem. Consequently, a node encapsulates a specific mathematical equation (defined by its constituent basis functions and their fitted weights) along with the historical sequence of decisions and refinements that led to its formulation.

The propose-and-prune procedure serves as the mechanism for generating successor states, which correspond to child nodes in the MCTS tree, from a given parent node. It is possible to generate multiple distinct successors from a single parent node by repeatedly executing the propose-and-prune, potentially introducing slight variations or leveraging inherent stochasticity in the LLM's responses (we use the latter). The evaluation of a node's quality, or its reward signal to be maximized, that we use for the MCTS algorithm, is its negative validation MSE, as a lower MSE indicates a better model. If the generation of successors is computationally expensive, the MCTS implementation can be set to use the immediate node reward for simulations or rollouts. A standard MCTS algorithm, governed by the Upper Confidence Bound for Trees (UCT) formula (Kocsis & Szepesvári, 2006) with the default exploration constant of $\sqrt{2}$ is used, balancing exploration and exploitation. The MCTS process continues until a predefined computational budget is exhausted, such as a maximum number of node expansions or a maximum search depth. The ultimate goal of the MCTS process is to identify the path through the search tree that culminates in exhibiting the best performance on the validation metric. Appendix B.3 provides full MCTS implementation details.

By enabling a parallel exploration of multiple refinement pathways, the MCTS approach helps SGED to potentially circumvent local optima that might ensnare a purely linear iterative refinement strategy.

2.3 Influence-Based Feedback and LLM Interaction

The effectiveness of SGED heavily relies on the quality of its interaction with the LLM. The prompts are designed to provide clear, unambiguous instructions and all necessary contextual information. The per-term influence scores, Δ_j, are pivotal during the pruning phase. The prompt directly instructs the LLM:

> *Inspect every row. Decide "keep" or "drop" for each term using the rule: Use the heuristic: "$\Delta_j \approx 0 \implies$ drop", "large $\Delta_j \implies$ keep" and your own judgement.*

This directive empowers the LLM to synergize a quantitative, data-driven metric (the influence score) with its extensive general knowledge and reasoning capabilities. These capabilities might include assessing term complexity, predicting potential for generalization, or understanding the semantic relevance of a term within the context of the specific scientific problem description.

Furthermore, the provision of a historical record of past decisions – what terms were kept or dropped, and the resultant impact on MSE before and after pruning – facilitates a form of meta-learning or in-context learning, allowing the LLM to refine its strategies over the duration of the discovery process (Appendices B.5 and B.6 contain full details on LLM interaction and prompts). The LLM is also explicitly encouraged to consider how well the proposed terms might generalize beyond the immediate validation set. Robustness is enhanced by post-processing steps that validate the LLM's output (whether they are proposed terms or keep/drop decisions), ensuring correct formatting and evaluability, and by incorporating retry mechanisms to handle occasional LLM errors or malformed responses.

3 Related Work

Table 2: Comparison of SGED with prior paradigms. SGED aims to overcome prior limitations via LLM guided proposal and refinement of basis functions using detailed influence-based feedback, optionally with MCTS.

Method Paradigm	Handles High Dim ($d \approx 150+$)	Automated Basis Func. Eng. (ψ_j)	Interpretable Output ($\sum w_j \psi_j(\mathbf{x})$)	Feedback Granularity
Classical Symbolic Reg.	Often struggles	Limited / Manual	✓	Basic (Loss)
Black-Box ML (NNs, GBDT)	✓	Implicit (Learned Rep.)	✗	Basic (Loss)
Neural ODEs	✓(if deep)	Implicit	✗	Basic (Loss)
LLM for Equations (e.g., D3)	Untested (low-d focus)	✗(Assumes features given)	✓/ Hybrid	Loss + Code Errors
SGED (Ours)	✓	**✓(LLM proposes ψ_j)**	**✓(Linear Comb. of ψ_j)**	**Detailed (Per-term Influence Scores)**

Our work, SGED, intersects with and differentiates itself from several research areas, as summarized in Table 2, and we provide an extended related work in Appendix A.

Symbolic Regression (SR). Traditional SR techniques, such as genetic programming (GP) (Koza, 1994; Schmidt & Lipson, 2009) and sparse regression methods like SINDy for dynamical systems (Brunton et al., 2016), aim to find explicit mathematical equations. While effective for certain problems, these methods often operate on a predefined set of input features and basic mathematical operations. They can struggle with high-dimensional inputs or require significant manual feature engineering to define relevant transformations. Some modern SR approaches like PySR (Cranmer, 2023) incorporate more sophisticated search algorithms and a wider range of operators but typically do not leverage the generative and reasoning capabilities of LLMs for proposing complex basis functions or utilize semantic feedback like per-term influence scores. SGED differentiates itself by employing an LLM to actively generate and refine these basis functions $\psi_j(\mathbf{x})$, which can be arbitrarily complex, guided by specific, quantitative influence feedback for each proposed component.

Black-Box Models. Machine learning models like neural networks (NNs) (Chen et al., 2018; Gorishniy et al., 2021) and gradient-boosted decision trees (GBDTs) (Chen & Guestrin, 2016) are highly effective at fitting complex patterns in data and can handle high-dimensional inputs. However, their internal workings are often opaque, making them "black boxes" that lack the interpretability of symbolic equations. While techniques such as SHAP (Lundberg & Lee, 2017) or LIME (Ribeiro et al., 2016) can provide post-hoc explanations for feature importance, they do not directly yield a concise, closed-form mathematical model. SGED, in contrast, aims to produce inherently interpretable models.

LLM-driven Equation Discovery. The use of LLMs for scientific discovery, including equation generation, is a rapidly advancing field. Systems like AI Feynman (Udrescu & Tegmark, 2020) have shown success in rediscovering physics equations from data. Eureka (Ma et al., 2023b) employed LLMs as part of a reward modeling system for reinforcement learning in SR tasks, but not as the direct generator and refiner of basis functions based on granular feedback. The D3 framework (Holt et al., 2024b) utilizes LLMs for discovering ODEs, focusing on dynamical systems primarily from lower-dimensional data. While D3 involves iterative refinement, its feedback mechanisms are generally coarser (e.g., overall loss, code execution errors) compared to the per-term influence scores used in SGED. Other recent methods also leverage LLMs in distinct ways. ICSR (Merler et al., 2024) uses in-context learning where an LLM is prompted with previous attempts and their scalar scores (combining MSE and complexity) to generate better candidates. LLM-SR (Shojaee

et al., 2025) treats equations as programs and uses data-driven feedback on the overall program fit to guide refinement. LaSR (Grayeli et al., 2024) evolves a high-level, abstract "concept library" (e.g., "exponential growth/decay") by observing patterns in successful equations.

SGED's novelty lies in its distinct feedback mechanism. Unlike the abstract concepts in LaSR or the single scalar scores in ICSR and LLM-SR, SGED provides a direct, quantitative vector of per-term influence scores (Δ_j). This feedback measures each basis function's marginal contribution to validation accuracy, offering interpretable, component-level credit assignment. This granular guidance, coupled with a dual-agent architecture for proposing and pruning terms within a constrained linear model structure ($\sum w_j \psi_j(\mathbf{x})$), allows for a more analytical and targeted model refinement process.

Influence Functions and Model Interpretability. The concept of influence functions in statistics (Cook & Weisberg, 1980), traditionally measures the impact of individual data points on model parameters or predictions. Our use of "influence scores" for terms in a linear model is analogous: it assesses the importance of a structural component (a basis function ψ_j) to the overall model fit, similar to a leave-one-out analysis performed at the term level. This provides a principled way to assign credit to parts of the model, which the LLM then uses for refinement.

4 Experiments and Evaluation

We evaluate SGED on a variety of datasets to demonstrate its ability to discover accurate, interpretable white-box models. Our experiments focus on biomedical, bioinformatics, and pharmacokinetic domains, reflecting real-world challenges where such models are highly valuable. Full experimental details, including dataset descriptions, method configurations, and evaluation protocols, are provided in the Appendices (Appendices B, C and C.5).

Benchmark Datasets. Our evaluation uses six datasets. Three are derived from a sophisticated biomedical Pharmacokinetic-Pharmacodynamic (PKPD) model of lung cancer tumor growth, simulating effects of chemotherapy and radiotherapy (Geng et al., 2017, Appendix C.1), used in prior research (Bica et al., 2020; Seedat et al., 2022; Melnychuk et al., 2022). These are: **Lung Cancer** (no treatment), **Lung Cancer (with Chemo.)**, and **Lung Cancer (with Chemo. & Radio.)**. We also use a COVID-19 epidemic agent-based simulator (**COVID-19**, Kerr et al., 2021, Appendix C.2). For bioinformatics, we use an eNET-seq dataset for predicting RNA Polymerase II pausing (**RNA Polymerase**, Fong et al., 2022, Appendix C.4). Finally, a real-world Pharmacokinetic (PK) dataset of Warfarin patients (**Warfarin**, Janssen et al., 2022, Appendix C.3) is included.

Benchmark Methods. We compare SGED against several relevant methods. For black-box comparisons, these include neural ODEs with action inputs (**DyNODE**, Chen et al., 2018; Alvarez et al., 2020), standard Recurrent Neural Networks (**RNN**), and a state-of-the-art Transformer model (**Transformer**, Vaswani et al., 2017). For white-box model discovery, we include Sparse Identification of Nonlinear Dynamics (**SINDy**, Brunton et al., 2016) and a Genetic Programming symbolic regression method (**GPLearn**, Stephens, 2015). We also compare against variants of LLM-based discovery: a zero-shot model generated by an LLM (**ZeroShot**), this model with optimized parameters (**ZeroOptim**), and an LLM-based iterative approach using only basic MSE feedback without influence scores (**ICL - Basic Feedback**). Furthermore, we benchmark against several recent state-of-the-art LLM-based frameworks: (**D3**, Holt et al., 2024b), which discovers ODEs through an iterative multi-agent approach; (**ICSR**, Merler et al., 2024), which uses in-context learning with previous attempts and their scalar scores to generate new candidates; (**LLM-SR**, Shojaee et al., 2025), which treats equations as programs and employs an evolutionary search; and (**LaSR**, Grayeli et al., 2024), which enhances genetic algorithms by using an LLM to evolve a library of abstract textual concepts.

Evaluation Metrics. To assess the performance of our benchmark methods, we use the mean squared error (MSE) on a held-out test dataset of state-action trajectories. This evaluation is conducted over multiple seeds, each initialized with different random seeds. We report the average MSE from these runs along with their 95% confidence intervals (see Appendix C.6 for the full protocol).

5 Main Results

Comprehensive evaluations across the benchmark datasets are presented in Table 3. SGED (referred to as "Ours" in the table, representing the full method with influence feedback with iterative refinement and MCTS) consistently demonstrates strong performance, often achieving the lowest MSE among

interpretable model classes and competitive results against black-box models. This indicates its ability to discover accurate and concise closed-form equations.

Table 3: **Evaluating Method Performance.** Test MSE (mean±95 % CI) on held-out data for six benchmarks. SGED demonstrates competitive or superior performance, particularly among interpretable models. Results are based on 25 seeds unless otherwise noted. Three vertical subsections correspond to baseline classes: (1) *white-box non-LLM baselines*, (2) *white-box LLM baselines*, (3) *black-box baselines* (dark gray font). Dashes (—) indicate not run or not applicable. Average rank computed for white-box methods only.

Method	Lung Cancer MSE ↓	Lung Cancer (with Chemo.) MSE ↓	Lung Cancer (with Chemo. & Radio.) MSE ↓	COVID-19 MSE ↓	RNA Polymerase MSE ↓	Warfarin PK MSE ↓	Avg. Rank ↓
DyNODE*	326±5.96	55.7±52.8	16.2±6.35	74±2.69	—†	0.726±0.17	6.80
SINDy*	325±5.95	11.8±0.442	13.7±0.635	93.5±0.509	—†	6.84±1.76	6.80
GPLearn	7.56±1.11	46.8±15.5	46.8±4.91	0.000713±0.000506	0.0204±0.000555	2.53±0.169	6.83
ZeroShot	2.13e+13±4.35e+13	4.97e+03±3.67e+03	2.54e+03±2.74e+03	1.34e+08±2.09e+08	1.35e+05±1.75e+05	5.3e+03±1.07e+04	10.50
ZeroOptim	0.142±0.119	86.2±27.3	122±6	1.41e-07±1.04e-07	0.0130±0.000287	0.861±0.177	5.67
ICL (Basic Feedback)	0.0557±0.0486	21.2±9.8	63.3±16.5	9.35e-08±1.77e-08	0.0119±0.000352	0.784±0.193	3.83
D3-white-box	1.01e+04±1.27e+04	45±28.9	253±273	7.81e-06±2.48e-07	0.043±0.0366	1.15±0.343	7.50
LLM-SR	33.4±0	42.2±35.6	32.1±48.4	0.000453±0.000912	1.44±1.91	1.24±0.564	6.50
LaSR	658±7.31	1.71±1.16	3.97±3.21	2.59e-06±8.66e-07	0.0172±0.000649	30.1±0.992	5.50
ICSR	0.407±0.244	0.688±0.39	6.1±1.05	1.03e-07±1.6e-08	—‡	**0.497**±0.0646	2.60
RNN*	1.16e+06±3.21e+04	719±94.3	137±5.88	1.39e+04±2.47e+03	—	**0.0495±0.0406**	—
Transformer*	7.07±0.558	0.346±0.0701	0.207±0.0318	0.261±0.0915	—	1.33±0.941	—
SGED (Ours)	**0.0033**±0.0035	**0.0054**±0.00107	**0.0521**±0.0178	**5.32e-08**±1.35e-09	**0.0115**±0.000312	0.646±0.105	**1.17**

∗Results reused from prior work (Holt et al., 2024b), based on 10 seeds.
†Not applicable as the baseline is designed for temporal data but RNA Polymerase dataset is static.
‡ICSR fails with this dataset due to the large number of features (263).

5.1 Case Study: RNA Polymerase II Pausing

The discovery of quantitative rules governing biological processes is crucial for advancing our understanding of life. Automated machine learning approaches like SGED offer a path to generate interpretable, data-driven hypotheses from complex biological datasets, potentially accelerating discovery.

Biological Background. RNA polymerase II (Pol II) transcription is a fundamental process involving initiation, elongation, and termination (Cramer, 2019). Transcription speed is non-uniform, influenced by frequent Pol II pausing (Noe Gonzalez et al., 2021; Jonkers & Lis, 2015; Danko et al., 2013; Bentley, 2014; Zamft et al., 2012). Pause sites, particularly at G residues preceding T/C on the non-template DNA strand, are key determinants of elongation speed (Fong et al., 2022; Gajos et al., 2021). Nucleosomes and histone modifications like H3K36me3 are also implicated (Bondarenko et al., 2006; Churchman & Weissman, 2011; Lee et al., 2024; Wen et al., 2014), but their precise roles and the sequence determinants of pausing in human cells remain incompletely understood.

Dataset. We analyzed eNET-seq data mapping Pol II pause sites in human cells at single-base resolution (Fong et al., 2022). A "pause score" ($N_{\text{reads at pause site}}/N_{\text{reads in 200bp window}}$) quantified pausing. This score was aligned with 263 features, including local DNA sequence context around potential pause sites (e.g., one-hot encoded nucleotides A/T/G/C at positions -3 to +3 relative to site), MNase-seq signal (nucleosome occupancy), H3K4me3 and H3K36me3 ChIP-seq signals (histone modifications), and gene region annotations (TSS, gene body, termination). A balanced dataset of 48,000 pause sites and 48,000 control sites (pause score = 0) was split into training, validation, and test sets.

Findings. SGED, guided by influence-based feedback, discovered the following interpretable equation (coefficients rounded for brevity):

$$
\begin{aligned}
\text{pause\_score} \;=\; & 0.0178\,\ln\!\big(1+\text{signal}_{\text{MNase}}\big) \\
& - 0.000246\,\text{signal}_{\text{H3K4me3}} + 0.00902\,\ln\!\big(1+\text{signal}_{\text{H3K4me3}}\big) \\
& + 0.0194\,\ln\!\Big(1+\sum_{\text{cond}}\text{signal}_{\text{H3K36me3,ds}}\Big) \\
& - 0.0291\,\big(\mathbb{1}_{\{\text{seq}_{-1}=A\}}+\mathbb{1}_{\{\text{seq}_{0}=A\}}+\mathbb{1}_{\{\text{seq}_{1}=A\}}+\mathbb{1}_{\{\text{seq}_{-1}=T\}}+\mathbb{1}_{\{\text{seq}_{0}=T\}}+\mathbb{1}_{\{\text{seq}_{1}=T\}}\big) \\
& + 0.0223\,\mathbb{1}_{\{\text{gene\_region=TSS}\}} + 0.0257\,\mathbb{1}_{\{\text{gene\_region=body}\}} + 0.0636\,\mathbb{1}_{\{\text{gene\_region=termination}\}} \\
& - 0.0146\,\big(\mathbb{1}_{\{\text{seq}_{-3}=T\}}+\mathbb{1}_{\{\text{seq}_{-2}=T\}}+\mathbb{1}_{\{\text{seq}_{-1}=T\}}\big) \\
& - 0.0402\,\big(\mathbb{1}_{\{\text{seq}_{-1}=G\}}+\mathbb{1}_{\{\text{seq}_{-1}=C\}}\big) + 0.0333\,\mathbb{1}_{\{\text{seq}_{0}=G\}} - 0.0397\,\mathbb{1}_{\{\text{seq}_{0}=C\}} \\
& + 0.0735\,\mathbb{1}_{\{\text{seq}_{1}=T\}} + 0.0243\,\mathbb{1}_{\{\text{seq}_{-1}=G\}},
\end{aligned}
$$

where "ds" sums over the H3K36me3 signals from several alternative data sources; seq_i is the nucleotide at relative position i; $\mathbb{1}_{\{\cdot\}}$ is the indicator function.

Expert review by an Anonymous Biologist confirmed that this SGED-discovered equation aligns with known biology and offers novel insights:

Expert review (Anonymous Biologist)

►**Confirms existing knowledge:** Positive association of nucleosome occupancy ($\text{signal}_{\text{MNase}}$) and H3K36me3 with pausing, and higher pausing in termination regions, consistent with prior studies (Bondarenko et al., 2006; Churchman & Weissman, 2011; Lee et al., 2024; Wen et al., 2014; Gromak et al., 2006).
►**Discovers novel sequence elements:** Beyond the known GT element at positions 0/+1 (Fong et al., 2022; Gajos et al., 2021), the model identifies C at positions 0 and -1, and T at -1, -2, -3 as significant negative predictors of pausing. These represent new, testable hypotheses about sequence-dependent pausing mechanisms.

This case study demonstrates SGED's capacity to learn complex relationships from high-dimensional biological data, producing interpretable models that both validate existing knowledge and generate novel scientific hypotheses. Further discussion is in Appendix D.

5.2 Insight Experiments: Impact of Feedback and Search Strategy

To understand the contributions of SGED's core components, we performed ablation studies on the Lung Cancer benchmark dataset.

Ablation Study: Influence Feedback and MCTS. We compared the full SGED model against variants where either the MCTS tree search component was disabled (falling back to iterative refinement) or the detailed influence based feedback was removed (LLM receives only basic MSE for pruning), or both. Results are shown in Table 4. The reported MSE values are for the Lung Cancer (no treatment) dataset, averaged over 25 seeds.

Table 4: **Ablation study on the Lung Cancer (no treatment) dataset.** We quantify the impact of removing the MCTS component and/or the influence-feedback module. Results are test MSE (lower is better) averaged over 25 seeds with 95% confidence intervals.

Variant	MCTS	Influence Feedback	MSE ↓
Full SGED (Ours)	✓	✓	**0.0033**±0.0035
w/o MCTS (Iterative + Influence Feedback)	✗	✓	0.350±0.505
w/o Influence Feedback (MCTS + Basic Feedback)	✓	✗	4.56±6.71
w/o MCTS or Influence Feedback (Iterative + Basic Feedback)	✗	✗	61.98±20.52

The results clearly indicate that both the influence-based feedback and the MCTS tree search contribute significantly to SGED's performance. Removing influence feedback (even with tree search) leads to a substantial increase in MSE (from 0.0033 to 4.56), demonstrating that granular, per-term guidance is crucial for the LLM to effectively prune and refine equations.

Similarly, removing the tree search (even with influence feedback, MSE increases to 0.350) also results in higher MSE, suggesting that systematic exploration helps in finding better solutions compared to a purely linear iterative approach for this benchmark. The variant without both components performs the worst (MSE of 61.98), underscoring the synergistic benefits of these design choices.

Iterative Improvement with Influence Feedback. Figure 2 illustrates the convergence behavior, comparing SGED with influence feedback to a variant relying on basic MSE feedback. SGED with influence feedback converges faster and to lower MSE values, as the detailed per-term information allows for more targeted and efficient exploration of the equation space. Each iteration leverages the insights from influence scores to prune unhelpful terms and focus on promising ones, leading to a more rapid discovery of accurate and parsimonious models. This is shown for the linear iterative refinement variant of SGED here, and analogously for the MCTS variant in Appendix E.1.

These insight experiments underscore the importance of SGED's core principles: providing LLMs with *rich, structured feedback at the component level* and employing *systematic search strategies* to navigate the complex landscape of possible equations. A suite of additional experiments in the appendix further substantiates these findings. We demonstrate that SGED's performance advantage is

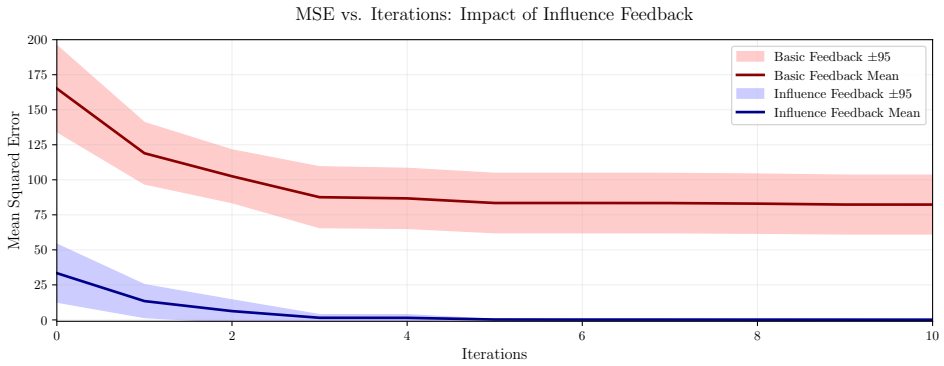

Figure 2: **MSE vs. Iterations: Impact of Influence Feedback.** Plot showing validation MSE convergence over iterations for SGED (linear iterative refinement variant) with full influence-based feedback versus a variant with only basic MSE feedback on the *Lung Cancer (with Chemo. & Radio.)* dataset. Shaded regions denote 95% confidence intervals, solid lines show means. Detailed influence feedback is leads to faster convergence and lowers final MSE.

consistent across nine different underlying LLMs, including open-weight models (Appendix E.5); that it is *robust to a large number of irrelevant features* (Appendix E.6); that it can successfully discover equations for diverse synthetic models (Appendix E.7); and, importantly, *generalizes robustly to unseen biological replicates*, indicating the discovered models capture reproducible scientific principles (Appendix E.8). Furthermore, the method *scales sub-linearly with an increasing number of input features*, making it suitable for high-dimensional problems (Appendix G). Critically, SGED also proves more computationally efficient, *achieving superior accuracy when constrained by a fixed LLM token budget* (Appendix G.3) and *converging significantly faster* than traditional methods like Genetic Programming (Appendix E.4). Methodological variants, including an extension for term-local constant optimization (Appendix E.10) and an ablation on alternative influence score calculations (Appendix E.9), are also explored.

6 Discussion

This paper introduced Structure Guided Equation Discovery (SGED), a framework that leverages Large Language Models for symbolic modeling by providing them with fine-grained, per-term influence scores as feedback. This structured guidance allows the LLM to iteratively propose, evaluate, and refine basis functions for constructing interpretable models of the form $f(\mathbf{x}) = \sum_j w_j \psi_j(\mathbf{x})$. Integration of Monte Carlo Tree Search further enhances the systematic exploration of the equation space. Our empirical results across diverse datasets, including a detailed case study on RNA Polymerase II pausing, demonstrate that SGED can discover accurate and scientifically plausible equations. The ablation studies confirm that both the influence-based feedback mechanism and the MCTS contribute significantly to the framework's effectiveness, leading to lower MSE compared to variants lacking these components. The ability to identify important terms via influence scores and to prune irrelevant ones based on this quantitative metric, combined with the LLM's reasoning capabilities, proves to be a powerful approach for navigating the vast search space of symbolic models and achieving superior accuracy.

Limitations & Future Work. Though SGED's architectural advantages provide a robust performance uplift across a range of LLMs, its performance is still ultimately tied to the capabilities of the underlying language model. While current state-of-the-art models show strong reasoning abilities, their capacity to generate highly novel or counter-intuitive scientific insights based on the provided feedback is an area for ongoing research. The complexity of basis functions that can be reliably proposed and evaluated also presents a frontier. While SGED is computationally efficient, running many LLM calls at scale can still be intensive. Future work could explore more efficient LLM prompting strategies, methods for distilling learned heuristics from the LLM's successful refinements, and extending the framework to other types of mathematical models (e.g., differential equations with more complex structures, causal graphs). Validating the novel discoveries from SGED, such as the new sequence determinants in the RNA Polymerase case study, through wet-lab experiments is a crucial next step for real-world scientific impact. Further research into the types of feedback that are most effective for LLM-guided discovery remains a rich area of investigation.

Ethics Statement. Our work promotes transparency in AI-driven science by developing a method, SGED, that generates interpretable symbolic models. The primary ethical consideration is the potential for misinterpretation; a discovered equation is a data-driven hypothesis, not a validated scientific law, and may reflect spurious correlations in the data. We stress that any model produced by SGED must be rigorously scrutinized and validated by domain experts before any consideration for real-world application to prevent potential harm from decisions based on flawed but plausible-looking equations. The datasets used in this research were either simulated or publicly available and anonymized, and were handled in accordance with their usage terms. We position SGED as a tool to augment, not replace, human scientific inquiry, acknowledging that the underlying Large Language Models may introduce biases and lack genuine scientific understanding.

Reproducibility Statement. To ensure full reproducibility of our findings, we provide a comprehensive account of our methodology, data, and experimental setup. The core Structure Guided Equation Discovery (SGED) framework is described in Section 2, with a detailed breakdown of the propose-and-prune cycle (Section 2.1), search strategies (Section 2.2), and the influence-based feedback mechanism (Section 2.3). For implementation, high-level pseudocode is available in Appendix B.4, and an in-depth description of all methodological components, including the calculation of influence scores and MCTS configuration, is provided in Appendix B. The specifics of our interaction with Large Language Models, including the models used and the exact prompt templates for the "Propose" and "Prune" agents, are documented in Appendix B.5 and Appendix B.6, respectively. All benchmark datasets are thoroughly described in Appendix C, which details the simulation parameters for the Cancer PKPD and COVID-19 environments and provides sources for the public Warfarin PK and RNA Polymerase datasets. The experimental evaluation protocol, including benchmark methods, metrics, and hyperparameters, is specified in Section 4 and further detailed in Appendix C.5. The computational resources used for our experiments are outlined in Appendix F. Upon publication, all code required to generate the datasets and reproduce the results will be made publicly available.

REFERENCES

Aerdem. Lofo importance - leave one feature out importance. https://github.com/aerdem4/lofo-importance, 2020. Accessed: 2024-05-23.

Ruta Agashe, Jayanth Krishnamurthy, and Daniel Khashabi. Leveraging large language models for scientific discovery: a survey. *arXiv preprint arXiv:2402.03236*, 2024.

Victor M Martinez Alvarez, Rareş Roşca, and Cristian G Fălcuţescu. Dynode: Neural ordinary differential equations for dynamics modeling in continuous control. *arXiv preprint arXiv:2009.04278*, 2020.

David Alvarez-Melis and Tommi S Jaakkola. On the robustness of interpretability methods. *arXiv preprint arXiv:1806.08049*, 2018.

Rajkumar Ashok, Manuel López-Ibáñez, and Nadarajen Veerapen. Mcts-ge: Monte carlo tree search for grammar-based genetic programming. In *Proceedings of the 2020 Genetic and Evolutionary Computation Conference Companion*, pp. 171–172. ACM, 2020.

David L Bentley. Coupling mrna processing with transcription in time and space. *Nature Reviews Genetics*, 15(3):163–175, 2014.

Tarek R Besold, Artur d'Avila Garcez, Sebastian Bader, Howard Bowman, Pedro Domingos, Pascal Hitzler, Thomas Icard, Kai-Uwe Kühnberger, Luís C Lamb, Rianne de Penning, et al. Neurosymbolic cognitive reasoning: A survey. *KI-Künstliche Intelligenz*, 31:337–357, 2017.

Ioana Bica, Ahmed M. Alaa, James Jordon, and Mihaela van der Schaar. Estimating counterfactual treatment outcomes over time through adversarially balanced representations. In *International Conference on Learning Representations*, 2020.

Luca Biggio, Tommaso Bendinelli, Alexander Neitz, Aurelien Lucchi, and Giambattista Parascandolo. Neural symbolic regression that scales. In *International Conference on Machine Learning*, pp. 936–945. PMLR, 2021.

Daniil A Boiko, Robert MacKnight, and Gabe Gomes. Emergent autonomous scientific research capabilities of large language models. *Nature*, 622(7981):101–108, 2023.

Vladimir A Bondarenko, Louise M Steele, Andrea Újvári, Daria A Gaykalova, Olga I Kulaeva, Yury S Polikanov, Donal S Luse, and Vasily M Studitsky. Nucleosomes can form a polar barrier to transcript elongation by rna polymerase ii. *Molecular cell*, 24(3):469–479, 2006.

Alana Bran, Alvin Rajkomar, Yanatan Matias, Valter Sagi, Catherine Cui, Anton Libov, Bowen Cole, Shefali Rao, Benjamin Van Durme, and Adam M Ringel. Beyond fact checking: Guiding biomedical hypothesis generation with large language models. *arXiv preprint arXiv:2308.14487*, 2023.

Leo Breiman. Random forests. *Machine learning*, 45(1):5–32, 2001.

Tom Brown, Benjamin Mann, Nick Ryder, Melanie Subbiah, Jared D Kaplan, Prafulla Dhariwal, Arvind Neelakantan, Pranav Shyam, Girish Sastry, Amanda Askell, et al. Language models are few-shot learners. *Advances in neural information processing systems*, 33:1877–1901, 2020.

Steven L Brunton, Joshua L Proctor, and J Nathan Kutz. Discovering governing equations from data by sparse identification of nonlinear dynamical systems. *Proceedings of the national academy of sciences*, 113(15):3932–3937, 2016.

Swarat Chaudhuri, Kevin Ellis, Oleksandr Polozov, Rishabh Singh, Armando Solar-Lezama, Yisong Yue, et al. Neurosymbolic programming. *Foundations and Trends® in Programming Languages*, 7 (3):158–243, 2021.

Pinxin Chen, Hieu Xu, Luke Zettlemoyer, and Alexey Leshchinskiy. Alphadev: Generating code with large language models and deep reinforcement learning. *arXiv preprint arXiv:2307.02319*, 2023.

Ricky TQ Chen, Yulia Rubanova, Jesse Bettencourt, and David K Duvenaud. Neural ordinary differential equations. *Advances in neural information processing systems*, 31, 2018.

Tianqi Chen and Carlos Guestrin. Xgboost: A scalable tree boosting system. In *Proceedings of the 22nd acm sigkdd international conference on knowledge discovery and data mining*, pp. 785–794, 2016.

Zhi-Feng Chen, Jing-Dun Lin, Cheng-Ming Fan, and Hsueh-I Wu. Incorporating actor-critic in monte carlo tree search for symbolic regression. *Applied Intelligence*, pp. 1–19, 2024.

Hanyu Cheng, Raghu Kansal, and Javier Duarte. Symbolnet: Neural symbolic regression with adaptive dynamic pruning for compression. *Machine Learning: Science and Technology*, 2024. doi: 10.1088/2632-2153/ad2a91. arXiv:2307.15720.

Kyunghyun Cho, Bart Van Merriënboer, Caglar Gulcehre, Dzmitry Bahdanau, Fethi Bougares, Holger Schwenk, and Yoshua Bengio. Learning phrase representations using rnn encoder-decoder for statistical machine translation. *arXiv preprint arXiv:1406.1078*, 2014.

L Stirling Churchman and Jonathan S Weissman. Nascent transcript sequencing visualizes transcription at nucleotide resolution. *Nature*, 469(7330):368–373, 2011.

R Dennis Cook and Sanford Weisberg. Characterizations of an empirical influence function for detecting influential cases in regression. *Technometrics*, 22(4):495–508, 1980.

Patrick Cramer. Eukaryotic transcription turns 50. *Cell*, 179(4):808–812, 2019.

Miles Cranmer. Interpretable machine learning for science with pysr and symbolicregression. jl. *arXiv preprint arXiv:2305.01582*, 2023.

Miles Cranmer, Alvaro Sanchez Gonzalez, Peter Battaglia, Rui Xu, Kyle Cranmer, David Spergel, and Shirley Ho. Discovering symbolic models from deep learning with inductive biases. In *Advances in Neural Information Processing Systems*, volume 33, pp. 17429–17442, 2020a.

Miles Cranmer, Alvaro Sanchez Gonzalez, Peter Battaglia, Rui Xu, Kyle Cranmer, David Spergel, and Shirley Ho. PySR: Fast & flexible symbolic regression. *arXiv preprint arXiv:2010.14131*, 2020b.

Charles G Danko, Nasun Hah, Xin Luo, André L Martins, Leighton Core, John T Lis, Adam Siepel, and W Lee Kraus. Signaling pathways differentially affect rna polymerase ii initiation, pausing, and elongation rate in cells. *Molecular cell*, 50(2):212–222, 2013.

Finale Doshi-Velez and Been Kim. Towards a rigorous science of interpretable machine learning. *arXiv preprint arXiv:1702.08608*, 2017.

Andrew G Dunn and Tom S Arrow. Gpt-3 a new tool for reproducible science? *Nature Machine Intelligence*, 4(12):1088–1089, 2022.

Aaron Fisher, Cynthia Rudin, and Francesca Dominici. All models are wrong, but many are useful: Learning a variable's importance by studying an entire class of prediction models simultaneously. *Journal of Machine Learning Research*, 20(177):1–81, 2019.

Nova Fong, Ryan M Sheridan, Srinivas Ramachandran, and David L Bentley. The pausing zone and control of rna polymerase ii elongation by spt5: Implications for the pause-release model. *Molecular cell*, 82(19):3632–3645, 2022.

Jerome H Friedman and Bogdan E Popescu. Predictive learning via rule ensembles. *The Annals of Applied Statistics*, 2(3):916–954, 2008.

Martyna Gajos, Olga Jasnovidova, Alena van Bömmel, Susanne Freier, Martin Vingron, and Andreas Mayer. Conserved dna sequence features underlie pervasive rna polymerase pausing. *Nucleic acids research*, 49(8):4402–4420, 2021.

Artur d'Avila Garcez and Luis C Lamb. Neurosymbolic ai: The 3 rd wave. *Artificial Intelligence Review*, pp. 1–20, 2023.

Changran Geng, Harald Paganetti, and Clemens Grassberger. Prediction of Treatment Response for Combined Chemo- and Radiation Therapy for Non-Small Cell Lung Cancer Patients Using a Bio-Mathematical Model. *Scientific Reports*, 7(1):13542, October 2017. ISSN 2045-2322. doi: 10.1038/s41598-017-13646-z.

Yury Gorishniy, Ivan Rubachev, Valentin Khrulkov, and Artem Babenko. Revisiting deep learning models for tabular data. *Advances in neural information processing systems*, 34:18932–18943, 2021.

Arya Grayeli, Atharva Sehgal, Omar Costilla-Reyes, Miles Cranmer, and Swarat Chaudhuri. Symbolic regression with a learned concept library. In A. Globerson, L. Mackey, D. Belgrave, A. Fan, U. Paquet, J. Tomczak, and C. Zhang (eds.), *Advances in Neural Information Processing Systems*, volume 37, pp. 44678–44709. Curran Associates, Inc., 2024. URL https://proceedings.neurips.cc/paper_files/paper/2024/file/4ec3ddc465c6d650c9c419fb91f1c00a-Paper-Conference.pdf.

Natalia Gromak, Steven West, and Nick J Proudfoot. Pause sites promote transcriptional termination of mammalian rna polymerase ii. *Molecular and cellular biology*, 26(10):3986–3996, 2006.

Frank R Hampel. The influence curve and its role in robust estimation. *Journal of the american statistical association*, 69(346):383–393, 1974.

Sepp Hochreiter and Jürgen Schmidhuber. Long short-term memory. *Neural computation*, 9(8): 1735–1780, 1997.

Samuel Holt, Zhaozhi Qian, Tennison Liu, James Owen Weatherall, and Mihaela van der Schaar. Data-driven discovery of dynamical systems in pharmacology using large language models - project page. https://www.vanderschaar-lab.com/papers/d3-data-driven-discovery-of-dynamical-systems-in-pharmacology-using-large-language 2024a. Accessed: 2024-05-23.

Samuel Holt, Zhaozhi Qian, Tennison Liu, Jim Weatherall, and Mihaela van der Schaar. Data-driven discovery of dynamical systems in pharmacology using large language models. *Advances in Neural Information Processing Systems*, 37:96325–96366, 2024b.

Shima Imani, Liang Du, and Harsh Shrivastava. Mathprompter: Mathematical reasoning using large language models. In *ICLR 2023 Workshop on Trustworthy and Reliable Large-Scale Machine Learning Models*, 2023.

Alexander Janssen, Frank C Bennis, and Ron AA Mathôt. Adoption of machine learning in pharmacometrics: an overview of recent implementations and their considerations. *Pharmaceutics*, 14(9): 1814, 2022.

Iris Jonkers and John T Lis. Getting up to speed with transcription elongation by rna polymerase ii. *Nature reviews Molecular cell biology*, 16(3):167–177, 2015.

Pierre-Alexandre Kamienny, Stéphane Le Tallec, François Charton, Sébastien Le, and Yann Ollivier. End-to-end symbolic regression with transformers. *Transactions on Machine Learning Research*, 2022.

Cliff C Kerr, Robyn M Stuart, Dina Mistry, Romesh G Abeysuriya, Katherine Rosenfeld, Gregory R Hart, Rafael C Núñez, Jamie A Cohen, Prashanth Selvaraj, Brittany Hagedorn, et al. Covasim: an agent-based model of covid-19 dynamics and interventions. *PLOS Computational Biology*, 17(7): e1009149, 2021.

Elias B Khalil, Pierre Le Bodic, Siyuan Liu, and Song Son. Bamcts: A bayesian approach to monte-carlo tree search. In *International Conference on Machine Learning*, pp. 10962–10976. PMLR, 2022.

Levente Kocsis and Csaba Szepesvári. Bandit based monte-carlo planning. In *European conference on machine learning*, pp. 282–293. Springer, 2006.

John R Koza. Genetic programming as a means for programming computers by natural selection. *Statistics and computing*, 4:87–112, 1994.

Jan Kubalík, Erik Derner, Vít Bíba, Martin Babjak, and Robert Babuska. Symbolicgpt: A generative transformer model for symbolic regression. *Genetic Programming and Evolvable Machines*, 24(1): 7, 2023.

Ian E Kumar, Suresh Venkatasubramanian, Michael Hoffman, and Alistair Goldstein. Problems with shapley-value-based explanations as feature importances. In *International Conference on Machine Learning*, pp. 5391–5400. PMLR, 2020.

Min Kyung Lee, Na Hyun Park, Soo Young Lee, and TaeSoo Kim. Context-dependent and locus-specific role of h3k36 methylation in transcriptional regulation. *Journal of Molecular Biology*, pp. 168796, 2024.

Jing Lei, James Robins, and Larry Wasserman. Distribution-free predictive inference for regression. *Journal of the American Statistical Association*, 113(523):1094–1111, 2018.

Aitor Lewkowycz, Anders Andreassen, David Dohan, Ethan Dyer, Henryk Michalewski, Vinay Ramasesh, Ambrose Slone, Cem Anil, Iman Misra, Nicolas Sonnerat, et al. Solving quantitative reasoning problems with language models. In *Advances in Neural Information Processing Systems*, volume 35, pp. 1289–1301, 2022.

Yingping Li, Zihang Liu, Weimin Song, Tao Huang, Erik D Goodman, Jie Yan, and Aimin Zhou. Differentiable genetic programming for high-dimensional symbolic regression. *IEEE Transactions on Evolutionary Computation*, 27(6):1877–1891, 2023a.

Yue-Yang Li, Zichao Xu, Shangce Tan, Hongming Song, Kai Zhang, Fan Guo, and Hong Liu. Transformer-based planning for symbolic regression. In *Thirty-seventh Conference on Neural Information Processing Systems*, 2023b. URL https://openreview.net/forum?id=FpCV7iSjP7.

Yujia Li, David Choi, Junyoung Chung, Nate Kushman, Julian Schrittwieser, Rémi Leblond, Tom Eccles, James Keeling, Felix Gimeno, Agustin Dal Lago, et al. Competition-level code generation with alphacode. *Science*, 378(6624):1092–1097, 2022.

Linyuan Lu, Shingo Mabu, and Kotaro Hirasawa. Contemporary symbolic regression methods and their relative performance. *Applied Soft Computing*, 111:107692, 2021.

Scott M Lundberg and Su-In Lee. A unified approach to interpreting model predictions. *Advances in neural information processing systems*, 30, 2017.

Chuan Ma, Zonglin Shen, Yefan Wu, M Shamim Hossain, Cong Tao, and Yang Li. Large language models in science and medicine. *Patterns*, 4(8):100835, 2023a.

Yecheng Jason Ma, William Liang, Guanzhi Wang, De-An Huang, Osbert Bastani, Dinesh Jayaraman, Yuke Zhu, Linxi Fan, and Anima Anandkumar. Eureka: Human-level reward design via coding large language models. *arXiv preprint arXiv:2310.12931*, 2023b.

Yecheng Jason Ma, William Liang, Guanzhi Wang, De-An Huang, Osbert Bastani, Dinesh Jayaraman, Yuke Zhu, Linxi Fan, and Anima Anandkumar. Eureka: Human-level reward design via coding large language models. https://eureka-research.github.io/, 2023c. Accessed: 2024-05-23.

Aman Madaan, Niket Tandon, Prakhar Gupta, Skyler Hallinan, Luyu Gao, Sarah Wiegreffe, Uri Alon, Nouha Dziri, Shrimai Prabhumoye, Hossein Mobahi, et al. Self-refine: Iterative refinement with self-feedback. In *Advances in Neural Information Processing Systems*, volume 36, 2023.

Valentyn Melnychuk, Dennis Frauen, and Stefan Feuerriegel. Causal transformer for estimating counterfactual outcomes. In *International Conference on Machine Learning*, pp. 15293–15329. PMLR, 2022.

Matteo Merler, Nicola Dainese, and Katsiaryna Haitsiukevich. In-context symbolic regression: Leveraging language models for function discovery. *CoRR*, abs/2404.19094, 2024. URL https://doi.org/10.48550/arXiv.2404.19094.

Subhrajit Monda, Sudipan Das, Lovesh Kumar, and Partha Talukdar. Deep symbolic regression: A survey and new results. In *Proceedings of the First Workshop on Neural Machine Translation and Generation*, pp. 123–133. Association for Computational Linguistics, 2021.

Melvin Noe Gonzalez, Daniel Blears, and Jesper Q Svejstrup. Causes and consequences of rna polymerase ii stalling during transcript elongation. *Nature reviews Molecular cell biology*, 22(1): 3–21, 2021.

OpenAI. Gpt-4 technical report. *ArXiv*, abs/2303.08774, 2023. URL https://api.semanticscholar.org/CorpusID:257532815.

Allen Pan, Jiasheng Xu, Hong-Cheng Chen, Xiaozhi Li, and He Ji. Automatically correcting large language models: Surveying and aco. *arXiv preprint arXiv:2308.08182*, 2023.

Brenden K Petersen, Mikel Landajuela Larma, Terrell N Mundhenk, Claudio Prata Santiago, Soo Kyung Kim, and Joanne Taery Kim. Deep symbolic regression: Recovering mathematical expressions from data via risk-seeking policy gradients. In *International Conference on Learning Representations*, 2020.

Zhaozhi Qian, Krzysztof Kacprzyk, and Mihaela van der Schaar. D-CODE: Discovering closed-form ODEs from observed trajectories. In *International Conference on Learning Representations*, 2022. URL https://openreview.net/forum?id=wENMvIsxNN.

Marco Tulio Ribeiro, Sameer Singh, and Carlos Guestrin. " why should i trust you?" explaining the predictions of any classifier. In *Proceedings of the 22nd ACM SIGKDD international conference on knowledge discovery and data mining*, pp. 1135–1144, 2016.

Cynthia Rudin. Stop explaining black box machine learning models for high stakes decisions and use interpretable models instead. *Nature machine intelligence*, 1(5):206–215, 2019.

David E Rumelhart, Geoffrey E Hinton, and Ronald J Williams. Learning representations by back-propagating errors. *nature*, 323(6088):533–536, 1986.

Michael Schmidt and Hod Lipson. Distilling free-form natural laws from experimental data. *science*, 324(5923):81–85, 2009.

Nabeel Seedat, Fergus Imrie, Alexis Bellot, Zhaozhi Qian, and Mihaela van der Schaar. Continuous-time modeling of counterfactual outcomes using neural controlled differential equations. *arXiv preprint arXiv:2206.08311*, 2022.

Noah Shinn, Beck Labash, and Ashwin Gopinath. Reflexion: Language agents with verbal reinforcement learning. In *Advances in Neural Information Processing Systems*, volume 36, 2023.

Parshin Shojaee, Kazem Meidani, Shashank Gupta, Amir Barati Farimani, and Chandan K. Reddy. LLM-SR: Scientific equation discovery via programming with large language models. In *The Thirteenth International Conference on Learning Representations*, 2025. URL https://openreview.net/forum?id=m2nmp8P5in.

David Silver, Aja Huang, Chris J Maddison, Arthur Guez, Laurent Sifre, George Van Den Driessche, Julian Schrittwieser, Ioannis Antonoglou, Veda Panneershelvam, Marc Lanctot, et al. Mastering the game of go with deep neural networks and tree search. *Nature*, 529(7587):484–489, 2016.

David Silver, Julian Schrittwieser, Karen Simonyan, Ioannis Antonoglou, Aja Huang, Arthur Guez, Thomas Hubert, Lucas Baker, Matthew Lai, Adrian Bolton, et al. Mastering the game of go without human knowledge. *Nature*, 550(7676):354–359, 2017.

Trevor Stephens. gplearn 0.4.2 documentation. https://gplearn.readthedocs.io/en/stable/, 2015. Accessed: 2025-5-16.

Georgi Tonchev, Theofilos Sainis, Stergios Nikolakopoulos, Zoe Kotti, Pavlos Papasarantopoulos, Prodromos Malakasiotis, and Ion Androutsopoulos. Automating systematic reviews with large language models: a competition-based perspective. *arXiv preprint arXiv:2401.06794*, 2024.

Silviu-Marian Udrescu and Hod Lipson. Fast function class discovery for symbolic regression. *Genetic Programming and Evolvable Machines*, 10(3):241–271, 2009.

Silviu-Marian Udrescu and Max Tegmark. Ai feynman: A physics-inspired method for symbolic regression. *Science advances*, 6(16):eaay2631, 2020.

Silviu-Marian Udrescu, Andrew Tan, Jiahai Feng, Orisvaldo Neto, Tailin Wu, and Max Tegmark. Ai feynman 2.0: Pareto-optimal symbolic regression exploiting graph modularity. In H. Larochelle, M. Ranzato, R. Hadsell, M.F. Balcan, and H. Lin (eds.), *Advances in Neural Information Processing Systems*, volume 33, pp. 4860–4871. Curran Associates, Inc., 2020. URL https://proceedings.neurips.cc/paper_files/paper/2020/file/33a854e247155d590883b93bca53848a-Paper.pdf.

Ashish Vaswani, Noam Shazeer, Niki Parmar, Jakob Uszkoreit, Llion Jones, Aidan N Gomez, Łukasz Kaiser, and Illia Polosukhin. Attention is all you need. *Advances in neural information processing systems*, 30, 2017.

Hua Wang, Zheng Fan, Pavel V Shliaha, Matthew Miele, Ronald C Hendrickson, Xuejun Jiang, and Kristian Helin. H3k4me3 regulates rna polymerase ii promoter-proximal pause-release. *Nature*, 615(7951):339–348, 2023.

Larry Wasserman. *All of Statistics: A Concise Course in Statistical Inference*. Springer Texts in Statistics. Springer, New York, NY, 1 edition, 2004. ISBN 978-0-387-40272-7. doi: 10.1007/978-0-387-21736-9. URL https://doi.org/10.1007/978-0-387-21736-9. Series ISSN 1431-875X; Series E-ISSN 2197-4136; eBook ISBN 978-0-387-21736-9 (published 2013-12-11); Softcover ISBN 978-1-4419-2322-6 (published 2010-12-01); First edition; *xx*+442 pp.

Hong Wen, Yuanyuan Li, Yuanxin Xi, Shiming Jiang, Sabrina Stratton, Danni Peng, Kaori Tanaka, Yongfeng Ren, Zheng Xia, Jun Wu, et al. Zmynd11 links histone h3. 3k36me3 to transcription elongation and tumour suppression. *Nature*, 508(7495):263–268, 2014.

Bradley Zamft, Lacramioara Bintu, Toyotaka Ishibashi, and Carlos Bustamante. Nascent rna structure modulates the transcriptional dynamics of rna polymerases. *Proceedings of the National Academy of Sciences*, 109(23):8948–8953, 2012.

Yifan Zhang, Yikang Sile, Chengyu Weng, Yuxin Zhang, and Chen Lin. Hypothesis generation with a large language model by identifying documents for relevant and novel connections. *arXiv preprint arXiv:2305.19225*, 2023.

Appendix

Table of Contents

Code. All code will be made available upon publication.

LLM Usage. Large Language Models (LLMs) were employed for refining the language, grammar, and clarity of the manuscript. Additionally, they were used to assist with code implementation and debugging. All intellectual content, research ideas, and scientific arguments were developed solely by the authors.

A Additional Related Work

Structure Guided Equation Discovery (SGED) synergizes concepts from symbolic regression, the rapidly evolving capabilities of Large Language Models (LLMs) in scientific reasoning, machine learning interpretability, and advanced search techniques. This extended related work section aims to provide a more comprehensive contextualization of SGED, elaborating on its distinctions and contributions by delving deeper into these intersecting domains.

A.1 Symbolic Regression: Foundations and Evolution

Symbolic Regression (SR) is the problem of identifying a mathematical expression that best fits a given dataset, without assuming a pre-specified model structure. This inherently seeks interpretable models.

Traditional Approaches: Genetic Programming (GP) has historically been a dominant paradigm for SR (Koza, 1994; Schmidt & Lipson, 2009; Stephens, 2015). GP-based SR typically evolves a population of candidate expressions (often represented as trees) using evolutionary operators like crossover and mutation. While powerful, traditional GP can face challenges such as premature convergence, code bloat (expressions becoming overly complex), and difficulties in efficiently exploring vast search spaces, especially with high-dimensional data or when a diverse set of mathematical operators is required (Cranmer, 2023; Lu et al., 2021; Monda et al., 2021; Li et al., 2023a). The search can be computationally intensive, and the quality of discovered equations can be sensitive to the choice of initial function sets and hyperparameters. Other early approaches, like Symbolic Regression via Fast Function Class Discovery (SRFC) (Udrescu & Lipson, 2009), focused on identifying general classes of functions as a preliminary step, which could then guide more detailed equation discovery.

Sparse Symbolic Regression: Methods like SINDy (Sparse Identification of Nonlinear Dynamics) (Brunton et al., 2016) leverage sparse regression. SINDy constructs a library of candidate (often nonlinear) functions of the state variables and uses techniques like LASSO or sequentially thresholded least-squares to find a sparse combination of these functions that best describes the system's dynamics, primarily for ODEs. While effective for systems where the basis functions are well-chosen, the library of candidate functions is often pre-defined by the user, which might limit discovery of truly novel functional forms not anticipated by the domain expert.

Modern Advancements in SR: More recent SR methods have introduced innovations to tackle these challenges. PySR (Cranmer, 2023; Cranmer et al., 2020b) incorporates techniques from simulated annealing, genetic algorithms, and a highly optimized search process with a broad library of operators to find Pareto-optimal equations (balancing accuracy and complexity). AI Feynman (Udrescu & Tegmark, 2020; Udrescu et al., 2020) introduced a recursive divide-and-conquer strategy inspired by physics problem-solving techniques. It attempts to discover symmetries, separability, and other properties of the target function to break it down into simpler components, often using neural networks to guide these decompositions. Deep Symbolic Regression (DSR) approaches (Petersen et al., 2020; Biggio et al., 2021; Kamienny et al., 2022) often use recurrent neural networks (RNNs) to generate expressions token by token, framing SR as a sequence generation problem, sometimes guided by reinforcement learning. Other neural approaches like SymbolNet (Cheng et al., 2024) focus on scalability to high-dimensional inputs and model compression by dynamically pruning operators and features.

SGED's Differentiation in SR: SGED distinguishes itself from these SR paradigms in several key aspects. Unlike traditional GP or sparse SR methods that rely on pre-defined or combinatorially generated basis functions, SGED tasks an LLM with proposing candidate basis functions $\psi_j(\mathbf{x})$. These can be arbitrarily complex and draw upon the LLM's vast pre-trained knowledge of mathematical and

scientific relationships. Crucially, SGED provides the LLM with highly granular, *per-term influence scores* Δ_j as feedback, guiding a second LLM agent in the pruning and refinement process. This explicit, quantitative credit assignment for each component of the proposed equation is a core novelty that enables more targeted and efficient exploration than typical fitness-based evolution in GP or the global loss signals used in many DSR approaches. While AI Feynman uses NNs for specific decomposition tasks, SGED employs LLMs more broadly for generative proposal and structured refinement based on component-wise utility.

A.2 Large Language Models in Scientific Discovery and Equation Formulation

LLMs are increasingly being explored as powerful tools for accelerating scientific discovery (OpenAI, 2023; Brown et al., 2020; Agashe et al., 2024). Their ability to process and generate human language, understand complex instructions, and synthesize information from vast training corpora makes them suitable for tasks ranging from hypothesis generation to experimental design and data analysis (Boiko et al., 2023; Dunn & Arrow, 2022; Ma et al., 2023a; Tonchev et al., 2024).

LLMs for Equation Discovery and System Modeling: Several works have specifically investigated LLMs for discovering mathematical models. Eureka (Ma et al., 2023b;c) leverages LLMs, particularly their code-writing capabilities, to design reward functions for reinforcement learning agents that then perform symbolic regression or other optimization tasks. While Eureka uses LLMs effectively for reward generation, SGED employs LLMs as the direct architects of the symbolic equations themselves, iteratively proposing and refining basis functions. The D3 framework (Holt et al., 2024b;a) uses LLMs to discover Ordinary Differential Equations (ODEs) for pharmacological systems. D3 employs multiple LLM agents for modeling, feature acquisition, and evaluation in an iterative loop. While sharing the iterative, LLM-driven discovery spirit with SGED, the feedback mechanism in D3 is generally coarser (e.g., overall model fit, code execution errors, qualitative evaluation). SGED's unique contribution is the fine-grained, per-term influence scores Δ_j provided to the LLM, enabling more precise credit assignment and refinement of the equation's structure, and its applicability to general symbolic models beyond just ODEs. D-CODE (Qian et al., 2022) also focuses on discovering closed-form ODEs, using a grammar-based approach and a coefficient optimizer, but does not involve LLMs in the same generative and iterative feedback loop as SGED or D3.

Broader LLM Capabilities for Science: LLMs have also shown promise in generating computer code for simulations (Li et al., 2022; Chen et al., 2023), assisting in mathematical reasoning (Imani et al., 2023; Lewkowycz et al., 2022), and forming hypotheses from literature (Bran et al., 2023; Zhang et al., 2023). SGED specifically harnesses the LLM's pattern recognition and generative capabilities to propose scientifically plausible basis functions and its reasoning capabilities to interpret and act upon the structured influence feedback for model refinement. This structured interaction, providing quantitative evidence for the utility of each proposed component, pushes the LLM beyond simple generation towards a more analytical role.

A.3 Interpretability in Machine Learning: Inherent vs. Post-Hoc

The demand for interpretable machine learning models is growing, especially in high-stakes domains like science and medicine where understanding the "why" behind a prediction is as important as the prediction itself (Rudin, 2019; Doshi-Velez & Kim, 2017).

Black-Box Models and Post-Hoc Explanations: Many high-performing machine learning models, such as deep neural networks (Gorishniy et al., 2021; Chen et al., 2018) and gradient-boosted decision trees (Chen & Guestrin, 2016), are often considered "black boxes" due to their complex internal structures. To shed light on their predictions, post-hoc explanation methods have been developed. Prominent examples include LIME (Local Interpretable Model-agnostic Explanations) (Ribeiro et al., 2016) and SHAP (SHapley Additive exPlanations) (Lundberg & Lee, 2017). LIME approximates the black-box model locally with a simpler, interpretable model. SHAP uses concepts from cooperative game theory (Shapley values) to attribute the prediction to individual features. While these methods provide valuable insights, they offer explanations of an already-trained (and often opaque) model rather than producing a model that is inherently transparent. Limitations can include computational cost, potential instability of explanations, and the fact that the explanation itself is an approximation of the original model's behavior (Rudin, 2019; Kumar et al., 2020; Alvarez-Melis & Jaakkola, 2018).

SGED's Pursuit of Inherent Interpretability: SGED directly addresses the need for interpretability by aiming to discover models of the form $f(\mathbf{x}) = \sum_j w_j \psi_j(\mathbf{x})$. Each basis function $\psi_j(\mathbf{x})$ is a symbolic expression, and its contribution to the final output is explicitly weighted by w_j. This structure is inherently interpretable, allowing domain experts to examine, understand, and potentially validate or refute the discovered relationships based on their domain knowledge. The per-term influence scores Δ_j further enhance this by quantifying the contribution of each ψ_j to the model's predictive power during the discovery process itself.

A.4 Neurosymbolic AI

Neurosymbolic AI seeks to combine the strengths of neural networks (e.g., learning from data, pattern recognition) with symbolic reasoning (e.g., logic, explicit knowledge representation, interpretability) (Garcez & Lamb, 2023; Chaudhuri et al., 2021; Besold et al., 2017). This integration aims to create AI systems that are more robust, generalizable, interpretable, and capable of incorporating existing domain knowledge.

SGED can be viewed as a neurosymbolic system. The LLM, a large neural network, acts as the "neuro" component, responsible for proposing candidate symbolic basis functions and for reasoning about their utility based on feedback. The symbolic regression task itself, the manipulation of mathematical expressions, and the resulting interpretable equation $f(\mathbf{x}) = \sum_j w_j \psi_j(\mathbf{x})$ represent the "symbolic" component. The per-term influence scores act as a critical bridge, translating numerical performance data into a structured format that the LLM can symbolically reason about to refine the symbolic model. This tight integration, where the neural component generates and refines symbolic structures based on quantitative feedback about those structures, aligns well with the goals of neurosymbolic AI, particularly in the context of scientific discovery (Cranmer et al., 2020a; Kubalík et al., 2023).

A.5 Influence Analysis: From Data Points to Model Components

The concept of "influence" in SGED, referring to the impact of individual terms $\psi_j(\mathbf{x})$ on the model's predictive performance, draws an analogy to classical influence functions in statistics and more recent feature importance techniques.

Classical Influence Functions: Influence functions, introduced in Hampel (1974) and further developed in Cook & Weisberg (1980), measure the effect of an individual data point on a model's parameters or predictions. They are valuable for outlier detection and understanding model sensitivity to specific observations.

Feature Importance and Leave-One-Out Analysis: In machine learning, various methods assess feature importance. Permutation feature importance (Breiman, 2001; Fisher et al., 2019) measures the decrease in model performance when a feature's values are randomly shuffled. Leave-One-Feature-Out (LOFO) importance involves retraining the model with one feature omitted and observing the performance change (Lei et al., 2018; Aerdem, 2020). These methods help identify which input features are most critical for a model's predictions.

SGED's Term Influence Scores: SGED's per-term influence scores Δ_j adapt this concept to the components of the *discovered equation itself*. Instead of assessing the impact of raw input features or individual data points, Δ_j quantifies how much the removal of a specific basis function $\psi_j(\mathbf{x})$ (and its corresponding weight w_j) would affect the model's validation MSE. This provides a direct, interpretable measure of each term's contribution to the model's accuracy, akin to a leave-one-term-out analysis. This granular credit assignment is then fed back to the LLM, enabling it to make informed decisions about which terms to retain, discard, or refine, thereby steering the discovery process towards more accurate and parsimonious equations.

A.6 Automated Feature Engineering and Basis Function Discovery

The performance of many machine learning models heavily depends on the quality of input features. Automated feature engineering aims to create new, informative features from existing ones.

Traditional and Deep Learning Approaches: Traditional techniques might involve polynomial expansions or predefined transformations. Deep learning models implicitly perform feature engineering

by learning hierarchical representations, but these learned features are often not symbolic or easily interpretable.

Rule-Based Feature Generation: Methods like RuleFit (Friedman & Popescu, 2008) generate new features in the form of decision rules. These rules, derived from an ensemble of decision trees, capture interactions between original features. A sparse linear model (e.g., using Lasso) is then fitted on both the original features and these new rule-based features. This yields an interpretable model that can capture non-linearities and interactions.

SGED's LLM-Driven Basis Function Proposal: SGED takes a distinct approach by using an LLM to propose candidate basis functions $\psi_j(\mathbf{x})$. These are not limited to simple rules but can be complex symbolic expressions involving various mathematical operations and combinations of input features. The LLM's generative capabilities allow for a much broader and potentially more creative exploration of the space of possible transformations than typical rule-generation algorithms. The subsequent linear combination $\sum_j w_j \psi_j(\mathbf{x})$ maintains interpretability, while the influence-guided pruning ensures that only valuable, LLM-generated transformations are retained.

A.7 Iterative Refinement and Search Strategies in Complex Spaces

Discovering optimal symbolic equations is a challenging search problem over a vast and complex space.

Iterative Refinement and Feedback: Many AI systems employ iterative refinement, where solutions are progressively improved based on feedback. The nature and granularity of this feedback are crucial. SGED's iterative propose-and-prune cycle, guided by per-term influence scores, provides a structured mechanism for self-improvement. The LLM learns from its past decisions (which terms were kept/dropped and their impact) and the specific utility of each component in the current proposal. This contrasts with approaches where feedback is only a single scalar loss, offering less guidance for targeted improvement. LLM self-correction and refinement, often through in-context learning, is an active area of research (Madaan et al., 2023; Shinn et al., 2023; Pan et al., 2023). SGED provides a domain-specific instantiation of this principle with a highly structured feedback signal.

Monte Carlo Tree Search (MCTS): For more systematic exploration, SGED can integrate its propose-and-prune cycle into an MCTS framework. MCTS is a heuristic search algorithm that has achieved remarkable success in domains like game playing (e.g., AlphaGo/AlphaZero (Silver et al., 2016; 2017)) and other optimization problems. In SGED, MCTS treats the equation discovery process as navigating a tree where nodes represent (sets of) basis functions and edges represent propose/prune actions. MCTS balances exploration of new equation structures with exploitation of promising ones. While MCTS has been explored for program synthesis and, more recently, symbolic regression (Khalil et al., 2022; Li et al., 2023b; Chen et al., 2024; Ashok et al., 2020), SGED's novelty lies in combining MCTS with LLM-driven proposal/pruning stages that are informed by the detailed influence-based feedback. The work Li et al. (2023b) also uses MCTS with transformers for symbolic regression, but their feedback and reward structure within MCTS differs from SGED's influence-score-driven pruning by an LLM agent.

By leveraging detailed, interpretable feedback and powerful search strategies, SGED aims to make significant strides in the automated discovery of accurate and understandable symbolic models from data.

B Method Details

This section provides further details on the Structure Guided Equation Discovery (SGED) framework, complementing the main description in Section 2. We elaborate on the core components, including the definition and calculation of influence scores, and the specifics of the Monte Carlo Tree Search (MCTS) implementation.

B.1 Overview of SGED

As outlined in Section 2 and depicted in Figure 1, SGED operates as an iterative symbolic modeling pipeline driven by Large Language Models (LLMs). The framework employs two primary LLM agents:

- A **"Propose" Agent**: This LLM agent is responsible for generating new candidate basis functions $\psi_j(\mathbf{x})$. It receives contextual information about the dataset, the scientific problem, the current set of basis functions, the best equation discovered so far, and a history of past decisions and outcomes to guide its suggestions.
- A **"Prune" Agent**: After candidate terms are evaluated, this LLM agent refines the set of basis functions. It is provided with the candidate terms, their fitted weights w_j, and crucially, their per-term influence scores Δ_j. Based on this granular feedback and its general knowledge, it decides which terms to keep or discard.

This propose-and-prune cycle forms the core iterative step. SGED can execute these cycles in a linear iterative refinement loop or integrate them within a Monte Carlo Tree Search (MCTS) framework for a more systematic and robust exploration of the equation space. The overall objective is to discover accurate, parsimonious, and interpretable models of the form $f(\mathbf{x}) = \sum_j w_j \psi_j(\mathbf{x})$. The hyperparameters related to LLM prompting, such as `terms_per_round` (default: 5), `first_round_n_candidates` (default: 10), and `keep_n_terms` (default: 6, but can be disabled to allow keeping *any* number of terms), guide the LLM agents' behavior during term generation and pruning.

B.2 Influence Score (Δ_j) Details

The per-term influence score, Δ_j, is a cornerstone of the SGED framework, providing the granular feedback necessary for the "Prune" LLM agent to make informed decisions.

Definition: For a linear model $f(\mathbf{x}) = \sum_{k=1}^{M} w_k \psi_k(\mathbf{x})$ with M basis functions, the influence score Δ_j for a specific term $\psi_j(\mathbf{x})$ is defined as the change in the model's Mean Squared Error (MSE) on the validation set if that term were removed from the model, *while all other term weights w_k ($k \neq j$) remain fixed at their originally fitted values*.

Let $\mathbf{\Phi}_{\text{val}}$ be the design matrix evaluated on the validation set using all M candidate basis functions, and $\mathbf{y}_{\text{val}}$ be the corresponding true target values. Let $\mathbf{w} = (w_1, w_2, \ldots, w_M)^T$ be the vector of weights obtained by fitting the full model to the training data (e.g., using Ordinary Least Squares, OLS). The prediction of the full model on the validation set is $\hat{\mathbf{y}}_{\text{val}} = \mathbf{\Phi}_{\text{val}}\mathbf{w}$. The MSE of the full model on the validation set is $\text{MSE}_{\text{full}} = \text{mean}((\mathbf{y}_{\text{val}} - \hat{\mathbf{y}}_{\text{val}})^2)$.

Now, consider removing term ψ_j. This is equivalent to setting its weight w_j to zero. The predictions of this reduced model, $f_{-j}(\mathbf{x})$, on the validation set are $\hat{\mathbf{y}}_{\text{val},-j} = \hat{\mathbf{y}}_{\text{val}} - \phi_{\text{val},j} w_j$, where $\phi_{\text{val},j}$ is the j-th column of $\mathbf{\Phi}_{\text{val}}$ (i.e., the evaluations of $\psi_j(\mathbf{x})$ on the validation set). The MSE of this reduced model is $\text{MSE}_{-j} = \text{mean}((\mathbf{y}_{\text{val}} - \hat{\mathbf{y}}_{\text{val},-j})^2)$. The influence score Δ_j is then:

$$\Delta_j = \text{MSE}_{-j} - \text{MSE}_{\text{full}}$$

A higher positive Δ_j indicates that removing term ψ_j increases the validation MSE, implying that the term is important for the model's predictive accuracy on unseen data. A $\Delta_j \approx 0$ suggests the term has little unique contribution to reducing validation MSE under the current model. This calculation is performed for each target variable if the model is multi-output.

Calculation: The calculation steps are:

1. Fit the full linear model (e.g., OLS) using the training data $(\mathbf{\Phi}_{\text{train}}, \mathbf{y}_{\text{train}})$ to obtain the weights $\mathbf{w}$.
2. Calculate the predictions $\hat{\mathbf{y}}_{\text{val}}$ and the baseline MSE_{full} on the validation set $(\mathbf{\Phi}_{\text{val}}, \mathbf{y}_{\text{val}})$.
3. For each term ψ_j (from $k = 1$ to M):
   (a) Calculate the predictions of the model without term j (effectively $w_j = 0$, other w_k fixed): $\hat{\mathbf{y}}_{\text{val},-j} = \hat{\mathbf{y}}_{\text{val}} - \phi_{\text{val},j} w_j$.

(b) Calculate MSE_{-j} using $\hat{\mathbf{y}}_{\text{val},-j}$.
(c) Compute $\Delta_j = \text{MSE}_{-j} - \text{MSE}_{\text{full}}$.

Computational Cost:

- Fitting the initial OLS model: Typically $O(N_{\text{train}}M^2 + M^3)$ if $N_{\text{train}} > M$ or $O(N_{\text{train}}^2 M)$ if $M > N_{\text{train}}$.
- Calculating $\hat{\mathbf{y}}_{\text{val}}$: $O(N_{\text{val}}M)$.
- Calculating MSE_{full}: $O(N_{\text{val}})$ (assuming multi-output m is small, otherwise $O(N_{\text{val}}m)$).
- For each of the M terms, calculating Δ_j:
  - Prediction $\hat{\mathbf{y}}_{\text{val},-j}$ adjustment: $O(N_{\text{val}})$.
  - MSE_{-j} calculation: $O(N_{\text{val}})$.
  - Total for all Δ_j: $M \cdot O(N_{\text{val}})$.

The calculation of influence scores is therefore efficient once the initial model is fitted and its predictions on the validation set are obtained.

Justification and Relation to Other Measures:

- **Direct Relevance to Predictive Performance**: Δ_j directly quantifies how much a term contributes to reducing error on unseen (validation) data, which is a primary goal.
- **Efficiency**: Calculating Δ_j by fixing other weights is much more computationally efficient than refitting the model M times (once for each term's removal). This makes it practical for iterative refinement loops with many candidate terms.
- **Interpretability for LLM Guidance**: The concept of "change in error if term is removed" is intuitive and can be effectively communicated to an LLM, especially with heuristics like "$\Delta_j \approx 0 \implies$ drop".
- **Differentiation from other importance measures**:
  - It is a form of "leave-one-out" importance but applied to model terms (basis functions) rather than individual data points (like statistical influence functions, e.g., Cook's distance).
  - It differs from SHAP values (Lundberg & Lee, 2017), which explain the contribution of features to individual predictions rather than the global impact of a term on overall model MSE.
  - It is distinct from feature importance measures derived from tree-based ensembles (e.g., Gini importance or permutation importance on raw input features), as Δ_j is specific to the contribution of pre-defined or LLM-proposed basis functions $\psi_j(\mathbf{x})$ within a linear model structure.
  - By not refitting the model for each term removal, Δ_j measures the unique contribution of a term *given the current set of other terms and their weights*. This is a deliberate choice to assess the marginal utility of a term in the specific context of the current full model. If terms are highly collinear, this score might be low for some of them, aiding in pruning redundant terms.

The use of validation data for calculating Δ_j is critical for assessing generalization and mitigating overfitting, guiding the LLM to select terms that are robustly beneficial.

We further explore and experimentally investigate alternative approaches to computing influence scores in Appendix E.9.

B.3 Monte Carlo Tree Search (MCTS) Implementation Details

When SGED employs a tree-based search strategy, it utilizes a Monte Carlo Tree Search (MCTS) algorithm to navigate the complex hypothesis space of symbolic equations. This approach allows for a more structured exploration than simple iterative refinement.

- **State (Node Representation)**: Each node in the MCTS tree represents a specific state in the equation discovery process. This state is defined by the current set of selected basis functions $\{\psi_j(\mathbf{x})\}$, the corresponding fitted weights $\{w_j\}$ that form the current best equation for that path, and the history of decisions (proposals, prunings, and feedback) that led to this state.
- **Action (Transition)**: An action involves transitioning from a parent node (current equation state) to a child node (a refined equation state). This transition is achieved by executing one full **propose-and-prune cycle** as described in Section 2.1. Specifically, from a selected leaf node, the "Propose" agent suggests new terms, these are evaluated, influence scores are calculated, and the "Prune" agent refines the term set. This results in a new equation that defines a child node.
- **Expansion**: During the expansion phase of MCTS, if a selected leaf node is not a terminal state (e.g., maximum depth not reached), child nodes are generated. SGED can generate multiple distinct successor states (child nodes) from a single parent node by repeatedly invoking the propose-and-prune cycle. The hyperparameter `n_successors` (default: 5) controls how many child nodes are attempted to be generated from a parent node during a single expansion step. Variation between these successors arises from the inherent stochasticity in the LLM's responses to the propose and prune prompts, even when given the same historical context up to the parent node. Each such generated child represents a distinct path for exploration.
- **Reward and Value Estimation (Simulation/Rollout Phase)**: The quality or *value* of a node (equation) needs to be estimated to guide the MCTS search.
  - In the default SGED configuration, referred to as **Heuristic MCTS** (when the hyperparameter `rollout_is_just_node_reward` is set to `True`, which is the default), no explicit rollout (simulation beyond the newly expanded node) is performed. Instead, the reward for a newly expanded child node is its immediate, directly computed quality. This quality is typically the negative validation Mean Squared Error ($-\text{MSE}_{\text{val}}$) of the equation associated with that child node (after the pruning step). A higher value (lower MSE) indicates a better node. This immediate reward is then directly backpropagated up the tree.
  - If `rollout_is_just_node_reward` is set to `False`, a simulation phase (rollout) would be executed from the newly expanded node for a number of steps defined by `rollout_depth` (default: 1, see Appendix E.3 for an investigation). The reward from the end of this simulated trajectory would then be backpropagated. However, the primary results in this paper use the Heuristic MCTS approach.
  - Other reward signals beyond simply the negated validation set MSE could be used, though are not explored here, e.g. incorporating alternative accuracy metrics or accounting for equation parsimony (e.g. as $R = -\text{MSE}_{\text{val}} - \alpha \cdot \textit{Complexity}$, where complexity may be defined as the number of terms, operator count, etc.).
- **Backpropagation**: After a node's value is determined (either through direct evaluation in Heuristic MCTS or via a rollout), this value is backpropagated up the tree from the expanded node to the root. The visit counts and average reward (or value) of all visited nodes along the path are updated.
- **Selection (Tree Policy)**: The MCTS algorithm uses the Upper Confidence Bound applied to Trees (UCT) formula to balance exploration and exploitation when selecting which node to traverse down the tree. From a current node, the child i selected is the one that maximizes:

$$\text{UCT}(i) = Q(i) + c\sqrt{\frac{\ln N(p)}{N(i)}}$$

  where:
  - $Q(i)$ is the current estimated average reward (exploitation term) for child i.
  - $N(p)$ is the number of times the parent node p has been visited.
  - $N(i)$ is the number of times child node i has been visited.
  - c is the exploration constant (hyperparameter, default: $\sqrt{2}$). A higher c encourages more exploration of less-visited nodes.

This selection process is repeated from the root until a leaf node (a node that has not been expanded, or a terminal node) is reached.

- **Termination**: The MCTS process continues until a predefined computational budget is exhausted. This is primarily controlled by the `total_budget` hyperparameter (default: 30), which defines the total number of MCTS iterations (selection, expansion, simulation/evaluation, backpropagation cycles). A `depth_limit` (default: 10) can also restrict the maximum depth of the tree.

- **Output**: After the MCTS process completes, the equation corresponding to the node that yielded the best validation MSE throughout the entire search is typically selected as the final discovered model.

- **Computational Cost**: The main computational costs in the MCTS-based SGED are the LLM API calls (for term proposal and pruning at each expansion, potentially multiple times if `n_successors` > 1), the evaluation of basis functions on data, and the fitting of linear models. The total number of MCTS iterations (`total_budget`) is the primary driver of the overall computational expense.

This MCTS framework allows SGED to systematically explore diverse pathways of equation refinement, potentially avoiding local optima that a simpler iterative approach might encounter.

B.4 SGED PSEUDOCODE

Below is a high-level pseudocode outlining the SGED framework. Algorithm 1 describes the overall MCTS-driven search. Algorithm 2 details the core propose-and-prune cycle (`PAPC`).

For brevity, Algorithm 1 illustrates the Heuristic MCTS case, but this can be easily adapted to the rollout with `rollout_depth` case.

Algorithm 1 Structure Guided Equation Discovery (SGED) - MCTS Loop

Input: Dataset $\mathcal{D}$ (containing train, validation, test sets), Problem Description P_d, MCTS Budget B_{MCTS}, LLM Agents (LLM_P, LLM_R), MCTS Parameters (exploration const c, num successors n_s, depth limit d_{lim})
Output: Best discovered symbolic equation f_{best}
Initialize $f_{\text{best}} \leftarrow$ None
Initialize $best\_val\_mse \leftarrow \infty$
Initialize MCTS Tree T with a root node (representing an initial empty state)
for $iteration = 1$ to B_{MCTS} **do**
  $selected\_node \leftarrow$ SelectPolicy(T, c) {Select a node using UCT}
  if $selected\_node$ is suitable for expansion (e.g., not terminal by d_{lim}, and not yet fully expanded for n_s children) **then**
    {Attempt to expand $selected\_node$ by generating up to n_s children}
    for $i = 1$ to n_s **do**
      $PAPC\_Inputs \leftarrow$ GatherInputsForPAPC$(selected_node, P_d, \mathcal{D}, LLM_P, LLM_R, f_{\text{best}})$
      $equation, val\_mse, new\_terms, history \leftarrow$ ProposeAndPruneCycle$(PAPC_Inputs)$
      if $equation$ was successfully generated **then**
        $child\_node \leftarrow$ AddChildNode$(T, selected_node, new_terms, equation, val_mse, history)$
        $current\_reward \leftarrow -val\_mse$ {Heuristic reward for UCT}
        BackpropagateValue$(child_node, current_reward, T)$
        if $val\_mse < best\_val\_mse$ **then**
          $best\_val\_mse \leftarrow val\_mse$
          $f_{\text{best}} \leftarrow equation$
        end if
      end if
    end for
    Update expansion status of $selected\_node$ in T.
  else
    $current\_reward \leftarrow -selected\_node.stored\_val\_mse$ {Use node's known value}
    BackpropagateValue$(selected_node, current_reward, T)$
  end if
end for
if f_{best} is not None **then**
  Evaluate f_{best} using test set from $\mathcal{D}$
end if
return f_{best}

Algorithm 2 Propose-and-Prune Cycle

Input: $current\_terms_{in}$, $history_{in}$, $best\_equation\_so\_far$, P_d, $\mathcal{D}_{\text{train}}$, $\mathcal{D}_{\text{val}}$, LLM_P, LLM_R

Output: $equation_{out}$, val_mse_{out}, $final\_terms_{out}$, $history_{out}$

// Term Generation Phase
Prompt LLM_P with P_d, current active terms $current\_terms_{in}$, $best\_equation\_so\_far$, $history_{in}$, and data preview.
$newly\_proposed\_terms \leftarrow LLM_P$.generate_terms()
$candidate\_terms \leftarrow current\_terms_{in} \cup newly\_proposed\_terms$

// Candidate Evaluation and Feedback Preparation
Evaluate all $\psi_j \in candidate\_terms$ on $\mathcal{D}_{\text{train}}$ to get design matrix $\mathbf{\Phi}_{\text{train}}$.
Fit linear model: $\mathbf{y}_{\text{train}} \approx \mathbf{\Phi}_{\text{train}}\mathbf{w}_{cand}$ to get candidate weights $\mathbf{w}_{cand}$.
Evaluate all $\psi_j \in candidate\_terms$ on $\mathcal{D}_{\text{val}}$ to get $\mathbf{\Phi}_{\text{val}}$.
Calculate full validation MSE: $\text{MSE}_{\text{val,cand}}$ using $\mathbf{w}_{cand}$ and $(\mathbf{\Phi}_{\text{val}}, \mathbf{y}_{\text{val}})$.
For each $\psi_j \in candidate\_terms$, calculate influence score Δ_j on validation set (as per Appendix B.2).

// Term Pruning Phase
Prompt LLM_R with P_d, $candidate\_terms$, their weights w_j, influence scores Δ_j, $\text{MSE}_{\text{val,cand}}$, $history_{in}$, and current equation form.
$pruning\_decisions \leftarrow LLM_R$.decide_terms_to_keep_drop() {keep: [...], drop: [...]}
$final\_terms_{out} \leftarrow$ terms marked "keep" in $pruning\_decisions$

// Final Model Fitting and State Update
Evaluate $final\_terms_{out}$ on $\mathcal{D}_{\text{train}}$ to get $\mathbf{\Phi}_{\text{train,final}}$.
Fit final linear model: $\mathbf{y}_{\text{train}} \approx \mathbf{\Phi}_{\text{train,final}}\mathbf{w}_{\text{final}}$ to get $\mathbf{w}_{\text{final}}$.
Form $equation_{out}$ using $final\_terms_{out}$ and $\mathbf{w}_{\text{final}}$.
Calculate val_mse_{out} for $equation_{out}$ on $\mathcal{D}_{\text{val}}$.
Record this cycle's details (terms before/after pruning, decisions, MSEs, equation) into $history_{out}$.

return $equation_{out}$, val_mse_{out}, $final\_terms_{out}$, $history_{out}$

This pseudocode provides a conceptual blueprint. Actual implementations would involve detailed prompt engineering, error handling, and specific choices for the linear model fitting procedure (e.g., OLS, Ridge).

B.5 LLM Details

Unless otherwise specified (e.g., in Appendix E.5 which details experiments across a range of different Large Language Models), the primary LLM employed for the core experiments presented in this work was a version of GPT-4o. Specific model versions were used as available at the time of experimentation. For example, one of the models used in comparative evaluations was:

- `GPT-4o`: model identifier `gpt-4o`, version `2024-11-20`.

B.6 Prompt Details

The interaction with the LLM is central to the SGED framework. We employ two primary types of interactions, mediated by distinct LLM agents: one for proposing new candidate basis functions (the "Propose" agent) and another for refining the set of terms based on evaluation feedback (the "Prune" agent). Below, we detail the structure of these prompts and provide illustrative examples of LLM interactions.

B.6.1 TERM GENERATION PHASE: THE "PROPOSE" AGENT

In this phase, the LLM is tasked with generating new candidate basis functions $\psi_j(\mathbf{x})$. The prompt provides comprehensive context, including the problem description, available features, the current set of basis functions (if any), the best equation found so far, and a history of previous interactions to facilitate learning from past attempts.

Prompt Template for "Propose" Agent: The following is a representative template for the prompt provided to the "Propose" agent. Specific details such as dataset descriptions, feature lists, and historical performance are dynamically inserted.

Listing 1: Prompt Template for "Propose" Agent

```
You are an automated assistant for proposing linear terms for the equations in a symbolic regression pipeline.

Your proposed terms will be:
1. Concatenated with the current candidate terms.
2. Sent to a LLM term pruner agent that will use various computed signals to decide which terms to keep and
     which to drop.

# Instructions:
Given below information, propose some candidate terms. The terms can be any valid numpy expressions.
Make use of the dataset and problem description to propose relevant terms.
Make sure to use the learnings from the history of previous rounds.

Return these between triple backticks and one term on each line.
The first backticks must be prepended with TERMS

Example output:

TERMS
```
x1
x2**2
np.sin(x3)
```

NOTES:
* Propose around {terms_per_round} terms, generally not too many unless this is the first round.
* If this *is* the first round, propose around {first_round_n_candidates} terms.
* You may propose no terms (nothing between the TERMS backticks) if you think it is appropriate.

DATASET AND PROBLEM DESCRIPTION
------------------------------
{dataset_and_problem_description}

CURRENT TERMS:
------------------------------
{current_terms}

# Current equation:
{current_equation}

HISTORY
------------------------------
{history}

=========
The input data and target variable(s) preview:
{input_preview}
```

The prompt template for the "Propose" agent dynamically incorporates several pieces of information. Key placeholders include:

`terms_per_round`: Hyperparameter specifying how many new basis functions the LLM should suggest in the current round. Default value: `5`.

`first_round_n_candidates`: Hyperparameter specifying how many new basis functions the LLM should suggest in the first round. Default value: `10`.

`dataset_and_problem_description`: Provides the LLM with context about the scientific problem and data, e.g.:

```
Prediction of Treatment Response for Combined Chemo- and Radiation-Therapy
for Non-Small Cell Lung Cancer Patients Using a Bio-Mathematical Model

Here you must model the state differential of **cancer_volume**, and **chemo_concentration**, which are **
     dv_dt** and **dc_dt**, driven by the input actions **chemo_dosage** and **radiotherapy_dosage**,
     together with relevant
laboratory and coagulation markers listed below.

Description of the variables
```

```
_____________________________
* cancer_volume          : Volume of the tumour (cm^3)
* chemo_concentration    : Plasma concentration of vinblastine (mg m^-3)
* chemo_dosage           : Administered vinblastine dose rate (mg m^-3 day^-1)
* radiotherapy_dosage    : Delivered external-beam RT dose rate (Gy day^-1)

Time unit: **days**

Typical value ranges
____________________
* cancer_volume        : 0.01433 - 1170.861 cm^3
* chemo_concentration  : 0 - 9.9975 mg m^-3
* chemo_dosage         : 0 - 5 mg m^-3 day^-1
* radiotherapy_dosage  : 0 - 2 Gy day^-1

Dataset summary
_______________
The training dataset consists of **1000** patients, each
followed for 60 days with daily resolution (delta_t = 1 day). Continuous variables are recorded once per day
      unless otherwise specified.
```

`current_terms`: Informs the LLM about terms already part of the active model in iterative steps, e.g.:

```
['cancer_volume', 'chemo_dosage', 'cancer_volume * chemo_concentration', 'cancer_volume * radiotherapy_dosage
      ', 'np.log(cancer_volume + 1)', 'np.sqrt(cancer_volume)']
```

`current_equation`: Shows the LLM the current best-performing model to potentially build upon or deviate from, e.g.:

```
dv_dt = 0.009194 cancer_volume - 0.0004414 chemo_dosage - 0.02797 cancer_volume * chemo_concentration -
      0.04775 cancer_volume * radiotherapy_dosage - 1.214 np.log(cancer_volume + 1) + 1.202 np.sqrt(
      cancer_volume)
dc_dt = - 0.004518 cancer_volume + 0.9776 chemo_dosage - 0.001191 cancer_volume * chemo_concentration - 3.691e
      -06 cancer_volume * radiotherapy_dosage - 1.442 np.log(cancer_volume + 1) + 0.5209 np.sqrt(cancer_volume
      )
```

`history`: Gives a history of terms decisions, and performance, enabling in-context learning, e.g.

```
Round node_0_0:  KEEP=['cancer_volume', 'cancer_volume * chemo_concentration', 'cancer_volume *
      radiotherapy_dosage', 'np.log(cancer_volume + 1)', 'np.sqrt(cancer_volume)', 'chemo_dosage']  |  DROP=['
      chemo_concentration', 'radiotherapy_dosage', 'chemo_dosage * radiotherapy_dosage', 'cancer_volume *
      chemo_dosage', 'cancer_volume * radiotherapy_dosage', 'np.log(cancer_volume + 1)', 'np.sqrt(
      cancer_volume)', 'radiotherapy_dosage']  |  MSE before pruning=0.005453 (per-output
      =[0.010905755578988435, 6.33977252002678e-27]) |  MSE after pruning=0.900026 (per-output
      =[0.011005448429060318, 1.789047395904737])
Round node_0_0_1: ...
```

Example LLM Response for "Propose" Agent: Below is an example response from the LLM acting as the "Propose" agent, based on the template above.

Listing 2: Example LLM Response from "Propose" Agent

```
TERMS
```
cancer_volume
chemo_concentration
chemo_dosage
radiotherapy_dosage
np.log(cancer_volume + 1)
np.sqrt(cancer_volume)
chemo_dosage * radiotherapy_dosage
cancer_volume * chemo_concentration
radiotherapy_dosage / (cancer_volume + 1)
chemo_dosage / (chemo_concentration + 1)
```
```

B.6.2 TERM PRUNING PHASE: THE "PRUNE" AGENT

After new terms are proposed and a model is fitted using the expanded set of basis functions, the "Prune" agent is invoked. This agent receives the full list of candidate terms, their fitted weights w_j, their per-term influence scores Δ_j (e.g., change in validation MSE if the term is removed), and the overall validation MSE. Its task is to decide which terms to keep or discard.

Prompt Template for "Prune" Agent: The following template illustrates the prompt given to the "Prune" agent.

Listing 3: Prompt Template for “Prune” Agent

```
You are an equation-pruning assistant for symbolic regression.

============================================================
INPUT YOU RECEIVE
============================================================

* A table (or dictionary/json representation) where each row has:

| field     | meaning                                                                          |
|-----------|----------------------------------------------------------------------------------|
| term      | Name of the symbolic basis function psi_k(x) (e.g. "x1", "sin(x2)", ...).  |
| weight    | Fitted scalar coefficient w_k obtained by ordinary least squares (OLS).    |
| influence | Influence score for term k (see definition below).                         |

* The validation set MSE.

**Influence definition (no refit)**

delta_k is the increase in mean-squared-error (MSE) if the k-th weight is deleted while all other weights stay
       fixed. For OLS this is

    delta_k = (w_k^2 / n) * sum phi_k(x_i)^2  (always >= 0).

* Note that the influence values are computed on the validation (rather than training) set, and thus may not
     always be >= 0.

Hence:
* If influence is large -> the term is important (its removal hurts the loss a lot).
* If influence ~= 0 -> the term is useless (its removal makes no noticeable difference).

============================================================
YOUR TASK
============================================================
1. **Inspect every row**.
2. **Decide "keep" or "drop"** for each term using the rule:

* Use the heuristic: "delta_k ~= 0 -> drop", "large delta_k -> keep" and your own judgement.

3. **Return** a python dictionary after "DECISION" with exactly the two keys

DECISION
```
{{
    "keep": ["term_a", "term_b", ...],
    "drop": ["term_c", "term_d", ...]
}}
````

Place each term name in either **keep** or **drop** - never both, never neither.

**IMPORTANT:**
* Make use of the dataset and problem description to make the best decision.
* Make sure to use the learnings from the history of previous rounds.
* (!) You must consider the generalization beyond the validation set and make decisions accordingly.
* (!) You should also consider BOTH the weights and the influence of the terms.
* (!) You MUST keep {keep_n_terms} terms at most, to keep the model interpretable.

------------------------------------------------------------
CONVENTIONS & NOTES
------------------------------------------------------------

# Important notes
* Treat terms independently; no need to refit or update weights.
* Note that everything was evaluated on the validation set to avoid overfitting.
* If there are multiple outputs (targets), you will see multiple tables, one for each target.
* Use all the information available, but keep in mind that you must only return one keep/drop decision even if
      there are multiple outputs.
* Keep only the most important terms for each output.

# Output format
* Feel free to comment briefly (<= 30 chars) about each decision, but keep the python dictionary in the right
     format.
* The dictionary MUST be provided between triple backticks, otherwise it cannot be parsed.
* It must be prepended with "DECISION", otherwise it cannot be parsed.

------------------------------------------------------------
EXAMPLE
------------------------------------------------------------
# INPUT TABLE(S):

y_1:
| term   | weight | influence |
| ------ | ------ | --------- |
| x1     | 3.00   | 12.21     |
| x2     | -1.96  | 5.14      |
| x1**2  | 0.53   | 0.91      |
| sin    | 0.93   | 0.52      |
| cos    | -0.05  | 0.0009    |

y_2:
```

```
| term   | weight | influence |
| ------ | ------ | --------- |
| x1     | 3.00   | 12.21     |
| x2     | -1.96  | 5.14      |

MSE (per-output): [0.217, 0.145]
MSE overall: 0.181

# Output:

DECISION
```
{{
    "keep": ["x1", "x2", "x1**2", "sin"],
    "drop": ["cos"]
}}
```

That's it - perform the keep/drop decision based on the information provided.


============================================================
DATASET AND PROBLEM DESCRIPTION
============================================================
{dataset_and_problem_description}


============================================================
CURRENT TERMS
============================================================
{current_terms}

# Current equation:
{current_equation}

============================================================
HISTORY
============================================================
{history}


============================================================
INPUT YOU RECEIVE
============================================================

INPUT TABLE(S):

{input}

MSE (per-output): [..., ...]
MSE overall: ...
```

The prompt template for the "Prune" agent is populated with the following key pieces of information to guide the pruning decision:

**`keep_n_terms`**: Hyperparameter specifying the maximum number of terms to keep. Default value: 6.

**`dataset_and_problem_description`**: Analogous to the "Propose" agent.

**`current_terms`**: Analogous to the "Propose" agent.

**`current_equation`**: Analogous to the "Propose" agent.

**`history`**: Analogous to the "Propose" agent.

**`input`**: This is a critical input, formatted as a table, showing each candidate basis function $\psi_j$, its fitted weight $w_j$, and its calculated influence score $\Delta_j$. For example:

```
INPUT TABLE(S):

dv_dt:
| term                                |       weight |     influence |
|:------------------------------------|-------------:|--------------:|
| cancer_volume                       |  0.0092651   |   2.7752      |
| chemo_concentration                 | -0.0035792   |   0.000354906 |
| chemo_dosage                        |  0.00120966  |   9.91133e-06 |
| radiotherapy_dosage                 |  0.00212704  |  -7.52432e-07 |
| cancer_volume * chemo_concentration | -0.027962    | 638.689       |
| cancer_volume * chemo_dosage        | -1.14907e-05 |   9.16085e-05 |
| cancer_volume * radiotherapy_dosage | -0.0477543   | 197.164       |
| chemo_dosage * radiotherapy_dosage  | -0.000750627 |   1.83055e-05 |
| np.log(cancer_volume + 1)           | -1.20511     |  17.425       |
| np.sqrt(cancer_volume)              |  1.19886     | 109.978       |

dc_dt:
| term                                |       weight |    influence |
```

```
|:-----------------------------------|-------------:|-------------:|
| cancer_volume                      |  4.8914e-16  | -5.36642e-27 |
| chemo_concentration                | -0.5         |  6.62719     |
| chemo_dosage                       |  1           | 10.8058      |
| radiotherapy_dosage                | -6.55278e-15 |  4.93846e-28 |
| cancer_volume * chemo_concentration |  1.86065e-17 | -1.98136e-27 |
| cancer_volume * chemo_dosage       | -8.391e-18   |  7.54011e-28 |
| cancer_volume * radiotherapy_dosage | -9.34055e-17 |  3.47305e-27 |
| chemo_dosage * radiotherapy_dosage | -1.90453e-16 |  3.39238e-29 |
| np.log(cancer_volume + 1)          |  5.50181e-16 | -2.14874e-28 |
| np.sqrt(cancer_volume)             | -2.09539e-16 |  2.65579e-28 |


MSE (per-output): [0.010905755578988435, 6.33977252002678e-27]
MSE overall: 0.005453
```

**Example LLM Response for "Prune" Agent:** An example of an LLM's response when acting as the "Prune" agent is shown below.

Listing 4: Example LLM Response from "Prune" Agent

```
To make the equation interpretable and preserve only the most meaningful terms, I will review the terms in
     both outputs (`dv_dt` and `dc_dt`) based on their influence and weight. I'll aim to retain at most 6
     terms.

---

### **Analysis for `dv_dt`:**
1. **Highly influential terms**:
    - `cancer_volume * chemo_concentration` (delta = 638.509) is critical.
    - `cancer_volume * radiotherapy_dosage` (delta = 197.209) is highly impactful.
    - `np.sqrt(cancer_volume)` (delta = 110.587) has substantial influence.
    - `np.log(1 + cancer_volume)` (delta = 17.6803).

2. **Moderately influential / less relevant**:
    - `cancer_volume` (delta = 2.7081): core variable, but delta suggests moderate importance.
    - `chemo_dosage`, `radiotherapy_dosage`: limited delta values.

3. **Negligible**:
    - Terms involving weighted interactions: e.g., `chemo_dosage / (1 + cancer_volume)` (delta ~= 0). These
         can be ignored safely.

---

### **Analysis for `dc_dt`:**
1. **Highly influential terms**:
    - `np.log(1 + cancer_volume)` (delta = 22.3107): critical.
    - `chemo_dosage` (delta = 18.8115): essential for modeling `dc_dt`.
    - `np.sqrt(cancer_volume)` (delta = 15.8203): quite significant.

2. **Moderately influential**:
    - `radiotherapy_dosage`: important as part of the model.
    - `cancer_volume`: relevant, but has relatively small delta compared to other terms.

3. **Negligible terms**:
    - Interactions like `radiotherapy_dosage / (1 + cancer_volume)` (small delta).

---

Considering both outputs, I aim to balance interpretability and prioritization based on influence across both
     equations. Here is the final decision:

---

DECISION
```
{
    "keep": [
    "cancer_volume * chemo_concentration",  # Very high delta for dv_dt
    "cancer_volume * radiotherapy_dosage",  # Very high delta for dv_dt
    "np.sqrt(cancer_volume)",               # Significant delta for both dv_dt and dc_dt
    "np.log(1 + cancer_volume)",            # Critical delta for both dv_dt and dc_dt
    "chemo_dosage",                         # Crucial delta for dc_dt
    "radiotherapy_dosage"                   # Balanced importance for dc_dt
    ],
    "drop": [
    "cancer_volume",                        # Moderate delta in both outputs
    "chemo_dosage * chemo_concentration",   # Insignificant in dv_dt (<0.0003)
    "radiotherapy_dosage * chemo_concentration",  # Similar to above
    "chemo_dosage / (1 + cancer_volume)",   # Negligible delta
    "radiotherapy_dosage / (1 + cancer_volume)"   # Negligible delta
    ]
}
```
```

# C Benchmark Dataset and Evaluation Details

Our evaluation utilizes several benchmark datasets, including three derived from a sophisticated biomedical Pharmacokinetic-Pharmacodynamic (PKPD) model, one from an epidemic simulator, one real-world clinical dataset, and one real-world biological dataset.

## C.1 Cancer PKPD Simulations

Three of our benchmark environments are based on a well-established biomedical Pharmacokinetic-Pharmacodynamic (PKPD) model of lung cancer tumor growth. This model simulates the combined effects of chemotherapy and radiotherapy and has been utilized in prior research (Geng et al., 2017; Seedat et al., 2022; Bica et al., 2020; Melnychuk et al., 2022; Holt et al., 2024b). We use this model to generate data for three distinct scenarios: **Lung Cancer** (no treatments), **Lung Cancer (with Chemo.)** (chemotherapy only), and **Lung Cancer (with Chemo. & Radio.)** (both chemotherapy and radiotherapy). Each scenario results in a separately sampled dataset. The comprehensive *Lung Cancer (with Chemo. & Radio.)* scenario, based on the general Cancer PKPD model, is described below, followed by how the other variations are derived.

**General Cancer PKPD Model Structure.** This model describes the tumor volume $x(t)$ (in $\text{cm}^3$) over time $t$ (in days) following diagnosis. It incorporates the effects of radiotherapy, $u_t^r$, and chemotherapy, $u_t^c$. The tumor dynamics are governed by the differential equation:

$$\frac{dx(t)}{dt} = \left(\rho \log\left(\frac{K}{x(t)}\right) - \beta_c C(t) - (\alpha_r d(t) + \beta_r d(t)^2)\right) x(t) \tag{1}$$

where the first term $\rho \log\left(\frac{K}{x(t)}\right)$ represents tumor growth dynamics, the term $\beta_c C(t)$ models the effect of chemotherapy, and $(\alpha_r d(t) + \beta_r d(t)^2)$ models the effect of radiotherapy. The patient-specific parameters $K, \rho, \beta_c, \alpha_r, \beta_r$ are adopted from Geng et al. (2017), and their values are summarized in Table 5.

Table 5: **Cancer PKPD model parameter values from Geng et al. (2017).**

| Model Component | Variable | Parameter Symbol | Value |
|---|---|---|---|
| Tumor Growth | Growth rate | $\rho$ | $7.00 \times 10^{-5}$ $\text{day}^{-1}$ |
| | Carrying capacity | $K$ | 30 $\text{cm}^3$ |
| Radiotherapy | Linear cell kill | $\alpha_r$ | 0.0398 $\text{Gy}^{-1}$ |
| | Quadratic cell kill | $\beta_r$ | Set such that $\alpha_r/\beta_r = 10$ Gy |
| Chemotherapy | Chemotherapy cell kill | $\beta_c$ | 0.028 $(\text{mg/m}^3)^{-1}$ $\text{day}^{-1}$ |

The concentration of the chemotherapy drug, $C(t)$, is modeled by an exponential decay with a one-day half-life:

$$\frac{dC(t)}{dt} = -0.5C(t)$$

A chemotherapy action $u_t^c$ corresponds to an increase in $C(t)$ by 5.0 $\text{mg/m}^3$ of Vinblastine administered at time $t$. The radiotherapy term $d(t)$ represents the daily dose, with $u_t^r$ corresponding to 2.0 Gy fractions of radiotherapy delivered at timestep $t$.

**Time-Dependent Confounding.** To introduce realistic complexities, the administration of chemotherapy and radiotherapy is modeled as Bernoulli random variables, with probabilities $p_c(t)$ and $p_r(t)$ dependent on the average tumor diameter $\bar{D}(t)$:

$$p_c(t) = \sigma\left(\frac{\gamma_c}{D_{\max}}(\bar{D}(t) - \delta_c)\right) \qquad p_r(t) = \sigma\left(\frac{\gamma_r}{D_{\max}}(\bar{D}(t) - \delta_r)\right) \tag{2}$$

where $\sigma(\cdot)$ is the sigmoid function, $D_{\max} = 13\,\text{cm}$ is the maximum tumor diameter, $\delta_c = \delta_r = D_{\max}/2$. The parameters $\gamma_c = \gamma_r = 2$ control the strength of this time-varying confounding.

**Dataset Generation.** For each of the three Cancer PKPD scenarios, we sample $N = 1,000$ patient trajectories. Initial tumor volumes $x(0)$ are drawn from a uniform distribution $\mathcal{U}(0, 1149)$ $\text{cm}^3$. Patient trajectories are simulated for 60 days using the PKPD model (Equation (1)) and the specified

action policy, employing a Euler stepwise numerical solver. This procedure generates one dataset sample. We create distinct training, validation, and test sets ($\mathcal{D}_{\text{train}}, \mathcal{D}_{\text{val}}, \mathcal{D}_{\text{test}}$) by repeating this sampling process with different random seeds. For each run of a benchmark method requiring a random seed, these datasets are re-sampled. The **Lung Cancer** scenario omits both treatment terms (effectively $C(t) = 0, d(t) = 0$). The **Lung Cancer (with Chemo.)** scenario omits the radiotherapy term only ($d(t) = 0$). The **Lung Cancer (with Chemo. & Radio.)** scenario uses the full model as described.

### C.2 COVID-19 Epidemic Simulation

We employ COVASIM, a detailed agent-based simulator for modeling COVID-19 epidemics (Kerr et al., 2021). COVASIM can simulate various non-pharmaceutical interventions (e.g., lockdowns, social distancing) and pharmaceutical interventions (e.g., vaccinations). In this model, each agent signifies an individual who can transition between states: susceptible, exposed, infectious, or recovered (which includes deaths).

We use COVASIM with its default parameters as provided in its open-source implementation[1]. To generate diverse epidemic trajectories, we simulate 24 distinct "countries" or populations. For each simulation, the population size is set to $1,000,000$ individuals, with each agent simulated individually (i.e., simulation rescaling is disabled). Each simulation starts with an initial number of infected individuals $I(0)$ sampled uniformly from $\mathcal{U}(10,000, 100,000)$, and the epidemic is simulated for 60 days.

This process is repeated with independent random seeds to generate training, validation, and test datasets ($\mathcal{D}_{\text{train}}, \mathcal{D}_{\text{val}}, \mathcal{D}_{\text{test}}$). For each benchmark method run that involves a random seed, these datasets are re-sampled.

### C.3 Warfarin Pharmacokinetics Dataset

We utilize a real-world clinical trial dataset focused on Warfarin pharmacokinetics (PK), which is publicly available (Janssen et al., 2022). This dataset, known as the NOMEN dataset, can be accessed from `https://github.com/Janssena/SI-AIEP-paper`. It comprises data from 32 patients who received a single dose of Warfarin. The dataset contains a total of 251 Warfarin concentration measurements, with a median of six measurements per patient. Warfarin was administered at $t = 0$, and concentration measurements were taken at predefined time points: $t \in \{0.25, 0.5, 1.0, 2.0, 4.0, 6.0, 12.0, 24.0, 48.0, 72.0, 96.0, 120.0\}$ hours. Covariates available for each patient include weight, age, and sex.

We adhere to the original pre-processing scripts provided with the dataset. The data is split into training, validation, and test sets using proportions of 70%, 15%, and 15%, respectively. These splits are performed chronologically to maintain temporal causality. This dataset is released under a GPL-3.0 license.

### C.4 RNA Polymerase II Pausing Dataset

This dataset, central to the case study presented in Section 5.1, focuses on predicting RNA Polymerase II (Pol II) pausing. It is derived from eNET-seq data that maps Pol II pause sites in human cells at single-nucleotide resolution (Fong et al., 2022). The primary objective is to predict the `pause_score`, a continuous variable between 0 and 1, where a higher score indicates increased Pol II pausing at a specific genomic location. The pause score is calculated as the ratio of sequencing reads at the pause site to the total reads in a 200bp window surrounding it.

The dataset comprises 263 features, including:

- **Genomic Coordinates and Context:** Features such as `start` (current position), `gene_start`, `gene_end`, `exon_intron_start`, `exon_intron_end`, distance to nearest downstream (`down_nuc_dist`) and upstream (`up_nuc_dist`) nucleosomes.
- **Chromatin Features:**

[1] COVASIM is available at `https://github.com/InstituteforDiseaseModeling/covasim`.

  - Nucleosome occupancy signal from MNase-seq (e.g., `SIGNAL_MNase_CONDITION_WT`).
  - Histone modification signals from ChIP-seq, such as H3K4me3 (e.g., `SIGNAL_ChIPseqH3K4me3_CONDITION_CDK7negWT`, where higher signal implies more H3K4me3 modification) and H3K36me3 under various conditions (e.g., `SIGNAL_ChIPseqH3K36me3_CONDITION_negU170K`, `SIGNAL_ChIPseqH3K36me3_CONDITION_posU170K`, where higher signal indicates more H3K36me3 modification).
- **RNA Structure Features:** DMS signal (e.g., `SIGNAL_DMS_CONDITION_WT_STRAND_neg`, where lower signal implies more RNA structure) and RNA structure scores (e.g., `SIGNAL_StructureScore_CONDITION_WT_STRAND_neg`, where higher score indicates more structure).
- **DNA Sequence Context:** One-hot encoded nucleotides at positions -20 to +20 relative to the potential pause site (e.g., `seq_neg1__A`, `seq_0__G`, `seq_1__T`). Possible nucleotide categories are `A`, `C`, `G`, `T`, and `N` (unknown).
- **Gene Region Annotations:** Categorical features like `chrom__<category>` (chromosome, e.g., `chr1`, `chrX`), `strand__<category>` (`pos` or `neg`), `gene_region__<category>` (one of `TSS`, `body`, `termination`), and `exon_intron__<category>` (one of `exon`, `intron`, `missing`). Categorical columns are one-hot encoded, with column names in the format `<column_name>__<category>`.

The target variable is `pause_score`. The dataset used for the experiments described in Section 5.1 was balanced, containing approximately 48,000 pause sites and a similar number of control sites (where pause score = 0), and was split into training, validation, and test sets. For each benchmark method run involving a random seed, this training/validation/test split was resampled.

### C.5 Benchmark Method Details

Our comparative evaluation includes several established benchmark methods to contextualize the performance of SGED. These methods span both black-box and white-box modeling paradigms.

#### C.5.1 White-box non-LLM baselines

**DyNODE** (Dynamical Neural Ordinary Differential Equations) is a method that learns the underlying dynamics of a system from observed data by parameterizing the derivative function of an ordinary differential equation (ODE) with a neural network (Chen et al., 2018). For systems involving external actions or interventions, the DyNODE framework can be extended to incorporate these action inputs directly into the learned dynamics, allowing it to model how treatments or other external factors influence the system's evolution over time (Alvarez et al., 2020). This approach offers a flexible black-box model for continuous-time dynamical systems.

**SINDy** (Sparse Identification of Nonlinear Dynamics) is a white-box method designed to discover governing differential equations directly from time-series data (Brunton et al., 2016). It operates by constructing a library of candidate nonlinear functions of the state variables and then employs sparse regression techniques (typically sequentially thresholded least-squares or Lasso) to identify a minimal set of active terms that best describe the observed dynamics. The result is an interpretable, parsimonious differential equation model.

**GPLearn** (Stephens, 2015) is a genetic programming approach for symbolic regression that algorithmically discovers mathematical expressions to model a given dataset. It works by evolving a population of candidate equations over a number of generations, applying genetic operators such as crossover and mutation to iteratively refine solutions based on a fitness metric, typically related to prediction accuracy. In the experiments, unless stated otherwise, GPLearn was configured with a `population_size` of 1000, run for 30 `generations`, and a `parsimony_coefficient` of 1.0. The `parsimony_coefficient` of 1.0 was selected to apply a considerable penalty to the complexity of the evolved expressions. This encourages the discovery of more concise equations, which aligns with the general aim of finding parsimonious models (e.g., around six terms in the primary SGED experiments), thus making shorter programs preferable during the evolutionary search.

### C.5.2 WHITE-BOX LLM BASELINES

To ensure fair comparison, we set the maximum number of terms allowed to be six (unless otherwise stated) in SGED, and ensured this was comparably set in all other corresponding methods. We use the same underlying LLM across all LLM-based methods (`GPT-4o` version `2024-11-20`, unless otherwise stated).

**ZeroShot** represents a baseline LLM-driven approach where the Large Language Model is prompted to generate a symbolic equation model in a single pass, based solely on the provided problem description and dataset characteristics. This method does not involve any iterative refinement or feedback based on the model's performance on actual data. Consequently, the parameters of the equation generated by the ZeroShot method are used as proposed by the LLM without any subsequent optimization against the training dataset. The number of terms in the equation generated by the LLM was constrained via prompting, typically to a maximum of six terms (unless stated otherwise), to align with the parsimony goals of SGED.

**ZeroOptim** builds directly upon the ZeroShot approach. An LLM first generates an initial symbolic equation model in a zero-shot manner, based on the problem description. However, unlike the pure ZeroShot baseline, the structural form of this LLM-proposed equation is then taken, and its constituent parameters (weights $w_j$) are subsequently optimized by fitting them to the training data. This optimization process is performed analogously to the final model fitting stage within the SGED framework, aiming to find the best parameter values for the LLM's proposed equation structure. As with ZeroShot, the LLM was prompted to generate equations with a limited number of terms, typically up to six (unless stated otherwise), for comparability.

**ICL - Basic Feedback** is an LLM-based iterative equation discovery method that serves as a key ablation and comparator to SGED. In this approach, the LLM iteratively proposes candidate equations (or modifications to existing ones). After each proposal, the equation's parameters are optimized analogously to SGED, and its performance is evaluated, typically yielding a scalar metric such as the overall Mean Squared Error (MSE) on a validation set. This scalar MSE, along with a history of previously attempted equations and their outcomes, is now provided back to the LLM to guide its proposal for the next iteration, facilitating in-context learning. Crucially, ICL - Basic Feedback lacks the granular, per-term influence scores ($\Delta_j$) that are central to SGED. Furthermore, it does not incorporate SGED's dedicated term pruning phase, where an LLM agent refines the equation structure based on these influence scores. For fair comparison with SGED, the maximum number of terms in the equations generated by the LLM was limited via prompting, with a default of six terms in the experiments unless specified otherwise.

**D3-white-box** (Holt et al., 2024b) refers to the Data-Driven Discovery framework when specifically configured to discover interpretable, white-box dynamical system models. This approach leverages Large Language Models (LLMs) within an iterative cycle involving three core agents: Modeling, Feature Acquisition, and Evaluation. For white-box discovery, the Modeling Agent is tasked by the LLM to propose and refine closed-form equation models. These equations are represented as executable Python code, typically PyTorch modules. After a model is proposed, its parameters are optimized against training data. The Evaluation Agent then assesses the model, providing feedback that includes quantitative metrics like validation Mean Squared Error (MSE) and qualitative verbal reflections on model structure and plausibility. This feedback informs the LLM for subsequent iterations of model generation and refinement. The Feature Acquisition Agent can also propose additional relevant features to incorporate, further guiding the discovery process, although for specific benchmark comparisons, it might be applied to a fixed set of predefined features. The overall D3 framework aims to autonomously navigate the model space, identify relevant system variables, and converge on accurate, interpretable equations. The implementation details and hyperparameters as per (Holt et al., 2024b) were used for this benchmark. The maximum number of input features in the white-box model was constrained via prompting, with a default of six, unless specified otherwise.

**LaSR** (Symbolic Regression with a Learned Concept Library, Grayeli et al., 2024) is a framework that enhances traditional genetic algorithms for symbolic regression by incorporating a learned library of abstract textual concepts. It uses an LLM to discover and evolve high-level concepts (e.g., "exponential decay") from successful equations. These concepts then guide the mutation and crossover operations in the search, biasing it towards scientifically plausible structures rather than refining the equations directly. The complexity hyperparameter `maxsize` of 30 was used to allow

for equations at least as complex as the six-term limit used elsewhere. The total number of cycles was set to 75. Other hyperparameters used were as per Grayeli et al. (2024).

**LLM-SR** (Scientific Equation Discovery via Programming with Large Language Models, Shojaee et al., 2025) frames equation discovery as program synthesis. It leverages an LLM's scientific prior knowledge and code generation capabilities to propose equation skeletons as Python programs. These programs are then combined with an evolutionary search, where data-driven feedback on the overall program's fit is used to guide the iterative refinement process. The complexity hyperparameter `max_nparams` was set to 8, in excess of SGED's six term limit. The rest of the hyperparameters were used as per Shojaee et al. (2025).

**ICSR** (In-Context Symbolic Regression, Merler et al., 2024) employs an LLM as an optimizer within an iterative refinement loop. The LLM is prompted with a set of previously evaluated equations and their corresponding scalar fitness scores (which typically combine accuracy and a complexity penalty). Through in-context learning, the LLM is tasked with generating a new candidate equation that is expected to achieve a better score, effectively navigating the solution space based on a history of successes and failures. The hyperparameter from Merler et al. (2024) were used, and `max_nodes` complexity parameter was set to 30 to allow for equations at least as complex as the six-term limit used in SGED and elsewhere.

### C.5.3 Black-box baselines

**RNN** (Recurrent Neural Network) models are a class of neural networks well-suited for sequential data, including time-series (Rumelhart et al., 1986). Standard RNN architectures, such as those using LSTM (Long Short-Term Memory) (Hochreiter & Schmidhuber, 1997) or GRU (Gated Recurrent Unit) (Cho et al., 2014) cells, maintain an internal hidden state that captures information from past inputs, enabling them to model temporal dependencies. For prediction tasks, the RNN processes input sequences (e.g., trajectories of state variables and actions) to predict future states or system outputs. These are generally considered black-box models due to the complexity of their internal representations.

**Transformer** models, originally introduced for natural language processing tasks (Vaswani et al., 2017), have demonstrated strong performance on a wide variety of sequential data, including time-series. The core mechanism of Transformers is the attention mechanism, particularly self-attention, which allows the model to weigh the importance of different elements in the input sequence when making predictions. This enables them to capture long-range dependencies effectively. Like RNNs, Transformer models are typically considered black-box due to their intricate architectures and large number of parameters.

## C.6 Evaluation Details

We assess the performance of all benchmark methods using the mean squared error (MSE) on a held-out test dataset, denoted as $\mathcal{D}_{\text{test}}$. The MSE is calculated based on the model's predictions against the true target values in this test set. Where there are multiple target variables, the mean MSE across all targets is used.

For each method, given per-seed test MSEs $x_1, \ldots, x_n$, we report two-sided 95% confidence intervals for the mean across seeds as $\bar{x} \pm t_{0.975,n-1}\,\frac{s}{\sqrt{n}}$, where $\bar{x}$ is the sample mean, $s$ is the unbiased sample standard deviation, and $t_{0.975,n-1}$ is the Student's $t$ critical value (see, e.g., Wasserman, 2004). Replicates are independent training runs (random seeds). We use the appropriate degrees of freedom for each method's $n$.

When a simulator is used to generate data (e.g., for the Cancer PKPD and COVID-19 benchmarks as described in Appendix C), new training, validation, and test datasets ($\mathcal{D}_{\text{train}}, \mathcal{D}_{\text{val}}, \mathcal{D}_{\text{test}}$) are independently generated for each random seed. Unless specified otherwise, the validation and test datasets are generated to contain a comparable number of samples or trajectories as the training set.

Each benchmark model is trained using its respective training dataset ($\mathcal{D}_{\text{train}}$). For methods that support it, early stopping (at patience 10) or default model selection heuristics are applied using the validation dataset ($\mathcal{D}_{\text{val}}$) to prevent overfitting and guide the learning process. For SGED, the validation set is critically used for calculating per-term influence scores and guiding the pruning

decisions, as detailed in Section 2. Maximum number of iterations or generations is set to 30 for all methods where this is applicable unless stated otherwise; SGED maximum node expansion budget for MCST is similarly set set to 30. For a complementary experiment comparing methods at a fixed computational (LLM token) budget, see Appendix G.3. The final reported performance for all methods is evaluated on the unseen test dataset ($\mathcal{D}_{\text{test}}$). This entire procedure of data generation (if applicable), training, validation-guided refinement (if applicable), and testing is repeated for each random seed to ensure robust and reliable comparisons. We use 25 random seeds for SGED results and other LLM-based method results, using the same underlying LLM. Given the evaluation is exactly the same as the baseline and datasets for some results of the baselines, we use previous values averaged over 10 random seeds for the non-LLM baselines from paper Holt et al. (2024b).

# D RNA Polymerase II Pausing Case Study – Further Discussion

In this section, we provide SHAP plots for the case study experiment (referred to as **Experiment 1** here), an additional experiment (referred to as **Experiment 2** here) conducted to further investigate the use of SGED with the RNA Polymerase II pausing problem, and a discussion given both sets of results. The aim is to illustrate how SGED can be used in scientific discovery and hypothesis generation process (e.g. note the extension to Experiment 2 from Experiment 1, given the results of the former). This case study is one of many potential use cases for SGED, illustrating the potential power of this method.

## D.1 Experiment 1 SHAP Plots

To further interrogate the interpretable equation discovered by SGED for RNA Polymerase II pausing (presented in Section 5.1), $f(\mathbf{x}) = \sum_j w_j \psi_j(\mathbf{x})$, we employed SHapley Additive exPlanations (SHAP) (Lundberg & Lee, 2017). SHAP is a game theoretic approach that explains the output of a model by assigning an importance value (SHAP value) to each of its input features for every individual prediction. In this application, the "features" provided to SHAP are the evaluated basis functions $\psi_j(\mathbf{x})$ that form the terms of the SGED equation. The SHAP values therefore quantify how much each term $w_j \psi_j(\mathbf{x})$ contributes to pushing the model's output (the pause score) from its base (average) prediction to the actual predicted value for a given sample. This analysis allows us to visualize the magnitude, variability, and directional impact of each constituent term in the discovered equation.

While the SGED equation $f(\mathbf{x}) = \sum_j w_j \psi_j(\mathbf{x})$ is already structured for interpretability as a weighted sum of basis functions, SHAP analysis provides a standardized framework to:

- Visualize the distribution of contributions for each basis function term $\psi_j(\mathbf{x})$ across all samples.
- Understand how the specific value of a basis function $\psi_j(\mathbf{x})$ (which itself is derived from the original input features like $\text{signal}_{\text{MNase}}$ or sequence indicators) influences its contribution to the final pause score.
- Confirm the relative importance and consistent impact of terms that were selected and weighted during the SGED discovery process.

Essentially, SHAP helps to decompose the prediction into contributions from each $\psi_j(\mathbf{x})$ term, providing insights at both a global (overall term importance) and local (individual prediction explanation) level.

We generated two types of SHAP plots to visualize these explanations, as shown in Figure 3: a beeswarm plot and a custom term influence bar plot.

The **beeswarm plot** (Figure 3a) summarizes the SHAP values for the most influential basis function terms $\psi_j(\mathbf{x})$ in the equation. Each point on the plot represents a single term's SHAP value for a specific sample (a potential pause site). The terms are ranked along the y-axis by their global importance (sum of absolute SHAP values across all samples). The x-axis shows the SHAP value, indicating the term's impact on the model output; positive SHAP values contribute to a higher predicted pause score, while negative values contribute to a lower score. The color of each point corresponds to the *value of the basis function* $\psi_j(\mathbf{x})$ for that sample (typically, red indicates high

values of $\psi_j(\mathbf{x})$ and blue indicates low values). This coloring reveals how the magnitude of each basis function's evaluation influences its contribution to the pause score.

The **custom term influence bar plot** (Figure 3b) provides an alternative view of global term importance and the general direction of each term's influence. The length of each bar corresponds to the mean absolute SHAP value for that basis function term $\psi_j(\mathbf{x})$, signifying its overall importance in the equation. The color and direction of the bar indicate the predominant direction of the term's influence on the pause score. This directionality is determined by calculating the Spearman's rank correlation coefficient ($\rho$) between the *values of the basis function* $\psi_j(\mathbf{x})$ for each sample and their corresponding SHAP values for that term. Spearman's correlation is employed here because:

- It assesses monotonic relationships. The SHAP value of a term $w_j\psi_j(\mathbf{x})$ will have a monotonic relationship with $\psi_j(\mathbf{x})$ (the direction determined by the sign of $w_j$). Spearman captures this robustly.
- It is robust to outliers in the evaluated basis function values or the SHAP values.
- It operates on the ranks of the data, suitable even if distributions are non-normal.

A positive Spearman correlation (typically shown in red, extending to the right) suggests that as the value of the basis function $\psi_j(\mathbf{x})$ increases, its SHAP value (and thus its effective contribution $w_j\psi_j(\mathbf{x})$ relative to its mean) tends to push the predicted pause score higher. Conversely, a negative correlation (typically shown in blue, extending to the left) suggests that an increasing value of $\psi_j(\mathbf{x})$ tends to push the pause score lower. This plot helps to quickly identify which terms in the SGED-discovered equation are most impactful and whether higher values of these terms generally promote or inhibit Pol II pausing.

### D.2 Experiment 2 and Discussion

**Experimental Setup.** Experiment 1 (discussed in Section 5.1) tasked SGED with predicting pause sites from an artificially balanced dataset comprising equal numbers of actual pause sites and control non-pause sites within genes. While this approach identified key features distinguishing pause sites from non-pause regions, a limitation is that pause sites are naturally much less frequent than non-pause sites. Furthermore, this setup primarily addresses the *presence* of a pause rather than the *strength* or characteristics of different pause sites relative to each other.

To delve deeper into the factors modulating the intensity of Pol II pausing, Experiment 2 adopted a different approach. Here, SGED was tasked with identifying terms that distinguish pause sites based on their varying pause scores, using a dataset consisting exclusively of identified pause sites (i.e., non-pause sites were excluded). This focuses the analysis on understanding what makes some pauses stronger or weaker than others, given that a pause event is already occurring. This also addresses any potential confounding effects of artifical balancing between pause and non-pause sites in Experiment 1.

**Results.** The equation discovered by SGED in this context is presented below.

$$
\begin{aligned}
\text{pause\_score} \;=\; & -0.01711\,\ln(1+\text{signal}_{\text{MNase}}) \\
& -0.0003407\,\text{signal}_{\text{H3K4me3}} \\
& -0.00216\,\ln(2+\text{signal}_{\text{H3K4me3}}) \\
& -0.0005086\sum_{\text{cond}}\text{signal}_{\text{H3K36me3, cond}} \\
& +0.01206\,\ln(1+\text{gene\_length}) \\
& -0.08414\,\mathbb{1}_{\{\text{gene\_region}=\text{TSS}\}} \\
& +0.0003421\,\mathbb{1}_{\{\text{gene\_region}=\text{TSS}\}}\cdot\text{signal}_{\text{H3K4me3}} \\
& +0.02143\,\mathbb{1}_{\{\text{seq}_0=G\}} \\
& +0.0006817\,\ln(1+\text{down\_nuc\_dist}) \\
& +0.01968\,\ln(1+\text{down\_nuc\_dist}+|\text{up\_nuc\_dist}|) \\
& +0.0001679\left(\text{signal}_{\text{H3K4me3}}-\sum_{\text{cond}}\text{signal}_{\text{H3K36me3, cond}}\right) \\
& -0.01338\left(\ln(2+\text{signal}_{\text{H3K4me3}})-\ln\left(2+\sum_{\text{cond}}\text{signal}_{\text{H3K36me3, cond}}\right)\right) \\
& +0.009823\,\mathbb{1}_{\{\text{seq}_{-1}=G\}} \\
& +0.01422\left(\mathbb{1}_{\{\text{seq}_0=G\}}\cdot\mathbb{1}_{\{\text{seq}_1=T\}}\right)
\end{aligned}
$$

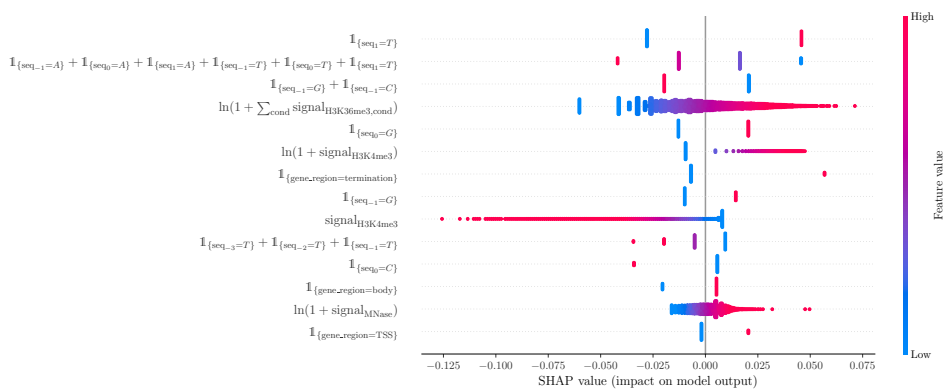


(a) SHAP Beeswarm Plot for Equation Terms

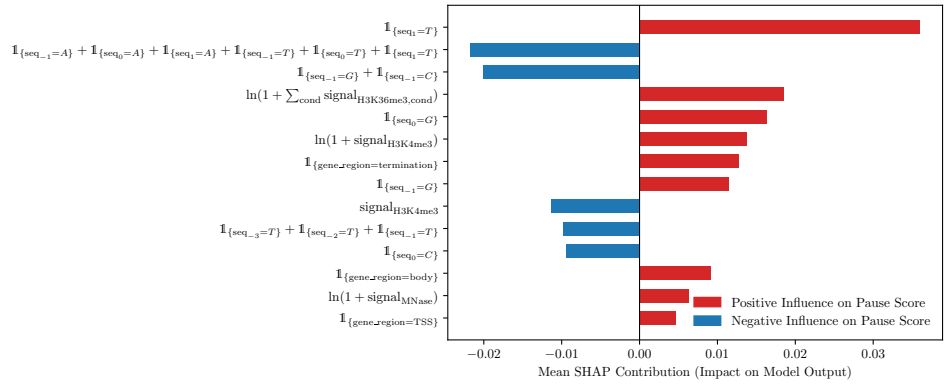


(b) SHAP Term Influence Bar Plot

Figure 3: SHAP analysis of the SGED-discovered equation for RNA Polymerase II pausing from **Experiment 1**. Each "feature" in the SHAP analysis corresponds to a basis function term $\psi_j(\mathbf{x})$ from the equation. (**a**) Beeswarm plot showing the distribution of SHAP values for the most important equation terms. Each point is a SHAP value for a term and a sample, colored by the value of the evaluated basis function $\psi_j(\mathbf{x})$ (red for high, blue for low). (**b**) Custom bar plot illustrating global term importance (mean absolute SHAP value) and the direction of influence. Red bars indicate a general positive correlation between the value of $\psi_j(\mathbf{x})$ and its contribution to the pause score (Spearman's $\rho > 0$), while blue bars indicate a negative correlation (Spearman's $\rho < 0$).

$$-0.01761\left(\mathbb{1}_{\{\text{seq}_{-1}=G\}} + \mathbb{1}_{\{\text{seq}_{-1}=C\}} + \mathbb{1}_{\{\text{seq}_0=G\}} + \mathbb{1}_{\{\text{seq}_0=C\}} + \mathbb{1}_{\{\text{seq}_1=G\}} + \mathbb{1}_{\{\text{seq}_1=C\}}\right),$$

The SHAP analysis for this equation (Figure 4) illustrates the relative effects of these different terms on the predicted pause score.

**Discussion.** Combining insights from both Experiment 1 and Experiment 2, SGED has revealed several features of potential functional importance to transcriptional pausing in human cells. A notable result emerging from this comparative analysis is that high H3K4me3 signal is generally associated with reduced pausing (i.e., lower pause scores in Experiment 2), consistent with a proposed a link between this mark and faster transcription (Wang et al., 2023). Regarding H3K36me3, Experiment 1 indicated its role as a significant predictor for the *presence* of pause sites. However, Experiment 2 suggests that higher levels of H3K36me3 are negatively related to the *strength* of these pause sites (lower pause scores), a finding that aligns with some genetic studies (Lee et al., 2024; Wen et al., 2014). Furthermore, SGED's discovered equations highlight the importance of the relative levels of these two histone marks. Specifically, terms reflecting a high ratio of H3K36me3 to H3K4me3 (e.g., through difference terms like $\text{signal}_{\text{H3K4me3}} - \sum \text{signal}_{\text{H3K36me3, cond}}$ with a positive coefficient,

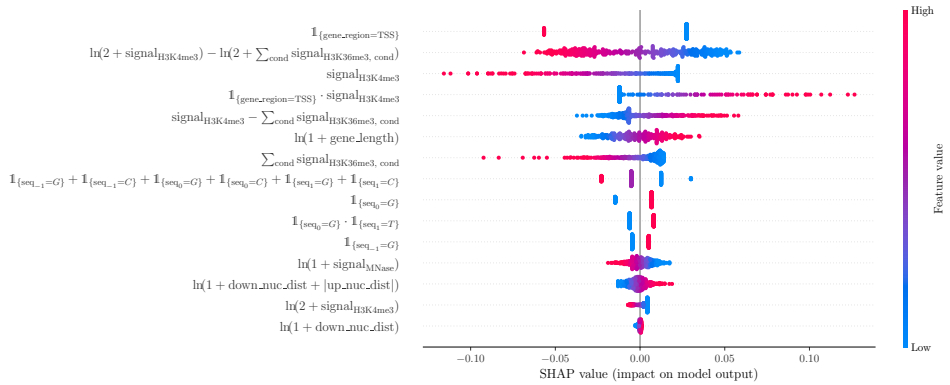


(a) SHAP Beeswarm Plot for Equation Terms

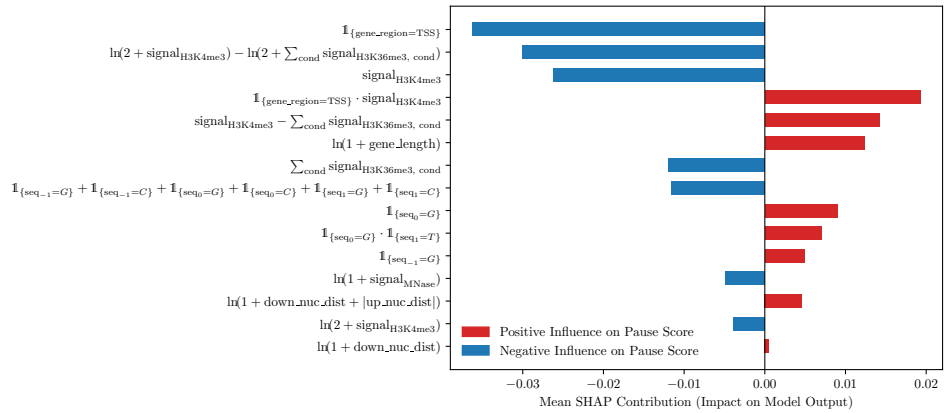


(b) SHAP Term Influence Bar Plot

Figure 4: SHAP analysis of the SGED-discovered equation for RNA Polymerase II pausing from **Experiment 2**. Analogous to Figure 3, but for **Experiment 2**.

or ratio-like terms in logarithmic form) are associated with higher pause scores, whereas a high H3K4me3 to H3K36me3 ratio appears linked to lower pause scores.

The analysis also found that the region downstream of genes (termination region) is associated with higher pausing scores relative to the gene body and the 5' end (TSS). This is consistent with the hypothesis that Pol II pausing plays a role in facilitating transcription termination (Gromak et al., 2006).

This work also refined our understanding of sequence specificity in pausing. Previous studies identified a G, T/C sequence element as enriched at the pause site (position 0) and the +1 position (Fong et al., 2022; Gajos et al., 2021). Our SGED models confirm that T at position +1 (often as part of a $G_0$–$T_{+1}$ motif) is a strong positive predictor for pause sites. Conversely, the models from both experiments, particularly when examining factors that disfavor pausing or reduce pause strength, identified new elements: C at position 0 and -1, and T at positions -1, -2, and -3 appear to disfavor pausing. Additionally, a cluster of G/C nucleotides at positions -1, 0, and +1 (captured by terms like $-(\mathbb{1}_{\{\text{seq}_{-1}=G\}} + \cdots + \mathbb{1}_{\{\text{seq}_1=C\}})$) was also found to be associated with reduced pausing or lower pause scores.

These results, derived from the interpretable equations generated by SGED, provide new, data-driven hypotheses that will help guide future experimental studies into the complex mechanisms of sequence-dependent transcriptional pausing and its regulation by the chromatin environment.

# E Additional Results

## E.1 Impact of Influence Feedback with MCTS

To further delineate the benefits of the per-term influence feedback mechanism, we conducted an additional comparative analysis focusing on scenarios where Monte Carlo Tree Search (MCTS) is employed as the overarching search strategy. In this setup, we compared SGED equipped with its full influence-based feedback against a variant that also uses MCTS but relies only on basic Mean Squared Error (MSE) for its pruning decisions (akin to the "MCTS + Basic Feedback" ablation in Table 4).

This comparison is particularly insightful as it highlights the value of granular feedback even when a powerful search algorithm like MCTS is exploring the equation space. While MCTS inherently provides a robust exploration framework, the detailed influence scores offer more directed guidance to the LLM agent during the pruning phase within each node expansion of the MCTS. This allows the search to more rapidly identify and prioritize promising branches in the search tree.

Figure 5 illustrates the expected convergence behavior in this MCTS context. The x-axis represents the number of nodes expanded in the MCTS, providing a measure of computational effort in the search process. As shown, SGED with full influence-based feedback converges more quickly to lower MSE values than the MCTS variant relying solely on basic feedback. This accelerated convergence underscores the efficiency gains afforded by providing the LLM with detailed, interpretable information about the contributions of individual equation components, even within a sophisticated tree search paradigm.

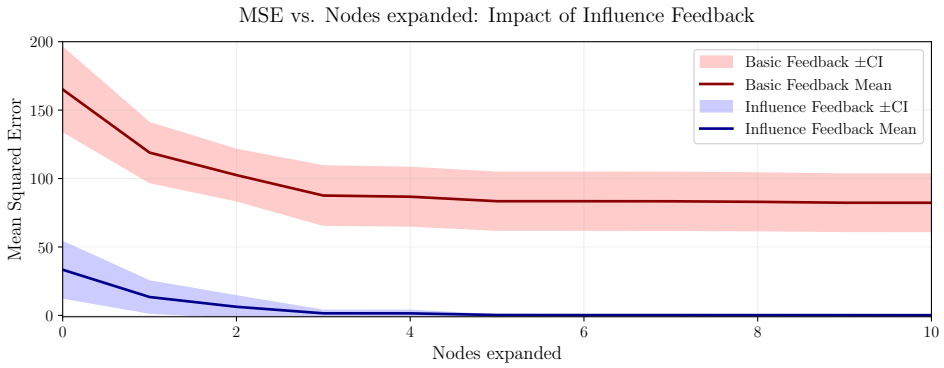


Figure 5: **MSE vs. Nodes Expanded (MCTS): Impact of Influence Feedback.** Plot showing validation MSE convergence as a function of MCTS nodes expanded. Compares SGED with full influence-based feedback against an MCTS variant using only basic MSE feedback on the Lung Cancer (with Chemo. & Radio.) dataset. Shaded regions denote 95% confidence intervals, and solid lines show means. Detailed influence feedback leads to faster convergence (fewer nodes expanded to reach a given MSE) and a lower final MSE within a given computational budget.

Both Figure 2 and Figure 5 are based on 25 seed runs for the Lung Cancer (with Chemo. & Radio.) dataset. In both figures, the best test MSE achieved so far as of # iteration or # node expansion is tracked.

## E.2 Illustration of SGED Equation Discovery

To provide a more concrete understanding of how SGED discovers and refines equations, this section illustrates the process using two example runs (Run A and Run B) on the Lung Cancer (with Chemo. & Radio.) benchmark dataset. Figure 6 depicts the progression of the best Mean Squared Error (MSE) achieved on the test set as the Monte Carlo Tree Search (MCTS) expands more nodes. Each significant drop in MSE, indicating the discovery of a more accurate equation, is annotated on the plot (e.g., A0, B9). Below, we present the specific equations and their corresponding MSEs at these key points, showcasing the iterative improvements made by SGED. This visualization highlights how the framework navigates the equation space, modifying and selecting terms to progressively enhance model performance.

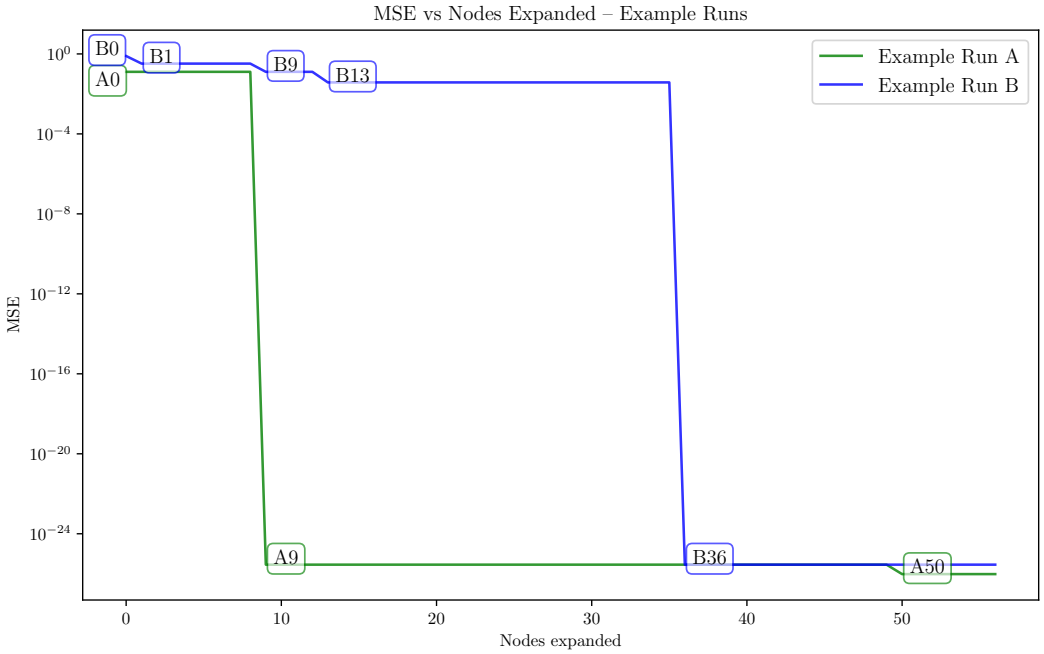


Figure 6: **Illustration of SGED Equation Discovery Process.** Test MSE achieved versus MCTS nodes expanded for two example SGED runs (Run A: green, Run B: blue) on the Lung Cancer (with Chemo. & Radio.) dataset. Points A0, A9, A50 for Run A, and B0, B1, B9, B13, B36 for Run B, indicate instances where a new, more accurate equation was discovered. The equations corresponding to these points are detailed below.

The equations discovered at pivotal moments during these SGED runs are as follows:

### Example Run A

- **Point A0** (Node 0):
  - MSE: $0.127$
  - Equations:

$$\begin{aligned}\text{dv\_dt} = {} & 0.02425 \cdot \text{cancer\_volume} - 0.08865 \cdot \text{chemo\_concentration} \\ & - 0.03812 \cdot \text{chemo\_dosage} \\ & - 0.02755 \cdot \text{cancer\_volume} \cdot \text{chemo\_concentration} \\ & - 0.04786 \cdot \text{cancer\_volume} \cdot \text{radiotherapy\_dosage} \\ & + 0.4913 \sqrt{\text{cancer\_volume}} \\ \text{dc\_dt} = {} & -0.5 \cdot \text{chemo\_concentration} + \text{chemo\_dosage}\end{aligned}$$

- **Point A9** (Node 9):
  - MSE: $2.85 \times 10^{-26}$
  - Equations:

$$\begin{aligned}\text{dv\_dt} = {} & 0.1389 \cdot \text{cancer\_volume} \\ & - 0.028 \cdot \text{cancer\_volume} \cdot \text{chemo\_concentration} \\ & - 0.04776 \cdot \text{cancer\_volume} \cdot \text{radiotherapy\_dosage} \\ & - 0.01453 \cdot \text{cancer\_volume} \cdot \ln(\text{cancer\_volume}) \\ \text{dc\_dt} = {} & -0.5 \cdot \text{chemo\_concentration} + \text{chemo\_dosage}\end{aligned}$$

- **Point A50** (Node 50):
  - MSE: $9.59 \times 10^{-27}$
  - Equations:

$$\begin{aligned}\text{dv\_dt} = {} & 0.1389 \cdot \text{cancer\_volume} \\ & - 0.028 \cdot \text{cancer\_volume} \cdot \text{chemo\_concentration} \\ & - 0.01453 \cdot \text{cancer\_volume} \cdot \ln(\text{cancer\_volume}) \\ & - 0.02388 \cdot \text{cancer\_volume} \cdot (\text{radiotherapy\_dosage})^2 \\ \text{dc\_dt} = {} & -0.5 \cdot \text{chemo\_concentration} + \text{chemo\_dosage}\end{aligned}$$

### EXAMPLE RUN B

- **Point B0** (Node 0):
  - MSE: $0.785$
  - Equations:

$$\begin{aligned}\text{dv\_dt} = {} & 0.04326 \cdot \text{cancer\_volume} + 0.1558 \cdot \text{chemo\_concentration} \\ & + 0.1157 \cdot \text{chemo\_dosage} \\ & - 0.02769 \cdot \text{cancer\_volume} \cdot \text{chemo\_concentration} \\ & - 0.04836 \cdot \text{cancer\_volume} \cdot \text{radiotherapy\_dosage} \\ \text{dc\_dt} = {} & -0.5 \cdot \text{chemo\_concentration} + \text{chemo\_dosage}\end{aligned}$$

- **Point B1** (Node 1):
  - MSE: $0.328$
  - Equations:

$$\begin{aligned}\text{dv\_dt} = {} & 0.03643 \cdot \text{cancer\_volume} - 0.08611 \cdot \text{chemo\_concentration} \\ & - 0.02803 \cdot \text{chemo\_dosage} \\ & - 0.02736 \cdot \text{cancer\_volume} \cdot \text{chemo\_concentration} \\ & - 0.04801 \cdot \text{cancer\_volume} \cdot \text{radiotherapy\_dosage} \\ & + 0.6666 \ln(\text{cancer\_volume} + 1) \\ \text{dc\_dt} = {} & -0.5 \cdot \text{chemo\_concentration} + \text{chemo\_dosage}\end{aligned}$$

- **Point B9** (Node 9):
  - MSE: $0.127$
  - Equations:

$$\begin{aligned}\text{dv\_dt} = {} & 0.02425 \cdot \text{cancer\_volume} - 0.08865 \cdot \text{chemo\_concentration} \\ & - 0.03812 \cdot \text{chemo\_dosage} \\ & - 0.02755 \cdot \text{cancer\_volume} \cdot \text{chemo\_concentration} \\ & - 0.04786 \cdot \text{cancer\_volume} \cdot \text{radiotherapy\_dosage} \\ & + 0.4913 \sqrt{\text{cancer\_volume}} \\ \text{dc\_dt} = {} & -0.5 \cdot \text{chemo\_concentration} + \text{chemo\_dosage}\end{aligned}$$

- **Point B13** (Node 13):
  - MSE: $0.0376$
  - Equations:

$$\begin{aligned}\text{dv\_dt} = {} & 0.005864 \cdot \text{chemo\_concentration} + 0.007118 \cdot \text{chemo\_dosage} \\ & - 0.02803 \cdot \text{cancer\_volume} \cdot \text{chemo\_concentration} \\ & - 0.04733 \cdot \text{cancer\_volume} \cdot \text{radiotherapy\_dosage} \\ & - 1.708 \ln(\text{cancer\_volume} + 1) \\ & + 1.544 \sqrt{\text{cancer\_volume}} \\ \text{dc\_dt} = {} & -0.5 \cdot \text{chemo\_concentration} + \text{chemo\_dosage}\end{aligned}$$

- **Point B36** (Node 36):
  - MSE: $2.85 \times 10^{-26}$
  - Equations:

$$\begin{aligned}\text{dv\_dt} = {} & 0.1389 \cdot \text{cancer\_volume} \\ & - 0.028 \cdot \text{cancer\_volume} \cdot \text{chemo\_concentration} \\ & - 0.04776 \cdot \text{cancer\_volume} \cdot \text{radiotherapy\_dosage} \\ & - 0.01453 \cdot \text{cancer\_volume} \cdot \ln(\text{cancer\_volume}) \\ \text{dc\_dt} = {} & -0.5 \cdot \text{chemo\_concentration} + \text{chemo\_dosage}\end{aligned}$$

### E.3 INVESTIGATION OF MCTS ROLLOUT DEPTH

The Monte Carlo Tree Search (MCTS) component of SGED plays a crucial role in systematically exploring the vast space of possible equations. A key parameter within MCTS is the rollout depth, which determines how far into the future the search simulates potential sequences of actions (in our case, "propose then prune terms" equation refinement steps) to estimate the value of a given state (equation). Deeper rollouts can provide more accurate value estimates, potentially leading to better search decisions and ultimately more accurate discovered equations. However, they also incur a higher computational cost. This investigation aims to quantify the impact of varying MCTS rollout depths on the performance of SGED, helping to understand this trade-off.

We evaluated the effect of rollout depth on two distinct benchmark datasets: the simulated **Lung Cancer (with Chemo. & Radio.)** dataset and the real-world **RNA Polymerase** dataset. Three MCTS configurations were tested:

- **No Rollout (Heuristic MCTS)**: In this configuration, the MCTS does not perform any simulation. Instead, the value of a newly expanded node (representing an equation) is directly estimated using an immediate heuristic, which in our case is the negative validation Mean Squared Error (MSE) of the equation at that node. This reward is then directly backpropagated.
- **Rollout Depth 1**: After selecting a leaf node for expansion, the MCTS performs a simulation of one additional propose-and-prune cycle. The reward obtained from this single-step rollout is used for backpropagation.
- **Rollout Depth 2**: Similar to the above, but the simulation (rollout) extends for two propose-and-prune cycles.

For each configuration and dataset, performance was measured by the test MSE, averaged over 10 random seeds, with 95% confidence intervals reported.

The results are presented in Table 6.

Table 6: **Impact of MCTS Rollout Depth on SGED Performance.** Test MSE (mean ± 95% CI) on the Lung Cancer with Chemo. & Radio. (simulated) and RNA Polymerase (real-world) datasets for different MCTS rollout depths. Results are averaged over 10 seeds. Lower MSE is better. The best performing variation for each dataset is indicated in bold.

| MCTS Rollout Variation | Lung Cancer with Chemo. & Radio. MSE ↓ | RNA Polymerase MSE ↓ |
|---|---|---|
| No Rollout (Heuristic MCTS) | 0.0571 ± 0.0367 | 0.0118 ± 0.000445 |
| Rollout Depth 1 | 0.0211 ± 0.0131 | 0.0114 ± 0.000720 |
| Rollout Depth 2 | **0.0130** ± 0.0123 | **0.0113** ± 0.000523 |

The findings from this investigation, as summarized in Table 6, indicate a trend consistent with expectations for MCTS performance. For both the simulated Lung Cancer with Chemo. & Radio. dataset and the real-world RNA Polymerase dataset, increasing the rollout depth generally leads to improved performance (i.e., lower test MSE). Specifically, moving from no rollout to a rollout depth of 1, and further to a rollout depth of 2, resulted in progressively lower mean MSE values.

On the Lung Cancer with Chemo. & Radio. dataset, a rollout depth of 2 achieved the lowest MSE (0.0130), a noticeable improvement over no rollout (0.0571) and rollout depth 1 (0.0211). Similarly, for the RNA Polymerase dataset, rollout depth 2 yielded the best mean MSE (0.0113), compared to 0.0118 for no rollout and 0.0114 for rollout depth 1. While the confidence intervals show some overlap, particularly for the RNA Polymerase dataset where the improvements are more modest, the consistent reduction in mean MSE suggests that deeper rollouts allow the MCTS to make more informed decisions during the search process. This enhanced lookahead capability helps SGED to better navigate the complex equation space and identify more accurate symbolic models. This benefit, however, should be weighed against the increased computational time required for deeper rollouts in practical applications.

Elsewhere in this work, unless otherwise specified, we use the Heuristic MCTS configuration.

### E.4 Convergence Efficiency

A critical aspect of any equation discovery algorithm is its efficiency in navigating the vast search space of potential mathematical expressions. Rapid convergence to accurate and parsimonious solutions is highly desirable, as it reduces computational cost and accelerates the scientific discovery process. This section investigates the convergence efficiency of SGED compared to a standard Genetic Programming (GP) approach, GPLearn. We aim to demonstrate that the structured, influence-based feedback mechanism within SGED, particularly when coupled with MCTS, leads to faster identification of high-quality symbolic models.

**Experimental Setup and Iteration Comparability:** To assess convergence efficiency, we tracked the best test Mean Squared Error (MSE) achieved against the number of "major evaluation iterations" for both SGED and GPLearn on the Lung Cancer (with Chemo. & Radio.) benchmark dataset. Experiments were conducted over 10 random seeds, and we report the mean MSE ± 95% confidence intervals.

For SGED, an "iteration" is defined as one MCTS node expansion. Each expansion involves the core propose-and-prune cycle: the LLM proposes candidate basis functions, these are evaluated, influence scores are calculated, and the LLM prunes the terms to form a new candidate equation. This new equation is then fully evaluated.

For GPLearn, an "iteration" corresponds to one generation. In each generation, a population of candidate equations undergoes genetic operations (e.g., crossover, mutation), and each new individual (equation) in the subsequent population is evaluated.

While the precise computational operations within an SGED MCTS expansion (involving LLM calls and influence score calculations) differ from those in a GPLearn generation (dominated by genetic operations and fitness evaluations of a population), both represent a fundamental step where a set of new candidate equations are generated, fully evaluated, and used to guide the subsequent search. By plotting performance against these respective "major evaluation iterations" or, more broadly, "number of candidate equations fully evaluated," we gain insight into how quickly each algorithm explores promising regions of the equation space and refines its solutions. This provides a broadly comparable measure of how efficiently each method utilizes its core search mechanism to improve solution quality.

The iteration count was set to 30 for both methods. GPLearn was run with the following parameters: `population_size = 1000`, `parsimony_coefficient = 0.01`, with the rest of the parameters set to their default values.

**Results:** The convergence behavior of SGED and GPLearn is illustrated in Figure 7. The plot clearly shows that SGED converges significantly faster to a substantially lower test MSE compared to GPLearn on this benchmark. SGED rapidly identifies high-performing equations within a smaller number of major evaluation iterations. Specifically, SGED reached a final mean test MSE of $0.0752 \pm 0.0295$. In contrast, GPLearn's convergence was slower, and it settled at a considerably higher final mean test MSE of $28.5 \pm 9.34$ within a comparable or number of its own evaluation iterations.

This superior convergence efficiency highlights the effectiveness of SGED's approach. The detailed, per-term influence feedback allows the LLM to make more informed decisions during the pruning phase, leading to more targeted exploration. Coupled with the systematic search of MCTS, SGED is able to more quickly discard unpromising avenues and focus on refining equation structures that demonstrate high predictive accuracy. This contrasts with the more stochastic and population-based exploration of GPLearn, which, in this case, required more evaluations to achieve a less optimal solution.

This demonstrates SGED's ability not only to find accurate equations but to do so with greater efficiency in terms of the number of core search and evaluation steps.

### E.5 Investigation of LLM sensitivity

Understanding the robustness of SGED's advantages across different underlying Large Language Models (LLMs) is crucial for assessing the generalizability of our approach. This investigation aims to determine if the performance gains observed with SGED are primarily due to its structured, influence-based feedback mechanism and search strategy, rather than being contingent on the specific capabilities of a single LLM. Demonstrating such robustness would imply that the architectural innovations of SGED provide consistent benefits, offering practical value to users who may employ a variety of LLMs, including proprietary and open-weight models.

To evaluate this sensitivity, we conducted a comprehensive set of experiments comparing SGED (Ours) with the baseline LLM-driven methods: ZeroShot, ZeroOptim, and ICL (Basic Feedback). These four methods were evaluated on all six main benchmark datasets detailed in Section 4 and Appendix C: Lung Cancer, Lung Cancer (with Chemo.), Lung Cancer (with Chemo. & Radio.), COVID-19, RNA Polymerase, and Warfarin PK. For each method and dataset combination, we utilized a diverse suite of nine different base LLMs. The models used, their classification, and version notes are as follows:

- **Open-weight Models:**
  - `Llama-3.3-70B`: `Llama-3.3-70B-Instruct`, version `5`.

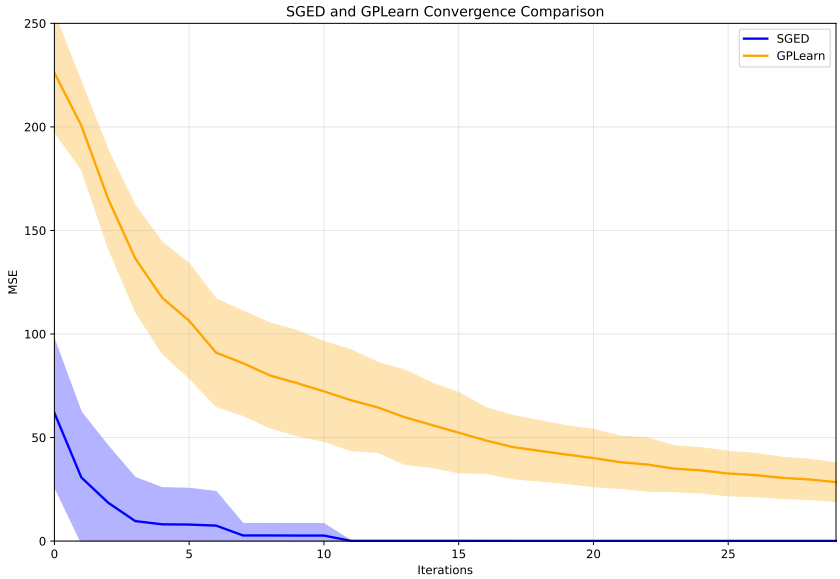


Figure 7: **Convergence Efficiency: SGED vs. GPLearn.** Test MSE (mean ± 95% CI over 10 seeds) versus number of major evaluation iterations for SGED (MCTS expansions) and GPLearn (generations) on the Lung Cancer (with Chemo. & Radio.) dataset. SGED demonstrates faster convergence to a lower MSE, indicating superior search efficiency.

  - `DeepSeek V3`: `DeepSeek V3`, version `0324`.
- **Proprietary Models:**
  - `GPT-4`: `gpt-4`, version `turbo-2024-04-09`.
  - `GPT-4o-Mini`: `gpt-4o-mini`, version `2024-07-18`.
  - `GPT-4o`: `gpt-4o`, version `2024-11-20`.
  - `GPT-4.1`: `gpt-4.1`, version `2025-04-14`.
  - `OpenAI o1`: `o1`, version `2024-12-17`.
  - `OpenAI o4-Mini`: `o4-mini`, version `2025-04-16`.
  - `OpenAI o3`: `o3`, version `2025-04-16`.

All inference hyperparameters were set to their default values for each model throughout the experiments.

The performance was measured using the Mean Squared Error (MSE) on the respective test sets, consistent with our main evaluations. Each experiment was run with 25 seeds[2] to ensure reliability, and average MSE values are reported.

The results of this extensive evaluation are presented systematically. Figure 8 presents bar plots for all six datasets, showing the MSE outcomes. Corresponding numerical results are detailed in Table 7.

The bar plots presented in Figure 8 facilitate visual comparison of method performance across different LLMs. Each subfigure in Figure 8 corresponds to a specific dataset. Within each such dataset-specific plot, results for the four methods—ZeroShot, ZeroOptim, ICL (Basic Feedback), and SGED (Ours)—are displayed in separate panels. In every panel, the x-axis lists the different base LLMs, while the y-axis represents the Mean Squared Error (MSE), where lower bars indicate better performance. The ± 95% CI is shown as error bars. For improved clarity, the y-axis MSE values are presented on a logarithmic scale. Notably, due to its significantly MSE, the ZeroShot method is plotted with a y-axis range distinct from the other three methods within each dataset. Conversely, the y-axis ranges for ZeroOptim, ICL (Basic Feedback), and SGED (Ours) are all aligned with each other within the context of a single dataset to enable their direct comparison.

[2]Except `Llama-3.3-70B-Instruct`, where 10 seeds were used, due to limitations to model throughput that was available at the time of the experiments.

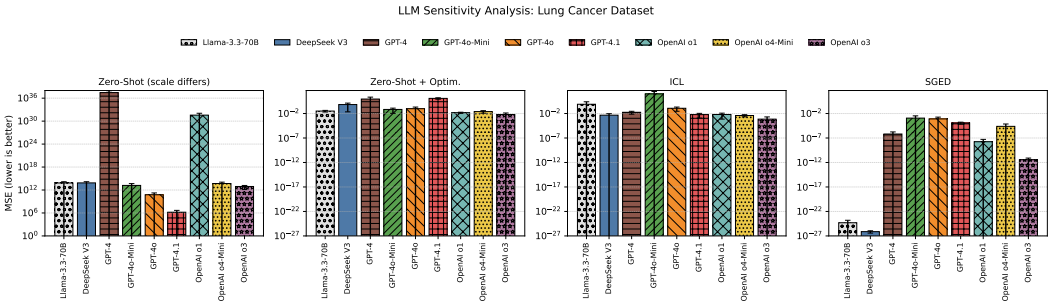


(a) Lung Cancer

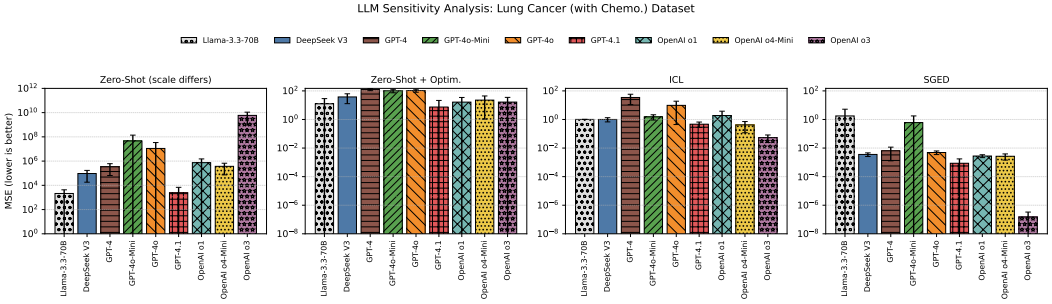


(b) Lung Cancer (with Chemo.)

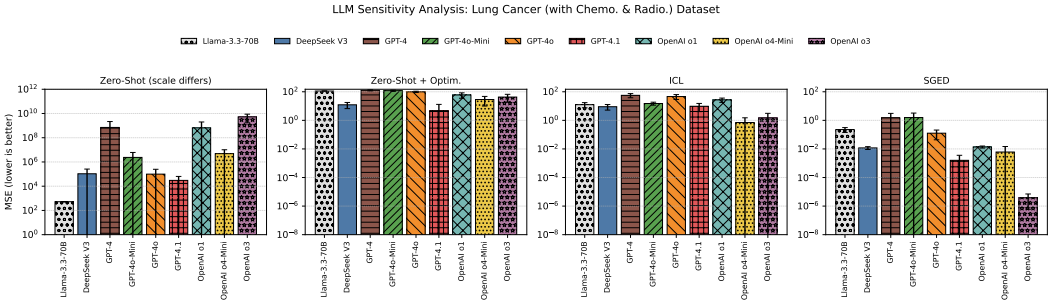


(c) Lung Cancer (with Chemo. & Radio.)

Figure 8: MSE (± 95% CI error bars) on benchmark datasets for ZeroShot, ZeroOptim, ICL (Basic Feedback), and SGED (Ours) across various base LLMs, including open-weight models. Each subfigure represents a different dataset. SGED outperforms the other methods across the datasets and base LLMs with few exceptions.

**Note:** The y axis (MSE) scale is logarithmic. For each dataset: the MSE range is different for the ZeroShot baseline, as its performance is significantly worse; the other methods are shown over matching ranges for clarity.

*(Figure continued to next page)*

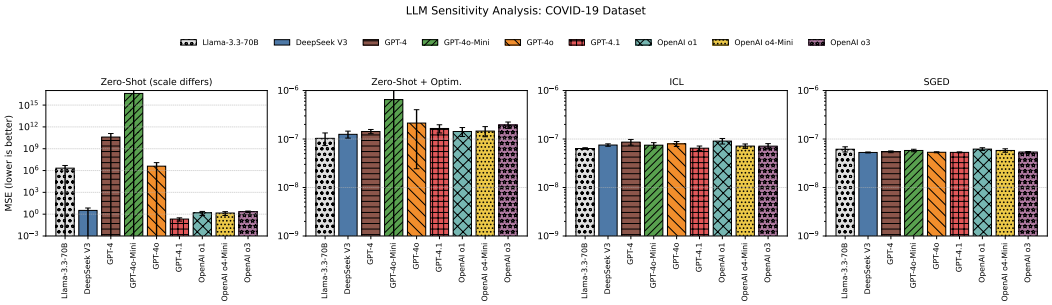


(d) COVID-19

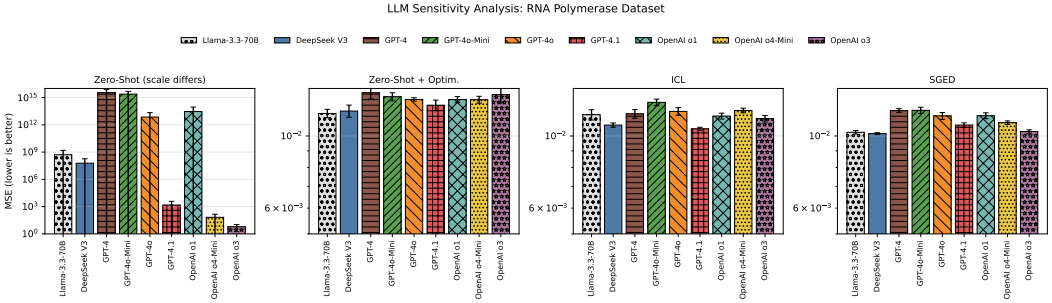


(e) RNA Polymerase

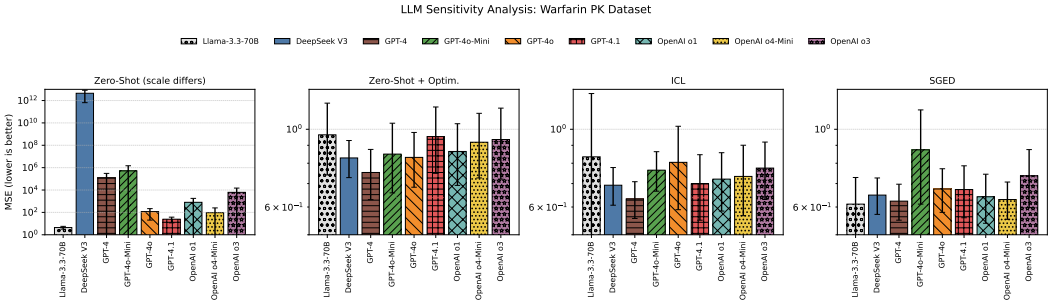


(f) Warfarin PK

Figure 8: MSE (± 95% CI error bars) on benchmark datasets for ZeroShot, ZeroOptim, ICL (Basic Feedback), and SGED (Ours) across various base LLMs, including open-weight models. Each subfigure represents a different dataset. SGED outperforms the other methods across the datasets and base LLMs with few exceptions.

**Note:** The y axis (MSE) scale is logarithmic. For each dataset: the MSE range is different for the ZeroShot baseline, as its performance is significantly worse; the other methods are shown over matching ranges for clarity.

*(Figure completed)*

Table 7: Test MSE (mean ± 95% CI) for different methods and base LLMs across all benchmark datasets. The best performing method for each LLM is bolded. If the best method's confidence interval overlaps with any other method's CI for that LLM, only its mean is bolded; otherwise, both mean and CI are bolded.

(a) Lung Cancer

| Base LLM | ZeroShot | ZeroOptim | ICL (Basic Feedback) | **SGED (Ours)** |
|---|---|---|---|---|
| `Llama-3.3-70B` | 6.88e+13 ± 7.74e+13 | 0.0319 ± 0.0117 | 0.782 ± 1.72 | **4.89e-25** ± 1.09e-24 |
| `DeepSeek V3` | 7.23e+13 ± 7.54e+13 | 0.679 ± 0.657 | 0.0046 ± 0.00468 | **7.55e-27** ± 3.76e-27 |
| `GPT-4` | 2.85e+37 ± 5.88e+37 | 9.06 ± 13.1 | 0.0179 ± 0.0106 | **6.57e-07** ± 1.09e-06 |
| `GPT-4o-Mini` | 1.59e+13 ± 3.18e+13 | 0.0682 ± 0.0575 | 102 ± 210 | **0.00116** ± 0.00218 |
| `GPT-4o` | 5.75e+10 ± 1.15e+11 | 0.0971 ± 0.111 | 0.119 ± 0.0899 | **0.000792** ± 0.00105 |
| `GPT-4.1` | 1.59e+06 ± 3.2e+06 | 12.4 ± 4.05 | 0.006 ± 0.00483 | **0.000118 ± 5.32e-05** |
| `OpenAI o1` | 3.71e+31 ± 7.66e+31 | 0.0146 ± 0.00384 | 0.00629 ± 0.00558 | **1.74e-08** ± 3.49e-08 |
| `OpenAI o4-Mini` | 4.98e+13 ± 6.34e+13 | 0.025 ± 0.0133 | 0.00395 ± 0.00183 | **2.39e-05** ± 4.87e-05 |
| `OpenAI o3` | 8.37e+12 ± 7.06e+12 | 0.00626 ± 0.00664 | 0.000717 ± 0.00131 | **3.54e-12 ± 4.4e-12** |

(b) Lung Cancer (with Chemo.)

| Base LLM | ZeroShot | ZeroOptim | ICL (Basic Feedback) | **SGED (Ours)** |
|---|---|---|---|---|
| `Llama-3.3-70B` | 2.13e+03 ± 2.14e+03 | 12.5 ± 16.4 | **1.01 ± 0.00448** | 1.76 ± 3.48 |
| `DeepSeek V3` | 9.44e+04 ± 7.63e+04 | 37.8 ± 25 | 1.01 ± 0.329 | **0.00358 ± 0.00102** |
| `GPT-4` | 3.38e+05 ± 2.73e+05 | 124 ± 20 | 34.7 ± 23.7 | **0.00644 ± 0.00516** |
| `GPT-4o-Mini` | 4.6e+07 ± 9.29e+07 | 101 ± 27.7 | 1.52 ± 0.608 | **0.603** ± 1.17 |
| `GPT-4o` | 1.11e+07 ± 2.28e+07 | 106 ± 25.1 | 9.74 ± 9.29 | **0.00489 ± 0.00139** |
| `GPT-4.1` | 2.44e+03 ± 4.4e+03 | 7.45 ± 14.1 | 0.468 ± 0.193 | **0.000864 ± 0.000883** |
| `OpenAI o1` | 7.39e+05 ± 7.73e+05 | 16.4 ± 18.3 | 1.89 ± 1.91 | **0.00277 ± 0.000628** |
| `OpenAI o4-Mini` | 3.7e+05 ± 2.97e+05 | 22.7 ± 21.6 | 0.417 ± 0.299 | **0.00267 ± 0.00123** |
| `OpenAI o3` | 5.92e+09 ± 4.99e+09 | 16.5 ± 18.7 | 0.0533 ± 0.029 | **1.52e-07 ± 1.8e-07** |

(c) Lung Cancer (with Chemo. & Radio.)

| Base LLM | ZeroShot | ZeroOptim | ICL (Basic Feedback) | **SGED (Ours)** |
|---|---|---|---|---|
| `Llama-3.3-70B` | 524 ± 18.4 | 113 ± 0.92 | 12.5 ± 4.91 | **0.227 ± 0.0846** |
| `DeepSeek V3` | 1.06e+05 ± 1.53e+05 | 12.2 ± 5.62 | 9 ± 3.8 | **0.0118 ± 0.00265** |
| `GPT-4` | 7.07e+08 ± 1.46e+09 | 126 ± 10.3 | 56.4 ± 18.2 | **1.47** ± 1.6 |
| `GPT-4o-Mini` | 2.38e+06 ± 3.7e+06 | 118 ± 11.8 | 15.1 ± 3.56 | **1.57** ± 1.66 |
| `GPT-4o` | 9.92e+04 ± 1.5e+05 | 98.6 ± 10.3 | 46.3 ± 17.3 | **0.127 ± 0.083** |
| `GPT-4.1` | 3.02e+04 ± 3.39e+04 | 4.76 ± 8.33 | 9.68 ± 5.6 | **0.0016** ± 0.00199 |
| `OpenAI o1` | 6.51e+08 ± 1.34e+09 | 59.7 ± 24.4 | 27.1 ± 9.04 | **0.0137 ± 0.00223** |
| `OpenAI o4-Mini` | 4.84e+06 ± 5.33e+06 | 28.7 ± 18.6 | 0.708 ± 0.801 | **0.00608** ± 0.00867 |
| `OpenAI o3` | 5.24e+09 ± 3.54e+09 | 42.7 ± 23.7 | 1.49 ± 1.61 | **3.82e-06 ± 3.22e-06** |

(d) COVID-19

| Base LLM | ZeroShot | ZeroOptim | ICL (Basic Feedback) | **SGED (Ours)** |
|---|---|---|---|---|
| `Llama-3.3-70B` | 2.13e+06 ± 2.84e+06 | 1.03e-07 ± 3.01e-08 | **6.38e-08 ± 2.41e-09** | 6.16e-08 ± 7.54e-09 |
| `DeepSeek V3` | 3.3 ± 3.76 | 1.25e-07 ± 2.05e-08 | 7.52e-08 ± 4.33e-09 | **5.28e-08 ± 1.18e-09** |
| `GPT-4` | 4.03e+10 ± 8.25e+10 | 1.43e-07 ± 1.44e-08 | 8.63e-08 ± 1.17e-08 | **5.45e-08 ± 2.28e-09** |
| `GPT-4o-Mini` | 4e+16 ± 8.26e+16 | 6.51e-07 ± 7.71e-07 | 7.47e-08 ± 9.47e-09 | **5.81e-08** ± 3.45e-09 |
| `GPT-4o` | 4e+06 ± 8.26e+06 | 2.13e-07 ± 1.89e-07 | 7.95e-08 ± 9.33e-09 | **5.33e-08 ± 1.27e-09** |
| `GPT-4.1` | 0.213 ± 0.102 | 1.65e-07 ± 3.17e-08 | 6.47e-08 ± 6.96e-09 | **5.31e-08 ± 1.17e-09** |
| `OpenAI o1` | 1.53 ± 0.857 | 1.43e-07 ± 2.99e-08 | 9.07e-08 ± 1.19e-08 | **6.2e-08** ± 4.14e-09 |
| `OpenAI o4-Mini` | 1.44 ± 0.791 | 1.46e-07 ± 3.45e-08 | 7.16e-08 ± 7.49e-09 | **5.81e-08** ± 4.81e-09 |
| `OpenAI o3` | 2.16 ± 0.514 | 1.95e-07 ± 2.92e-08 | 7.13e-08 ± 9.05e-09 | **5.4e-08 ± 1.28e-09** |

(e) RNA Polymerase

| Base LLM | ZeroShot | ZeroOptim | ICL (Basic Feedback) | **SGED (Ours)** |
|---|---|---|---|---|
| `Llama-3.3-70B` | 5.08e+08 ± 1.05e+09 | 0.0117 ± 0.00035 | 0.0116 ± 0.000425 | **0.0103 ± 0.000129** |
| `DeepSeek V3` | 6.01e+07 ± 1.24e+08 | 0.0119 ± 0.000514 | 0.0108 ± 0.000163 | **0.0102 ± 6.65e-05** |
| `GPT-4` | 3.46e+15 ± 4.49e+15 | 0.0136 ± 0.000579 | 0.0117 ± 0.000362 | **0.012** ± 0.00016 |
| `GPT-4o-Mini` | 2.36e+15 ± 2.46e+15 | 0.0132 ± 0.000381 | 0.0127 ± 0.000295 | **0.012 ± 0.000268** |
| `GPT-4o` | 7.16e+12 ± 1.48e+13 | 0.013 ± 0.000156 | **0.0119** ± 0.000323 | 0.0115 ± 0.000279 |
| `GPT-4.1` | 1.5e+03 ± 2.36e+03 | 0.0124 ± 0.00046 | **0.0105 ± 0.000118** | 0.0108 ± 0.000168 |
| `OpenAI o1` | 2.91e+13 ± 6e+13 | 0.0129 ± 0.000275 | **0.0115** ± 0.00024 | 0.0115 ± 0.000242 |
| `OpenAI o4-Mini` | 66.9 ± 78.7 | 0.0129 ± 0.000315 | 0.012 ± 0.000196 | **0.011 ± 0.000137** |
| `OpenAI o3` | 6.18 ± 4.42 | 0.0134 ± 0.000774 | 0.0113 ± 0.000258 | **0.0103 ± 0.000124** |

(f) Warfarin PK

| Base LLM | ZeroShot | ZeroOptim | ICL (Basic Feedback) | **SGED (Ours)** |
|---|---|---|---|---|
| `Llama-3.3-70B` | 4.42 ± 1.23 | 0.964 ± 0.223 | 0.834 ± 0.43 | **0.612 ± 0.117** |
| `DeepSeek V3` | 4.46e+12 ± 3.82e+12 | 0.828 ± 0.1 | 0.692 ± 0.0853 | **0.649 ± 0.0773** |
| `GPT-4` | 1.21e+05 ± 1.86e+05 | 0.753 ± 0.123 | 0.633 ± 0.076 | **0.624 ± 0.0734** |
| `GPT-4o-Mini` | 5.15e+05 ± 9.64e+05 | **0.85** ± 0.191 | 0.764 ± 0.0987 | 0.874 ± 0.262 |
| `GPT-4o` | 119 ± 98.5 | 0.831 ± 0.148 | 0.805 ± 0.215 | **0.675 ± 0.0961** |
| `GPT-4.1` | 24.6 ± 13 | 0.953 ± 0.205 | 0.698 ± 0.148 | **0.673 ± 0.114** |
| `OpenAI o1` | 798 ± 995 | 0.864 ± 0.173 | 0.721 ± 0.137 | **0.642 ± 0.103** |
| `OpenAI o4-Mini` | 94.1 ± 158 | 0.918 ± 0.192 | 0.734 ± 0.167 | **0.63 ± 0.0768** |
| `OpenAI o3` | 6.24e+03 ± 8.68e+03 | 0.935 ± 0.214 | 0.775 ± 0.144 | **0.736 ± 0.139** |

Across all datasets and underlying LLM choices, SGED consistently outperforms ZeroShot, ZeroOptim, and ICL (Basic Feedback), with only a few exceptions (see Table 7). This strongly suggests that the structured feedback and systematic search strategy integral to SGED are key drivers of its enhanced equation discovery capabilities, providing a robust advantage irrespective of the specific foundational LLM employed. These findings underscore the value of SGED's methodology in leveraging LLMs for scientific discovery.

### E.6 Investigation of Robustness to a Large Number of Irrelevant Features

Scientific datasets, particularly in fields like genomics or high-throughput screening, can often present a high-dimensional feature space where many features may be irrelevant or noisy. A critical aspect of an effective equation discovery method is its ability to identify the truly influential variables amidst a large number of distractors. This section investigates the robustness of SGED to an increasing number of such irrelevant features.

We conducted experiments using the **Lung Cancer (with Chemo. & Radio.)** benchmark dataset. To simulate scenarios with varying degrees of feature space complexity, we augmented the original dataset by adding 5, 75, or 150 additional "distractor" features. These features were populated with values drawn from a standard normal distribution ($\mathcal{N}(0, 1)$) and were designed to have no causal relationship with the target variables. The performance of SGED (denoted as "**SGED (Ours)**" in the table) was compared against the LLM-based baselines: ZeroShot, ZeroOptim, and ICL (Basic

Feedback). All methods were evaluated based on their Mean Squared Error (MSE) on the test set, averaged over 25 random seeds, with 95% confidence intervals reported.

The results are presented in Table 8.

Table 8: **Performance with Increasing Numbers of Irrelevant Features.** Test MSE (mean ± 95% CI) on the Lung Cancer (with Chemo. & Radio.) dataset, augmented with varying numbers of normally distributed, irrelevant features. Results are averaged over 25 seeds. Lower MSE is better. "+0 Features" corresponds to the original dataset.

| Method | +0 Features (Original) | +5 Features | +75 Features | +150 Features |
|---|---|---|---|---|
| ZeroShot | 2.54e+03 ± 2.74e+03 | 1.48e+03 ± 2.35e+03 | 3.08e+03 ± 6.18e+03 | 1.57e+04 ± 2.18e+04 |
| ZeroOptim | 122 ± 6 | 142 ± 12.2 | 131 ± 27.8 | 132 ± 22.7 |
| ICL (Basic Feedback) | 63.3 ± 16.5 | 111 ± 32.6 | 118 ± 32.5 | 126 ± 22.5 |
| **SGED (Ours)** | **0.0521 ± 0.0178** | **0.0843 ± 0.0421** | **2.99 ± 5.95** | **4.88 ± 9.8** |

As evident from Table 8, SGED consistently achieves the lowest MSE across all conditions, even when a substantial number of irrelevant features are introduced. While the performance of SGED does show some degradation as the number of distractor features increases (MSE from 0.0521 with 0 extra features to 4.88 with 150 extra features), its accuracy remains significantly better—often by orders of magnitude—than the other LLM-based approaches. For instance, with 150 additional irrelevant features, SGED achieves an MSE of 4.88, whereas the next best LLM-based method, ICL (Basic Feedback), has an MSE of 126.

The other methods (ZeroShot, ZeroOptim, ICL) show varied responses to the additional features but consistently perform much worse than SGED. Their inability to effectively filter out the noise, even with optimization (ZeroOptim) or basic iterative feedback (ICL), highlights the challenge distractor features pose. These findings suggest that SGED's architecture, particularly its use of per-term influence scores and systematic search (with MCTS), equips the LLM with a more robust mechanism to discern and prioritize relevant features.

### E.7 Investigation of Synthetic Model Benchmark

To further assess the robustness and generalization capabilities of SGED, particularly its performance on model structures that may not be prevalent in its LLM's training data, we conducted evaluations on a procedurally generated synthetic model benchmark. By creating synthetic models with known ground-truth equations incorporating diverse mathematical operators and interactions, we can test the ability of SGED to discover accurate equations even when faced with potentially unfamiliar functional forms.

These synthetic datasets were derived by introducing specific modifications to the underlying structure of the previously described lung cancer model with chemotherapy and radiotherapy. The modifications included the incorporation of trigonometric operators, division operators, and novel interaction terms, resulting in five distinct synthetic models:

- **Synthetic 1 (inc. $\gamma \sin(\omega t)$)**: Introduces a sinusoidal forcing term. The underlying differential equation is:
$$\frac{dx(t)}{dt} = \left( \rho \log\left(\frac{K}{x(t)}\right) - \beta_c C(t) - (\alpha_r d(t) + \beta_r d(t)^2) + \gamma \sin(\omega t) \right) x(t)$$
- **Synthetic 2 (inc. $-\delta I(t)$)**: Incorporates an additional linear negative feedback term $I(t)$.
$$\frac{dx(t)}{dt} = \left( \rho \log\left(\frac{K}{x(t)}\right) - \beta_c C(t) - (\alpha_r d(t) + \beta_r d(t)^2) - \delta I(t) \right) x(t)$$
- **Synthetic 3 (inc. $\log(\frac{K}{x(t)+N(t)})$)**: Modifies the growth term to include an additional variable $N(t)$ in the denominator of the logistic term.
$$\frac{dx(t)}{dt} = \left( \rho \log\left(\frac{K}{x(t)+N(t)}\right) - \beta_c C(t) - (\alpha_r d(t) + \beta_r d(t)^2) \right) x(t)$$

- **Synthetic 4 (inc. $\epsilon \cos(\phi t)$)**: Adds a cosine forcing term.

$$\frac{dx(t)}{dt} = \left(\rho \log\left(\frac{K}{x(t)}\right) - \beta_c C(t) - (\alpha_r d(t) + \beta_r d(t)^2) + \epsilon \cos(\phi t)\right) x(t)$$

- **Synthetic 5 (inc. $\theta C(t)d(t)$)**: Introduces a multiplicative interaction term between chemotherapy $C(t)$ and radiotherapy $d(t)$.

$$\frac{dx(t)}{dt} = \left(\rho \log\left(\frac{K}{x(t)}\right) - \beta_c C(t) - (\alpha_r d(t) + \beta_r d(t)^2) - \theta C(t) d(t)\right) x(t)$$

Here, $x(t)$ represents the tumor volume, $C(t)$ is the chemotherapy effect, $d(t)$ is the radiotherapy effect, and other parameters ($\rho, K, \beta_c, \alpha_r, \beta_r, \gamma, \omega, \delta, N(t), \epsilon, \phi, \theta$) are constants or time-varying inputs specific to each synthetic model.

The performance of SGED was compared against the LLM-based baselines: ZeroShot, ZeroOptim, and ICL (Basic Feedback). The results, in terms of test Mean Squared Error (MSE), are presented in Table 9.

Table 9: **Synthetic Model Benchmark Performance.** Test MSE (mean ± 95% CI) on five procedurally generated synthetic datasets. Results are averaged over 25 seeds. Lower MSE is better. SGED (Ours) consistently outperforms other LLM-based methods.

| Method | Synthetic 1 | Synthetic 2 | Synthetic 3 | Synthetic 4 | Synthetic 5 |
|---|---|---|---|---|---|
| ZeroShot | 3.42e+03 ± 2.59e+03 | 1.14e+04 ± 2.17e+04 | 1.11e+03 ± 470 | 3.12e+05 ± 6.36e+05 | 7.8e+03 ± 5.55e+03 |
| ZeroOptim | 153 ± 13.5 | 65.3 ± 7.53 | 106 ± 14.6 | 147 ± 14.8 | 118 ± 12.3 |
| ICL (Basic Feedback) | 102 ± 17.7 | 48.3 ± 10.7 | 40.4 ± 11.3 | 89.2 ± 12 | 42.6 ± 16.3 |
| **SGED (Ours)** | **52.7 ± 0.307** | **0.189 ± 0.158** | **0.0272 ± 0.0153** | **52.5 ± 0.296** | **0.036 ± 0.0202** |

As shown in Table 9, SGED consistently achieves significantly lower MSE compared to ZeroShot, ZeroOptim, and ICL (Basic Feedback) across all five synthetic datasets. This strong performance on models with varied and potentially novel structures (such as trigonometric terms or modified logistic growth factors) underscores SGED's ability to effectively search the equation space and adapt its discovery process. The granular, influence-based feedback appears crucial in guiding the LLM to identify relevant terms and construct accurate models, even when the underlying system dynamics deviate from more common forms. These results further highlight the robustness of the SGED framework and its potential for discovering meaningful equations in diverse scientific domains.

### E.8 Generalization Study on the RNA Polymerase Dataset

A crucial test for any equation discovery method aiming for scientific relevance is its ability to generalize not just to held-out data from the same experiment, but to entirely new, independent measurements. A model that performs well on a new biological replicate is more likely to have captured true underlying biological principles rather than just fitting noise or artifacts specific to a single experiment.

To rigorously assess this, we obtained a second biological replicate for the RNA Polymerase II pausing measurements, representing a separate laboratory experiment (used as the target `pause_score`; henceforth, *"Replicate 2"*). We then took the final equations discovered by SGED and several LLM-based baselines – which were trained and selected using only the original dataset (*"Replicate 1"*) – and evaluated their predictive performance on this new, unseen replicate without any re-fitting. This provides a strong test of out-of-distribution generalization.

The results, summarized in Table 10, demonstrate the robust generalization of the SGED-discovered models. While all methods experienced a predictable and modest drop in performance when evaluated on the new replicate – an expected outcome given inter-experiment variability – SGED maintained its superior accuracy.

On *Replicate 2*, SGED achieved the lowest Mean Squared Error (MSE) of $0.00793 \pm 0.000214$ and the highest coefficient of determination ($R^2$) of $0.142 \pm 0.0232$. This indicates that the SGED-discovered equation explained the most variance in the independent dataset, outperforming the next-best method, ICL (Basic Feedback), which achieved an MSE of $0.00815$ and an $R^2$ of $0.119$.

The strong performance on a true biological replicate provides compelling evidence that the structured, influence-based feedback mechanism of SGED guides the discovery process towards equations that capture genuine, reproducible biological principles.

Table 10: **Generalization to an Independent Biological Replicate.** Performance of discovered equations on the original test set (Replicate 1) versus a new, unseen biological replicate (Replicate 2) for the RNA Polymerase dataset. Models were trained/selected using only Replicate 1 data. Results are mean ± 95% CI over 25 seeds. SGED shows the best generalization, maintaining the lowest MSE and highest $R^2$ on the new replicate.

| | Performance on Original Test Set (Replicate 1) | | | Performance on New Biological Replicate (Replicate 2) | | |
|---|---|---|---|---|---|---|
| Method | MSE ↓ | $R^2$ ↑ | NRMSE ↓ | MSE ↓ | $R^2$ ↑ | NRMSE ↓ |
| ZeroShot | 1.35e+05 ± 1.75e+05 | -9.80e+06 ± 1.28e+07 | 1.55e+03 ± 1.15e+03 | 1.40e+05 ± 1.72e+05 | -1.52e+07 ± 1.87e+07 | 1.97e+03 ± 1.42e+03 |
| ZeroOptim | 0.0130 ± 0.000287 | 0.0724 ± 0.0199 | 0.963 ± 0.0101 | 0.00887 ± 0.000159 | 0.0406 ± 0.0188 | 0.979 ± 0.00937 |
| ICL (Basic Feedback) | 0.0119 ± 0.000352 | 0.149 ± 0.0251 | 0.922 ± 0.0137 | 0.00815 ± 0.000246 | 0.119 ± 0.0262 | 0.938 ± 0.0140 |
| **SGED (Ours)** | **0.0115 ± 0.000312** | **0.176 ± 0.0226** | **0.907 ± 0.0125** | **0.00793 ± 0.000214** | **0.142 ± 0.0232** | **0.926 ± 0.0126** |

### E.9 Influence Score Variants

In SGED, the per-term influence score, $\Delta_j$, is computed on a *validation* split by deleting a single term (setting $w_j \leftarrow 0$) while holding the remaining coefficients fixed. This is the explicit definition of $\Delta_j$ used throughout the method and its pruning phase. The corresponding pruning prompt includes, as an illustration, an OLS identity, $\Delta_k = \frac{w_k^2}{n} \sum_i \phi_k(x_i)^2$, with the comment "always $\geq 0$" and an instruction to "treat terms independently; no need to refit or update weights."

The applicability of these statements hinges on the OLS orthogonality that nullifies cross-terms, a property that holds for the *training* data at the optimum but does not necessarily extend to a disjoint validation set. To ensure this distinction is clear, the prompt contains an explicit note that validation-computed values "may not always be $\geq 0$".

Here, as part of an additional investigation, we also implement and evaluate two *refit-aware* influence score alternatives that align the definition more closely with extra-sum-of-squares logic.

#### Influence score computation

**Notation.** Let $X \in \mathbb{R}^{n\times p}$ and $y \in \mathbb{R}^n$ denote training data; $X_{\mathrm{val}} \in \mathbb{R}^{n_{\mathrm{val}}\times p}$, $y_{\mathrm{val}} \in \mathbb{R}^{n_{\mathrm{val}}}$ denote validation data; $W \in \mathbb{R}^{p\times m}$ the fitted full–model coefficients (one column per output). On validation, $\widehat{Y}_{\mathrm{val}} = X_{\mathrm{val}}W$, with residuals $R_{\mathrm{val}} = Y_{\mathrm{val}} - \widehat{Y}_{\mathrm{val}}$. We use $\mathrm{MSE}_{\mathrm{val}}(W)_j = \frac{1}{n_{\mathrm{val}}}\|y_{\mathrm{val}}^{(j)} - (X_{\mathrm{val}}W)_{:,j}\|_2^2$.

**(A) No–refit** (default in SGED)**.** Deleting term $k$ is implemented by $\widehat{y}^{(j)}_{\mathrm{val},-k} = (X_{\mathrm{val}}W)_{:,j} - \varphi_k^{\mathrm{val}}\, w_{k,j}$, where $\varphi_k^{\mathrm{val}} = X_{\mathrm{val}}e_k$. Expanding the squares yields the exact validation–split change

$$\Delta^{\mathrm{val}}_{k,j} \;=\; \frac{2w_{k,j}}{n_{\mathrm{val}}}\,(\varphi_k^{\mathrm{val}})^\top r^{(j)}_{\mathrm{val}} \;+\; \frac{w_{k,j}^2}{n_{\mathrm{val}}}\,\|\varphi_k^{\mathrm{val}}\|_2^2, \quad r^{(j)}_{\mathrm{val}} = y^{(j)}_{\mathrm{val}} - (X_{\mathrm{val}}W)_{:,j}.$$

The cross–term vanishes on the *training* split at the OLS optimum (residuals orthogonal to columns of $X$), making the classic "$\geq 0$" identity a good approximation there; on validation the cross–term generally does not vanish and $\Delta^{\mathrm{val}}_{k,j}$ can be slightly negative. This approach is how SGED computes $\Delta_j$ before pruning, by default.

**(B) Refit–aware (full refit).** Define the refit–aware influence as the *validation* MSE change after *refitting on train* with column $k$ removed:

$$\Delta^{\mathrm{refit}}_{k,j} \;=\; \mathrm{MSE}_{\mathrm{val}}\big(W^{(-k)}\big)_j - \mathrm{MSE}_{\mathrm{val}}(W)_j, \qquad W^{(-k)}_{:,j} = \arg\min_{u\in\mathbb{R}^{p-1}} \frac{1}{n}\|y^{(j)} - X_{(-k)}u\|_2^2$$

(or ridge adds $\lambda\|u\|_2^2$). This aligns with extra-sum-of-squares on train and yields a clean validation readout.

**(C) Refit–aware (efficient)**, compatible with OLS and ridge. Let $A = X^\top X$ (OLS) or $A = X^\top X + \lambda I$ (ridge), $B = A^{-1}$. Partition index $k$ from the rest and denote $\alpha_k = B_{kk}$, $\beta_{-k} = B_{-k,k}$. Writing $W = \begin{bmatrix} W_{-k,:} \\ W_{k,:} \end{bmatrix}$,

$$W^{(-k)}_{-k,:} = W_{-k,:} - \frac{\beta_{-k}}{\alpha_k} W_{k,:}$$
$$\widehat{Y}^{(-k)}_{\text{val}} = X^{(-k)}_{\text{val}} W^{(-k)}_{-k,:}$$
$$\Delta^{\text{refit}}_{k,j} = \frac{1}{n_{\text{val}}} \left\| y^{(j)}_{\text{val}} - \widehat{y}^{(j)(-k)}_{\text{val}} \right\|_2^2 - \text{MSE}_{\text{val}}(W)_j.$$

This avoids an explicit fit–loop, reusing $B$ to update all $p$ leave–one–out solutions in $O(p^2)$ per term (after a one–time $O(p^3)$ factorization), and works columnwise for multi–output.

**Where this is used in SGED.** The pipeline computes $\Delta_j$ on validation to guide pruning (Section 2, Appendix B.2); the prompt receives the per–term weights $w_j$ and validation–computed $\Delta_j$ to guide its term keep/drop decisions.

### Ablation across six benchmarks: accuracy vs. cost

We compared the three influence score variants—(i) No–refit, (ii) Refit–aware (full), and (iii) Refit–aware (efficient)—across the six benchmark datasets described in Tables 11 and 12. To ensure a fair comparison of test performance, the same set of 15 random seeds was used for each variant.

Table 11: Test MSE (mean ± 95% CI) across datasets for the three influence variants.

| Variant | COVID-19 | Lung Cancer (with Chemo. & Radio.) | Lung Cancer (with Chemo.) | Lung Cancer | RNA Polymerase | Warfarin PK |
|---|---|---|---|---|---|---|
| No–refit | 5.35e-08 ± 1.93e-09 | 0.0311 ± 0.027 | 0.00304 ± 0.00194 | 3.55e-09 ± 5.3e-09 | 0.0114 ± 0.000398 | 0.597 ± 0.0821 |
| Refit–aware (full) | 5.24e-08 ± 1.67e-09 | 0.0337 ± 0.0064 | 0.00903 ± 0.0043 | 0.0065 ± 0.00561 | 0.0118 ± 0.000373 | 0.622 ± 0.0943 |
| Refit–aware (efficient) | 5.14e-08 ± 1.97e-09 | 0.0476 ± 0.0226 | 0.00756 ± 0.00169 | 0.0028 ± 0.00192 | 0.0119 ± 0.000391 | 0.639 ± 0.0888 |

Table 12: Wall–clock optimization time (mean ± 95% CI; seconds).

| Variant | COVID-19 | Lung Cancer (with Chemo. & Radio.) | Lung Cancer (with Chemo.) | Lung Cancer | RNA Polymerase | Warfarin PK |
|---|---|---|---|---|---|---|
| No–refit | 0.752 ± 0.0103 | 4.46 ± 0.564 | 5.54 ± 0.712 | 2.83 ± 0.193 | 13.5 ± 1.17 | 0.482 ± 0.0415 |
| Refit–aware (full) | 0.891 ± 0.0159 | 10.6 ± 1.56 | 10.7 ± 1.22 | 9.87 ± 1.14 | 23.1 ± 1.59 | 0.607 ± 0.0848 |
| Refit–aware (efficient) | 0.779 ± 0.0139 | 4.55 ± 0.512 | 4.31 ± 0.61 | 5.04 ± 0.662 | 18 ± 1.69 | 0.53 ± 0.0753 |

A repeated-measures ANOVA confirmed that there was *no significant difference* in test MSE among the three variants on any of the six datasets (all $p \geq 0.09$).[3] As expected, the refit–aware variants incur a non–trivial extra cost (Table 12) without providing a corresponding gain in accuracy (Table 11).

### Distribution of influence values

We examined the empirical distribution of $\Delta$ values encountered during runs for *Lung Cancer (with Chemo. & Radio.)* and *RNA Polymerase* across all three variants. Two representative histograms (symlog $x$–axis for readability; outliers lightly clipped at extreme quantiles) are included in Fig. 9–10.

**Key summaries:**

**Lung Cancer (with Chemo. & Radio.)**: share of influences (%)

| Variant | $\Pr(\Delta < 0)$ | $\Pr(\Delta = 0)$ | $\Pr(\Delta > 0)$ | $n$ |
|---|---|---|---|---|
| No–refit | 18.19 | – | 81.81 | 21,912 |
| Refit–aware (full) | 24.59 | 0.05 | 75.37 | 21,590 |
| Refit–aware (efficient) | 29.53 | 0.14 | 70.33 | 22,398 |

[3] We conducted a one-factor repeated-measures ANOVA with Greenhouse-Geisser correction for each dataset. The statistics ($F(2, 18)$, $p_{\text{GG}}$, partial $\eta^2$) were: Lung Cancer ($F = 0.19, p = 0.72, \eta_p^2 = 0.02$); Lung Cancer (with Chemo.) ($F = 2.17, p = 0.17, \eta_p^2 = 0.20$); Lung Cancer (with Chemo. & Radio.) ($F = 1.74, p = 0.22, \eta_p^2 = 0.16$); Warfarin PK ($F = 2.78, p = 0.09, \eta_p^2 = 0.24$); RNA Polymerase ($F = 1.49, p = 0.26, \eta_p^2 = 0.14$); and COVID-19 ($F = 1.05, p = 0.34, \eta_p^2 = 0.10$).

**RNA Polymerase**: share of influences (%)

| **Variant** | $\Pr(\Delta < 0)$ | $\Pr(\Delta = 0)$ | $\Pr(\Delta > 0)$ | $n$ |
|---|---|---|---|---|
| No–refit | 4.71 | – | 95.29 | 7,190 |
| Refit–aware (full) | 9.08 | 1.40 | 89.52 | 6,696 |
| Refit–aware (efficient) | 8.75 | 2.28 | 88.97 | 6,526 |

**Observations:** (i) negative values are infrequent, and where present their magnitudes are typically small compared to the bulk positive mass (see symlog histograms); (ii) the *shape* of the distribution is broadly similar across the three variants; (iii) taken together with the within–seed ANOVA analysis, these results suggest the validation–computed $\Delta$ is *stable enough* for pruning decisions even without per–term refits.

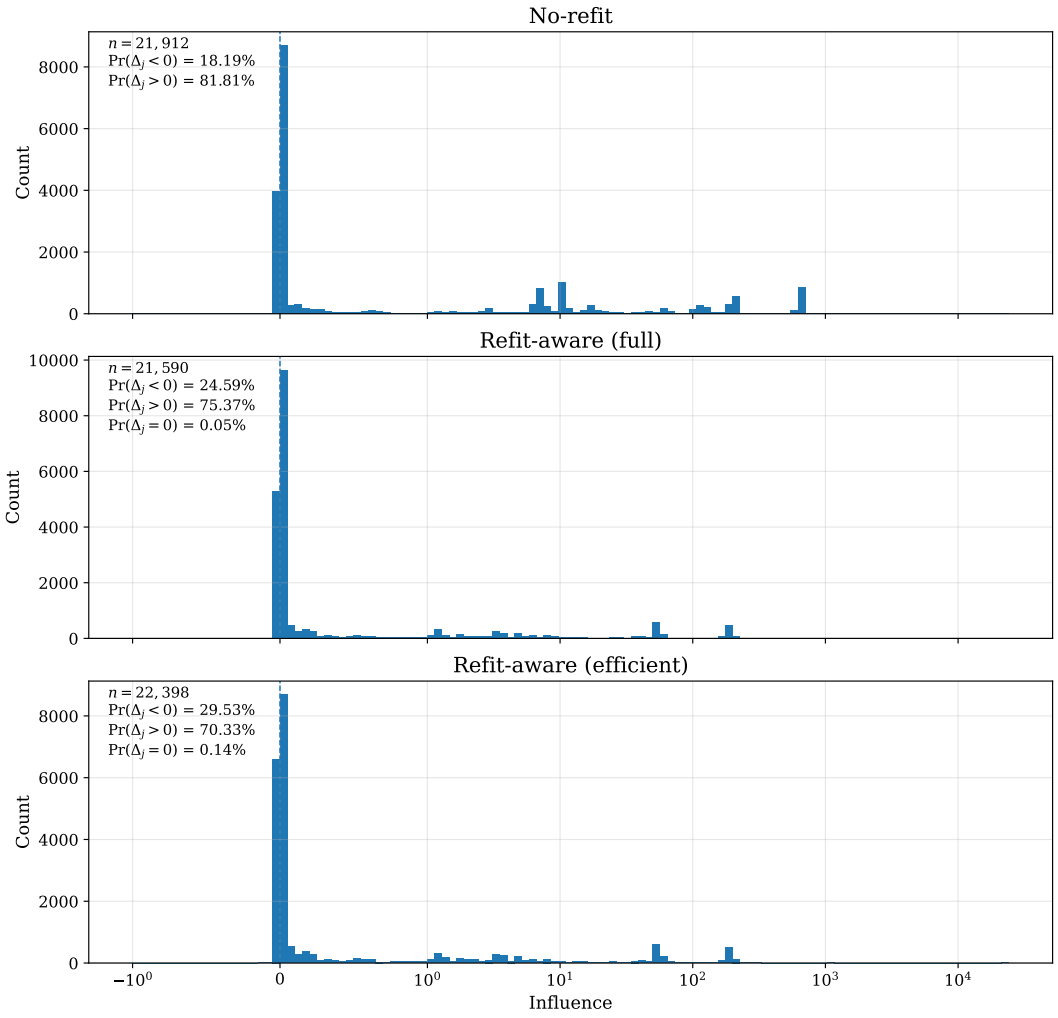


Figure 9: Distribution of influence values $\Delta$ on **Lung Cancer (with Chemo. & Radio.)** (symlog $x$–axis; extreme outliers clipped at the 0.01% tails for legibility).

### Summary of Findings

- **The Nature of the Influence Score.** Because the influence score, $\Delta$, is computed on a validation set *without* refitting the model, it is not constrained to be non-negative. Occasional small negative values are an expected result of this design and indicate that a feature has low or redundant influence in the context of the full model.
- **Performance vs. Cost.** Our experiments across six diverse datasets show that the test accuracy of the default, no-refit, and refit-aware variants is statistically indistinguishable. Given

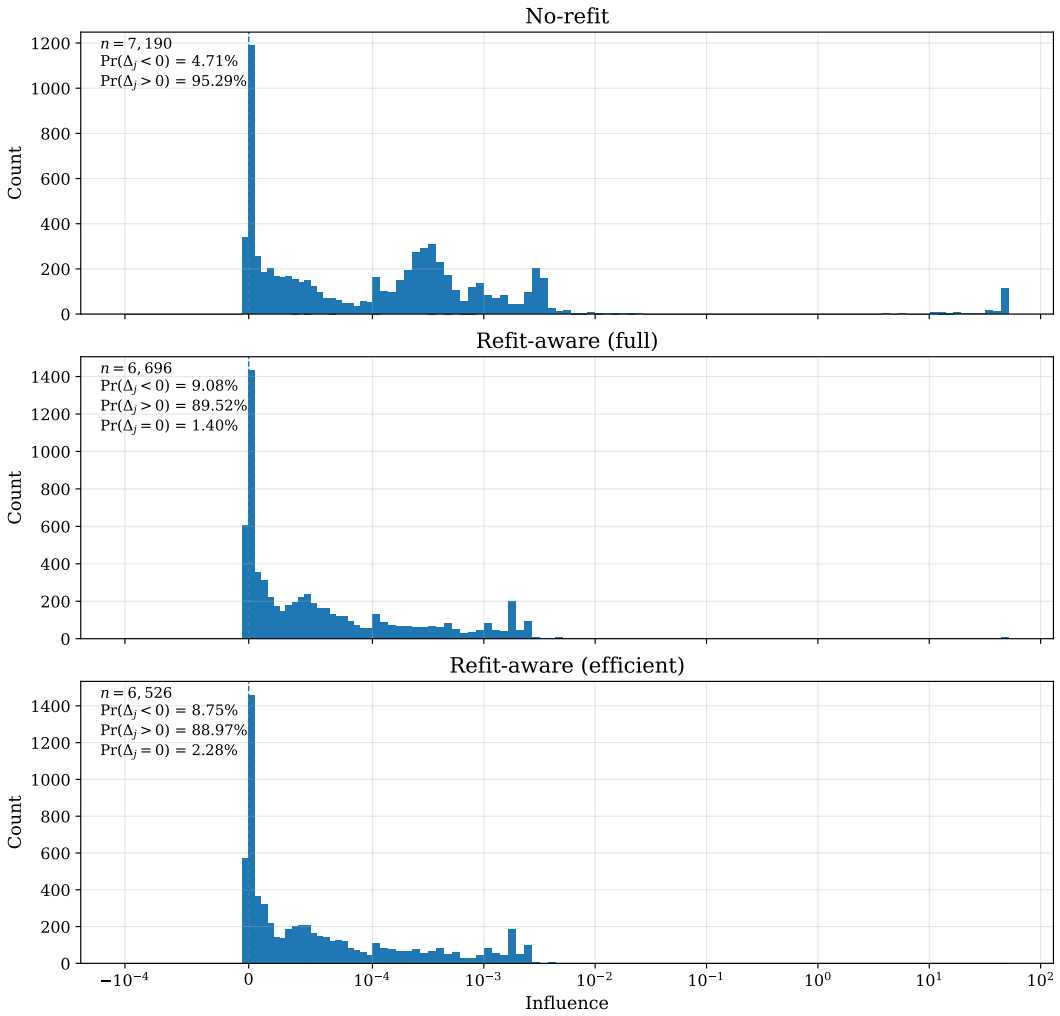


Figure 10: Distribution of influence values $\Delta$ on **RNA Polymerase** (symlog $x$–axis; extreme outliers clipped).

that the refit-aware variants are more computationally expensive, this finding establishes the default **no-refit** method as an efficient approach that does not compromise test accuracy.

- **Implementation Flexibility.** For applications where a refit-aware analysis is specifically required, two alternatives are available via configuration. Setting `refit_aware=True` performs a full refit for each term, while `refit_aware_efficient=True` uses a faster computational update. Both methods provide the extra-sum-of-squares style score, $\Delta^{\text{refit}}$, evaluated on the validation set.

### E.10 TERM-LOCAL OPTIMIZATION

To enhance SGED's flexibility, we introduce a variant that allows for the discovery of optimal scalar constants *within* the basis functions proposed by the LLM. This extension, which we refer to as SGED with Term-Local Optimization (SGED-TLO), addresses scenarios where an equation's true functional form involves specific constants that an LLM is unlikely to guess *a priori* (e.g., a decay rate in an exponential term or a frequency in a sinusoidal term). SGED-TLO integrates a dedicated optimization step to fine-tune these constants, enabling the discovery of more precise and potentially more accurate symbolic models.

The core principle is to augment the standard SGED loop: the "Propose" agent can now suggest basis functions containing tunable parameters, which are subsequently optimized before the "Prune" agent performs its influence-guided term selection.

**Parametric Basis Functions** In this variant, the "Propose" LLM agent can include tunable scalar constants in its proposed terms using the syntax `c(init)`, where `init` is an initial value for the parameter. For example, an agent might propose a term like `np.sin(c(1.0) * x1)`. Each basis function $\psi_j$ can thus be a parametric function $\psi_j(\mathbf{x}; \theta_j)$, where $\theta_j$ is a vector of the tunable constants within that term. The collection of all such constants across all candidate terms is denoted by $\theta$.

To maintain the model's primary structure as a linear combination of basis functions, the use of `c()` is disallowed as a direct outer multiplier (e.g., `c(1.5) * x1`), as the per-term linear coefficient $w_j$ is already learned by the outer model. The "Propose" agent's prompt in SGED-TLO variant contains clear instructions and examples to reflect this setup.

**Term-Local Optimization Objective** After the "Propose" agent suggests a new set of candidate terms, an additional optimization step is introduced before pruning. This step tunes the vector of all constants $\theta$ by minimizing an objective function $J(\theta)$. Crucially, this is a nested optimization problem. For any given set of constants $\theta$, the outer linear model weights $W$ are first re-computed by fitting on the training data. The objective $J(\theta)$ is then the Mean Squared Error (MSE) evaluated on the validation set using these optimal weights $W(\theta)$. This ensures that the constants are optimized for generalization performance.

Formally, for a given $\theta$, the design matrix on a data split $S \in \{\text{train, val}\}$ is $\Phi_S(\theta)$, where $[\Phi_S(\theta)]_{ik} = \psi_k(\mathbf{x}_i; \theta_k)$. The optimal outer weights are a function of $\theta$:

$$W(\theta) = \arg\min_{W'} \frac{1}{n_{\text{train}} m} \|Y_{\text{train}} - \Phi_{\text{train}}(\theta) W'\|_F^2 \; (+ \lambda \|W'\|_F^2 \text{ for ridge})$$

The objective for the inner-term constants is then to minimize the validation loss:

$$J(\theta) = \frac{1}{n_{\text{val}} m} \left\| Y_{\text{val}} - \Phi_{\text{val}}(\theta)\, W(\theta) \right\|_F^2$$

This objective is minimized with respect to $\theta$ using a quasi-Newton method (L-BFGS-B by default), with gradients estimated via finite differences.

**Dynamic Re-optimization and Agent Interaction** A key feature of this variant is that the constants are not optimized once and then fixed. After optimization, the symbolic representation of the terms retains the `c(value)` markers, where `value` is now the optimized value. These symbolic forms are what the "Prune" agent sees in its feedback tables.

In each subsequent iteration of the SGED loop, the constants within *all* surviving and newly proposed terms are re-optimized together. This dynamic re-optimization allows the ideal value for a constant in one term to adapt to the presence or absence of other terms in the model, preserving maximal flexibility throughout the discovery process. The "Prune" agent is explicitly prompted that these constants are not static and will be re-tuned in subsequent rounds.

**Algorithm Flow** The SGED-TLO propose-and-prune cycle proceeds as follows:

1. The LLM Propose agent suggests new terms, which may contain `c(init)` syntax. These are combined with surviving terms from the previous iteration.

2. The set of all constants $\theta$ from all current candidate terms is optimized by minimizing $J(\theta)$.
3. After optimization, the resulting terms are evaluated on the data splits (train, validation, test).
4. The standard pruning phase proceeds. The Prune agent receives the terms (with their optimized `c(value)` markers), their fitted outer weights $w_j$, and their per-term influence scores $\Delta_j$.
5. The agent returns keep/drop decisions. Surviving terms, retaining their `c()` markers, are passed to the next iteration.

This entire cycle is embedded within either the linear iterative refinement or the MCTS search strategy, just as in the standard SGED framework.

#### E.10.1 PROOF OF CONCEPT EXPERIMENT

To provide a clear illustration of the specific advantage offered by term-local optimization, we conducted a proof-of-concept experiment on a simple synthetic dataset. The data was generated from the ground-truth equation $y = 1/(0.123 + x_1^2)$, which contains a non-trivial constant, $0.123$, that an LLM is highly unlikely to propose spontaneously. We ran both the standard SGED and the SGED-TLO variant on this dataset, using their non-tree-based iterative refinement modes for simplicity.

As hypothesized, SGED-TLO was uniquely capable of recovering the exact ground-truth equation. During its iterative search, the "Propose" agent eventually suggested the correct functional form with a tunable constant: `1 / (x_1**2 + c(init))`. The subsequent optimization step successfully tuned the constant to match the ground truth value of $0.123$. In the final pruning round, the feedback provided to the "Prune" agent was unambiguous. The correct parametric term had an influence score of $17.59$, while all other candidate terms had negligible influence (on the order of $10^{-17}$ or less). Guided by this overwhelming signal, the agent correctly kept only the single correct term and discarded all others, resulting in the exact solution with a final MSE of effectively zero ($1.07 \times 10^{-29}$). The final discovered equation was:

```
y = 1 / (x_1**2 + 0.123)
```

By contrast, the standard SGED variant was unable to discover the true equation. Without the ability to tune the constant, it could not find a single basis function to accurately model the data. Instead, it was forced to approximate the target function by constructing a linear combination of multiple, non-parametric basis functions. After ten iterations, the best model it found was a complex five-term approximation:

```
y = 17.33 x_1 + 102.2 np.exp(-x_1) + 38.73 x_1 * np.exp(-x_1)
    - 18.34 np.abs(x_1) - 186.4 * 1 / (1 + np.exp(x_1))
```

While this model achieved a respectable test MSE of $0.0372$, it failed to capture the simple, parsimonious structure of the underlying data-generating process. In this experimental setting, with a 10 iteration budget, SGED-TLO was able to discover the exact expression in 10/25 runs, while vanilla SGED was able discover it in 0/25 runs (never). The experiment clearly demonstrates that for problems where precise constants are integral to the model's form, the term-local optimization capability of SGED-TLO is essential for discovering the correct symbolic solution.

#### E.10.2 BENCHMARK RESULTS WITH TERM-LOCAL OPTIMIZATION

To assess the practical impact of term-local optimization, we compared the performance of SGED-TLO against the vanilla SGED framework across our six benchmark datasets. The results, presented in Table 13, show that the inclusion of tunable constants yields mixed outcomes depending on the dataset's characteristics. However, it is important to note that SGED-TLO's performance remains highly competitive, and is often superior, when compared to the broader set of baselines presented in Table 3.

For the **Lung Cancer** and **Lung Cancer (with Chemo.)** datasets, SGED-TLO demonstrates a marked improvement in accuracy. This is likely attributable to the increased flexibility afforded by parametric terms, which can more closely approximate the underlying system dynamics. In the discovered equations for these datasets, we observe the selection of basis functions with optimized constants, such as those with the functional form $w_j \log(x + \theta)$ or $w_j \exp(\theta \cdot x)$. For instance, a

Table 13: **Comparison of SGED vs. SGED-TLO.** Test MSE (mean ± 95% CI) across all benchmark datasets. Results are averaged over 25 seeds. Lower is better. Bold indicates the better-performing variant for each dataset (if confidence intervals overlap, only the mean of the better-performing variant is bold.)

| Benchmark Dataset | SGED | SGED-TLO |
|---|---|---|
| Lung Cancer | 0.0033 ± 0.0035 | **7.59e-06 ± 1.33e-05** |
| Lung Cancer (with Chemo.) | 0.0054 ± 0.00107 | **0.000877 ± 0.000548** |
| Lung Cancer (with Chemo. & Radio.) | **0.0521 ± 0.0178** | 0.239 ± 0.127 |
| COVID-19 | **5.32e-08** ± 1.35e-09 | 5.33e-08 ± 1.77e-09 |
| RNA Polymerase | **0.0115** ± 0.000312 | 0.0119 ± 0.000124 |
| Warfarin PK | **0.646** ± 0.105 | 0.663 ± 0.111 |

high-performing equation discovered for the Lung Cancer (with Chemo.) task includes such adaptive terms:

$$\begin{aligned}\text{dv\_dt} = &-0.0002279 \cdot \text{chemo\_concentration} + 0.0001333 \cdot \text{chemo\_dosage} \\ &- 2.358 \cdot \text{np.log}(\text{cancer\_volume} + \mathbf{4.06858}) \\ &- 0.02799 \cdot \text{cancer\_volume} \cdot \text{chemo\_concentration} \\ &+ 1.736 \cdot \text{np.sqrt}(\text{cancer\_volume}) \\ &+ 1.945 \cdot \text{np.exp}(\mathbf{-0.00875506} \cdot \text{cancer\_volume}) \\ \text{dc\_dt} = &-0.5 \cdot \text{chemo\_concentration} + \text{chemo\_dosage}\end{aligned}$$

Conversely, on datasets like **Lung Cancer (with Chemo. & Radio.)** and **RNA Polymerase**, the performance of SGED-TLO is slightly worse than that of vanilla SGED. We speculate that this may be due to the significantly more complex and potentially non-convex optimization landscape introduced by the tunable constants $\theta$. The L-BFGS-B optimizer, while effective, may converge to local minima, particularly if the LLM's initial guesses for the constants are far from an optimal region. This could result in a set of basis functions that are locally optimal with respect to their internal constants but globally suboptimal for the final linear model, leading to a higher test MSE compared to the simpler, non-parametric terms found by the standard SGED. Performance on the COVID-19 and Warfarin PK datasets was comparable between the two variants.

The promising results on several datasets indicate that SGED-TLO is a valuable extension of the core framework. The approach and its variants warrant further investigation in future work, which could explore more sophisticated global optimization algorithms or improved heuristics for initializing the tunable constants. We provide the implementation of SGED-TLO as described in this section with the codebase for this work.

## F Computational Resources

The computational experiments for this research were conducted using a combination of cloud-based services for Large Language Model (LLM) inference and local or server-based machines for model optimization and equation evaluation.

**LLM Inference:** The inference for the majority of the Large Language Models employed in this study was performed using the serverless API provided by Azure AI Foundry. This allowed for scalable access to various proprietary LLM endpoints.

For the `Llama-3.3-70B` model, inference was conducted on a dedicated Azure Virtual Machine, specifically a Standard_NC96ads_A100_v4 instance. Key specifications of this VM include:

- **Processor:** 96 non-multithreaded 3rd Gen AMD EPYC™ 7V13 (Milan) cores.
- **GPU Accelerators:** 4 NVIDIA A100 PCIe GPUs, each with 80GB of memory.
- **System Memory:** 880 GiB.

**Model Optimization and Equation Evaluation:** The optimization of model parameters (i.e., fitting the linear model $\mathbf{w}$ for basis functions $\psi_j(\mathbf{x})$) and the evaluation of equations were carried out on the following types of local workstations and servers:

- A workstation equipped with a 10-core Intel Core i9-10900K CPU and 64 GiB of RAM.

- A server equipped with an 80-Core AMD EPYC 9V84 CPU and approximately 630 GiB of RAM.

It is important to note that the optimization step of SGED, which involves fitting a linear model (we use the `scikit-learn` library's implementation), does not require GPU acceleration and can be efficiently performed on any reasonably powerful desktop computer.

**Execution Time:** The time of execution for SGED varied depending on several factors, including the complexity of the dataset, the number of terms explored, the depth and breadth of the Monte Carlo Tree Search (if utilized), and the response latency of the LLM APIs. Individual propose-and-prune cycles involving LLM calls typically took seconds to minutes, while full MCTS runs could extend to several hours for comprehensive exploration. No single run took longer than 3 hours total wall-clock time. Fitting the linear models for equation evaluation was generally swift, on the order of seconds.

The total compute resources for the entire research project, including preliminary experiments and hyperparameter tuning, naturally exceeded that of the final reported experimental runs. However, the resources outlined above are representative of those required to reproduce the main findings.

# G Computational Cost and Scalability Analysis

To address the practical feasibility of SGED, we conducted a comprehensive analysis of its computational cost and scalability.

## G.1 Cost and Wall-Clock Time Comparison

We benchmarked SGED's monetary cost (in USD, based on LLM API calls) and total wall-clock time against several baseline methods on the Lung Cancer (with Chemo. & Radio.) dataset. Cost is based on GPT-4o API pricing at the time of experimentation: \$0.000005 per input token and \$0.00002 per output token. The total cost and wall clock results, averaged over 5 seeds, are shown in Table 14, as well as the Test MSE taken from the Table 3 main experiment results where available. Hyperparameters used were the same as in the Table 3 experiment, and default parameters were used for the additional PySR baseline, as set in the PySR implementation shipped with the LaSR (Grayeli et al., 2024) code base.

SGED's runtime is competitive with other modern symbolic regression methods and significantly faster than computationally intensive approaches like LaSR, while achieving a substantially lower Test MSE. For results under a comparable LLM token budget, see Appendix G.3, which makes the per-token performance efficiency of SGED especially clear.

Table 14: **Computational Cost and Performance Comparison.** Benchmarks on the Lung Cancer (with Chemo. & Radio.) dataset. Cost is based on GPT-4o API pricing at the time of experimentation.

| Method | Total Cost (USD) ↓ | Wall Clock (s) ↓ | Test MSE ↓ |
|---|---|---|---|
| GPLearn | - | $92.2 \pm 5.8$ | $46.8 \pm 4.9$ |
| PySR (Cranmer, 2023) | - | $282.7 \pm 6.0$ | $0.399 \pm 0.123$ |
| D3-white-box (Holt et al., 2024b) | $0.589 \pm 0.138$ | $203.4 \pm 39.5$ | $253 \pm 273$ |
| LaSR (Grayeli et al., 2024) | $72.40 \pm 3.48$ | $1444.5 \pm 137.5$ | $3.97 \pm 3.21$ |
| ICSR (Merler et al., 2024) | $1.08 \pm 0.16$ | $774.2 \pm 140.6$ | $6.1 \pm 1.05$ |
| LLM-SR (Shojaee et al., 2025) | $0.80 \pm 0.02$ | $371.7 \pm 18.7$ | $32.1 \pm 48.4$ |
| **SGED (Ours)** | $1.87 \pm 0.71$ | $382.8 \pm 137.6$ | $\mathbf{0.052 \pm 0.018}$ |

## G.2 Scalability with High-Dimensional Inputs

A key concern for symbolic regression methods is scalability with a large number of input features. We evaluated SGED's runtime on the RNA Polymerase dataset, which has 263 features. All hyperparameters were kept the same as in the Table 3 main experiment. As shown in Figure 11, SGED's runtime scales exceptionally well. The total wall-clock time increases only sub-linearly as the feature count grows from 10 to 263. This is a significant advantage of our framework, as

the influence-based feedback allows the LLM to efficiently identify and prune irrelevant features, avoiding the combinatorial explosion that challenges many other methods. This demonstrates SGED's practical feasibility for large-scale, high-dimensional scientific problems.

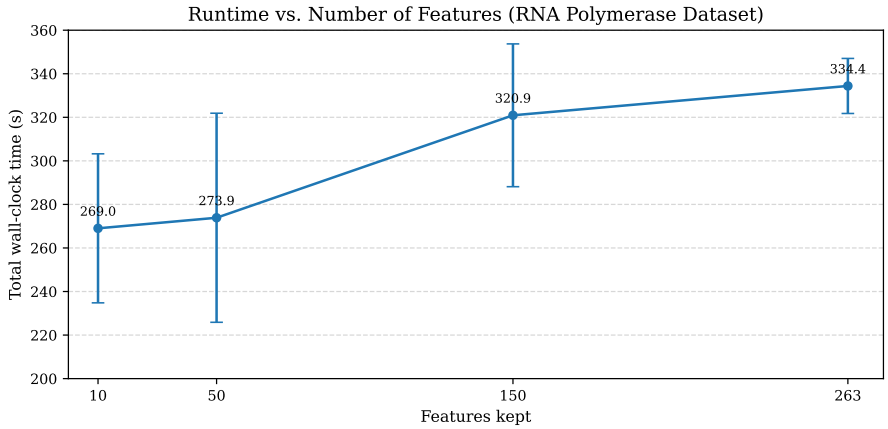


Figure 11: **Scalability with Increasing Number of Features.** Mean total wall-clock time on the RNA Polymerase dataset versus number of features used, averaged over 10 seeds. Points indicate means; error bars denote 95% confidence-interval half-widths. Runtime increases sub-linearly as the feature count grows from 10 to 263, indicating strong scalability of SGED.

### G.3 Performance Under a Fixed Computational Budget

To provide a direct and fair comparison of computational efficiency, we conducted an experiment where all LLM-based baselines were benchmarked under a fixed computational budget with respect to LLM usage – as the LLM calls are the most computationally intensive aspect of these methods. In order to ensure the methods consumed a nearly identical number of total LLM tokens (approximately 265k) we either adjusted the hyperparameters controlling itrative execution length of the method (number of iterations / generations or equivalent), or added early stopping based on the cumulative number of tokens consumed in the experiment run. All other hyperparameters were unchanged from the Table 3 main experiment setting. The Lung Cancer (with Chemo. & Radio.) dataset was used and the results were averaged over 5 seeds.

The results, presented in Table 15, are conclusive. When the LLM computational resources are held equal, SGED's performance advantage is clear. It achieves an MSE that is nearly 50 times better than the next-best performing method (ICSR). This demonstrates that SGED's architecture uses its computational budget more efficiently to find a superior solutions. While some simpler methods (like ICL with Basic Feedback) have a faster wall-clock time, they produce substantially less accurate results. SGED strikes an optimal balance, achieving a competitive runtime while delivering superior final equation(s).

Table 15: **Performance Comparison Under a Fixed Token Budget (≈265k Tokens).** Results on the Lung Cancer (with Chemo. & Radio.) dataset, averaged over 5 seeds.

| Method | Test MSE ↓ | Total Tokens | Wall Clock (s) |
|---|---|---|---|
| ICL (Basic Feedback) | 16.04 ± 22.1 | 265,199 ± 8,729 | 82.4 ± 3.8 |
| D3-white-box (Holt et al., 2024b) | 809.7 ± 1754.4 | 262,636 ± 2,406 | 302.1 ± 33.3 |
| LaSR (Grayeli et al., 2024) | 101.3 ± 112.1 | 272,606 ± 15,209 | 409.3 ± 28.1 |
| ICSR (Merler et al., 2024) | 2.66 ± 2.11 | 261,989 ± 71,813 | 1031.5 ± 319.3 |
| LLM-SR (Shojaee et al., 2025) | 9.88 ± 20.1 | 259,639 ± 12,820 | 1208.2 ± 58.1 |
| **SGED (Ours)** | **0.054 ± 0.074** | 272,743 ± 111,859 | 382.8 ± 137.6 |